Anti-miRNA Delivery Systems Based on Self-assembled Nanostructure

By
YU ZHANG
B.S., Northeast Forestry University, China, 2007
M.S. Northeast Forestry University, China, 2010

Dissertation
Submitted as partial fulfillment of the requirements
for the degree of Doctor of Philosophy in Biopharmaceutical Sciences in the Graduate College of the University of Illinois at Chicago, 2015
Chicago, IL

Defense Committee:

Richard A. Gemeinhart, Chair and Advisor
Debra Tonetti,
Seungpyo Hong,
Rohit Kolhatkar,
Mahesh V. Chaubal, Baxter

I would like to dedicate my dissertation to

my beloved parents, Baomin Zhang and Yunli Yu,

my husband, Yang Liu, and my daughter, Sophia T. Liu,

for believing in me and giving me encouragement, strength and

support to pursue my dreams.

Acknowledgement

My Ph.D. time at UIC is truly transformative. I am grateful to the Biopharmaceutical Sciences Department for the opportunity to pursue my dreams. First and for most, I would like to thank my thesis adviser, Professor Richard A. Gemeinhart, for his support and guidance. He taught me to always look at my own work with critical eyes and give my dedication to everything I do. The academic freedom he establishes in the lab and in daily communications fostered my ability to think independently and creatively. I am also very appreciative of my committee members, Dr. Debra Tonetti, Dr. Seungpyo Hong, Dr. Rohit Kolhatkar, Dr. Mahesh V. Chaubal and Dr. Xiaolong He for their helpful feedback and discussions.

I would like to acknowledge my former and current lab members for always providing help, Dr. Melanie Köllmer, Jason Buhrman, Jamie Rayahin, Mary Tang, Amy Ross and the undergraduate student researcher that has worked with me on this research project, Elizabeth Ramirez. I am also very appreciative of my collaborators, Dr. Petr Král and Soumyo Sen in his group, who performed the molecular dynamics simulations. I would also like to thank Dr. Larry L. Klein for helpful discussion about polymer conjugation and Dr. Gerd Prehna for assistance with ITC experiments.

I also thank Drs. Beck, Onyuksel, Tonetti and Hong for sharing of equipment and resources. I also would like to thank other students in the BPS department, especially, Dr. Ja Hye Myung, Dr. Suhair Sunoqrot, Dr. Yang Yang, Dr. Ryan Pearson, and Dr. Fatima Khaja for discussions and showing lab techniques. I also appreciate our wonderful office staff Celina Tejada, Connie Bouye and Tonya Kuzmis for their support.

Contribution of Authors

The first part of Chapter 1 is a published literature review [Yu Zhang, Zaijie Wang, Richard A. Gemeinhart. J Control Release. 2013 Dec 28;172(3):962-74] that summarizes the current progress of microRNA delivery research. I was the first author and wrote major portion of the manuscript. Dr. Zaijie Wang and my advisor, Dr. Richard A. Gemeinhart, also contributed to the writing of the review. Chapter 2 is a published manuscript (Yu Zhang, Melanie Köllmer, Jason S. Buhrman, Mary Y. Tang, Richard A. Gemeinhart. Peptides, 2014, 58:83-90). I was the first author and major driver of the research. Dr. Melanie Köllmer assisted me in the RT-PCR experiment of Figure 2.4. Jason S. Buhrman helped me with the Confocal Microscope imaging of Figure 2.3. Mary Y. Tang had some discussion with me about the manuscript structure. Dr. Richard A. Gemeinhart contributed to the writing of the manuscript. Chapter 3 represents a published manuscript (Yu Zhang, Yang Liu, Soumyo Sen, Petr Král, Richard A. Gemeinhart. Nanoscale. 2015, 7, 7559-7564). I was the first author and major driver of the research. Yang Liu assisted me with the NMR analysis in Figure 3.1 and 3.4. Soumyo Sen and Dr. Petr Král generated Figure 3.5. Dr. Richard A. Gemeinhart contributed to the writing of the manuscript. Chapter 4 represents my own unpublished work investigating the contribution of redox-responsive feature on anti-miRNA release from micelleplexes and micelleplexes stability in bodily fluids. I plan to publish this chapter as first author together with several other co-authors. Chapter 5 summarizes my overarching conclusions. The overall scientific contribution of my dissertation to the field and future directions are discussed.

TABLE OF CONTENTS

CHAPTERS

1 Introduction 1

1.1 Discovery and action of miRNAs 1

1.2 MicroRNA therapeutic approaches 7

1.3 Synthetic materials for miRNA and anti-miRNA oligonucleotide delivery 17

1.4 Challenges for developing short oligonucleotides delivery system 20

1.5 Dissertation outline and objectives 25

1.6 References 27

2 Arginine-rich, Cell Penetrating Peptide–anti-microRNA Complexes Decrease Glioblastoma Migration Potential 53

2.1 Abstract 53

2.2 Introduction 54

2.3 Materials and Methods 58

2.4 Results and Discussion 65

2.5 Conclusion 81

2.6 References 81

3 Charged Group Surface Accessibility Determines Micelleplexes Formation and Cellular Interaction 90

3.1 Abstract 90

3.2 Introduction 91

3.3 Materials and Methods 93

3.4 Result and Discussion 100

3.5 Conclusion 120

3.6 References 121

4 Redox-responsive Anti-miRNAs Delivery System Demonstrates Superior Potential for Releasing MiRNAs 131

4.1 Abstract 131

4.2 Introduction 132

4.3 Materials and Methods 137
4.4 Result and Discussion 146
4.5 Conclusions 162
4.6 References 163
5 Conclusion and Future Work 170
5.1 MiRNA Delivery Overview 170
5.2 Scientific Contribution of This Study 171
5.3 Recommended Future Research 174
5.4 References 178
APPENDICES 182
VITA 193

LIST OF FIGURES

Figure 1.1. Schematic representation of the biogenesis of miRNA. From genomic DNA, RNA is transcribed either as (1) an independent miRNA sequence or (2) an intron that is removed from mRNA. Following loop formation, the pre-miRNA is processed by DROSHA into pre-miRNA. The pre-miRNA is exported from the nucleus by Exportin5 before maturation by Dicer. Upon loading into the RISC complex, the miRNA duplex is unwound and the mature strand (red strand) retained within the miRISC complex. The passenger strand (green strand) is degraded. 4

Figure 1.2. Mechanism of natural miRNA-mRNA action. The roles of miRNA in protein production have been proposed to be through many routes. The majority of the actions inhibit protein production, but several modes of promotion of protein production have also been proposed. Binding of miRNA to DNA may promote transcription directly or through the recruitment of other factors. In addition, translation can be promoted by 5'UTR binding. Inhibitory action is likely through a combination of the mechanisms shown which include (1) direct mRNA degradation, (2) deadenylation, (3) initiation repression, (4) ribosomal stalling, (5) ribosomal drop-off, (6) co-translational degradation, and (7) translation repression following DNA binding. 5

Figure 1.3. Chemistry and structure of miRNA therapeutic molecules. RNA molecules (RNA) has several bonds that have been modified for stability including the alpha oxygen of phosphate (red), 4′ hydrogen (green), 2′ hydroxide (orange), 4′ hydrogen (purple), and the 1′ amide linkage to the base (blue). Peptide nucleic acids (PNAs) substitute a peptide bond at the 1′ amide linkage to the base. Phosphorothioates, methylphosphonates, and boranophosphates substitute a sulfur, methyl, and a borano group, respectively, for the alpha-oxygen of the phosphate. Locked nucleic acids (LNAs) add a secondary linkage between the 4′ carbon and the 2′ hydroxide while 2′ -O-(2-methoxyethyl)- (2′ -O-MOE), 2'-O-methyl- (2′ -O-Me), and 2′ -fluoro- (2′ -F) RNAs substitutes less reactive groups for the 2′ hydroxyl group. 10

Figure 1.4. Therapeutic Strategies for miRNA activity. Delivered DNA or RNA (green) can

act to augment, mimic miRNA activity or prevent activity of miRNA. MicroRNA can be produced by plasmid DNA (gene therapy) that is introduced into the cell, or by introducing agents to increase by translation promoters or cofactors, or delivered directly (in the forms of pri-, pre-, or mature with or without passenger). To prevent the activity of expressed miRNAs, miRNA binding with mRNA may be inhibited by masks of the binding of miRNA with the RISC complex may be inhibited with a sponge or a single binding anti-miRNA. Finally, translation may be directly repressed at the DNA level. 13

Figure 2.1. Physicochemical characterization of complexes. (A) Mobility of siRNA (upper panel) and anti-miRNA (lower panel) was retarded in the presence of R_8 peptide above a threshold charge (+/-) ratio. (B) Fluorescence was also quenched above a threshold charge (+/-) ratio, indicating double stranded siRNA (■) and single stranded anti-miRNA (◆) were condensed by the R_8 peptide (mean ± S.E.M., n=3). Similarly, R_8 complex (C) diameters and (D) ζ potential were measured by dynamic light scattering (mean ± S.E.M., n=3) for siRNA/R_8 complexes (■) and anti-miRNA/R_8 complexes (◆) further indicating complex formation at the given charge (+/-) ratios (mean ± S.E.M., n=3). 67

Figure 2.2. Cell association of RNA/R_8 complexes. Relative association of anti-miRNA/R_8 (blue bars) and siRNA/R_8 (red bars) with U251 glioblastoma cells after 4-hour interaction *in vitro* measured by flow cytometry (mean ± S.E.M., n=3). 68

Figure 2.3. Evaluation of endosomal escape efficiencies of anti-miRNA/R_8 and siRNA/R_8. (A) Representative confocal micrographs of siRNA/R_8 (left) and anti-miRNA/R_8 (right) complex-endosome colocalization showing RNA (red), endosome (green), nuclei (blue), and the composite of the three pseudocolor images where the RNA concentration was 55 nM and mixed with R_8 at a charge ratio of 50. (B) Quantitative comparison of endosome escape efficiency, $\mathcal{E}_{ee}$, between anti-miRNA/R_8 and siRNA/R_8. Endosome escape efficiency was calculated for 20 random, individual cells ($p < 0.001$). 72

Figure 2.4. Indirect measurement of anti-miRNA activity by detecting the mRNA of downstream miR-21 targets. (A) PDCD4 and (B) SERPINB5 mRNA levels relative to

GAPDH mRNA in cells treated with the R_8 peptide, control (ctrl) anti-miRNA/R_8 complexes, and anti-miRNA-21/R_8 complexes where the RNA concentration was 55 nM and mixed with R_8 at a charge ratio of 50 (mean±S.E.M.; n=3). Statistical significance compared to the anti-miRNA/R_8 group (†), ctrl anti-miRNA/R_8 group (‡), and R_8 treatment group (§) is presented as one ($0.01 < p < 0.05$), two ($0.001 < p < 0.01$), or three ($p < 0.001$) symbols. 74

Figure 2.5. Relative U251 survival (mitochondrial activity). After incubation with the anti-miR21/R_8 complex (▩) or control (ctrl) anti-miRNA/R_8 complex (▩) for varying times (mean±S.E.M.; n=3). 75

Figure 2.6. Inhibition of U251 cell migration after anti-miR-21/R_8 transfection. (A) Micrographs of U251 cells immediately after (0 hr) and 48 hours after wounding. (B) Wound recovery (P) measured 72 hours post transfection following treatment with R_8 peptide, ctrl anti-miRNA/R_8 complexes, or anti-miRNA-21/R_8 complexes where the RNA concentration was 55 nM and mixed with R_8 at a charge ratio of 50 (mean±S.E.M.; n=3) The wound recovery (P) of the three groups were normalized to the cell control group underwent wounding assay but no treatment. Statistical significance compared to the anti-miRNA/R_8 group (†) and control anti-miRNA/R_8 group (‡) treatment group is presented ($0.001 < p < 0.01$). 77

Figure 3.1. ^{1}H NMR spectra of (A) mPEG-PLA-COOH (B) CR_x (C) mPEG-PLA-R_8 (D) mPEG-PLA-R_{15}^{Low} (E) mPEG-PLA-R_{15}^{High}. The purified products have characteristic peaks from both PLA segment (a, δ 5.19, 1H) and guanidine group (b, δ 7.43, 4H) in R_x. 101

Figure 3.2. mPEG-PLA-R_x copolymers have CMC similar to mPEG-PLA. CMC plots of (A) mPEG-PLA (B) mPEG-PLA-R_8 (C) mPEG-PLA-R_{15}^{Low} and (D) mPEG-PLA-R_{15}^{High}. Data represent mean ± standard deviation, N=3. 104

Figure 3.3. TEM images of mPEG-PLA-R_8, mPEG-PLA-R_{15}^{Low} and mPEG-PLA-R_{15}^{High} micelles and micelleplexes (+/- charge ratio 30). 105

Figure 3.4. Micelles properties and surface oligoarginine presence. (A) Schematic representation of the micelles formed and the relevant molecular weights of the components. (B) ^{1}H NMR analysis of the peptides (CR_8 and CR_{15}) and micelles

(mPEG-PLA-R_8, mPEG-PLA-R_{15}^{Low}, and mPEG-PLA-R_{15}^{High}) showing the arginine a proton (1; δ 4.40, 1H), d protons (2; δ 3.20, 2H), or ω-terminal methoxyl protons (arrow; δ 3.40, 3H). 107

Figure 3.5. Molecular dynamics simulation of mPEG-PLA-R_8 micelle. Each monomer consisted of a methoxy-poly(ethylene-glycol)(mPEG; MW ~ 2,000 g/mol; blue) block coupled to the α-hydroxide of poly(lactide) (PLA; MW ~ 3,000 g/mol; red). As in the experiments, 28% of total monomers were modified with oligoarginine (R_8; green) on the ω-carboxylate of the PLA block. The micelles were prepared with total 60 monomers. 109

Figure 3.6. MiRNA complexation with micelles occurs at lower charge ratios for longer oligoarginine regardless of oligoarginine density. (A) mPEG-PLA-R_8, mPEG-PLA-R_{15}^{Low}, and mPEG-PLA-R_{15}^{High} complexation with miRNA at +/- charge ratios of 1, 5, 10 and 30 (B) mPEG-PLA-R_{15}^{Low} and mPEG-PLA-R_{15}^{High} complexation with miRNA at +/- charge ratios 1, 1.5, 2 and 30.....111

Figure 3.7. Thermodynamic profiles of single stranded miRNA binding to micelles indicate different interactions occur dependent upon oligoarginine length and density. (A) mPEG-PLA-R_8 (B) mPEG-PLA-R_{15}^{Low} (C) mPEG-PLA-R_{15}^{High} (D) Thermodynamic parameters, derived from ITC, of miRNA binding to mPEG-PLA-R_8, mPEG-PLA-R_{15}^{Low}, and mPEG-PLA-R_{15}^{High} micelles. 113

Figure 3.8. Micelleplexes are stable to heparin competition. Micelleplexes were prepared at (A) +/- charge ratio 20 or (B) 30 and incubated with heparin at a heparin to miRNA weight ratio (w/w) of 0:1, 4:1, or 8:1 prior to electrophoresis and staining. 116

Figure 3.9. Cellular association mediated by different micelleplexes. (A) The mean fluorescence intensity observed on U251 glioma cells following interaction with mPEG-PLA-R_8, mPEG-PLA-R_{15}^{Low}, and mPEG-PLA-R_{15}^{High} micelleplexes or untreated cells or Cy3-labeled miRNA. (B) The relative population (%) of cells associated with the mPEG-PLA-R_8, mPEG-PLA-R_{15}^{Low}, and mPEG-PLA-R_{15}^{High} micelleplexes or untreated cells or Cy3-labeled miRNA. N=3, mean ± standard error of the mean. 119

Figure 4.1. Schematic illustration of micelleplexes assembly. 135

Figure 4.2. Schematic illustration of micelleplexes disassembly in the presence of intracellular reducing environment. 136
Figure 4.3. Chemical reaction scheme for redox (A) and nonredox (B) polymer conjugates. 147
Figure 4.4. ^{1}H NMR spectra of (A) CR_{15} (B) mPEG-PLA-COOH (C) mPEG-PLA-SS-R_{15}. The purified products have characteristic peaks from both guanidine group (a, δ 7.43, 4H) in R_{15} and PLA segment (b, δ 5.19, 1H). 148
Figure 4.5. Micelleplexes characterization. (A) Redox-R_{15} and Nonredox-R_{15} micelles complexation with anti-miRNA at +/- charge ratios of 1, 2, 5, 10, 30 and 50. (B) Particle size and zeta potential of Redox-R_{15} and Nonredox-R_{15} micelles. (C) TEM characterization of Redox-R_{15} and Nonredox-R_{15} micelles and micelleplexes morphology, the scar bar is 100 nm. 150
Figure 4.6. Stability of micelleplexes and micelles in different media. (A) Micelleplexes stability in PBS, CSF and human plasma (B) Micelles stability in PBS, CSF and human plasma (C) Stability of the association between Cy3-anti-miRNA and micelles in PBS, CSF and human plasma. Data were presented as the mean plus or minus (±) standard error of the mean (S.E.M.). Three independent replicates of each experiment were performed. 153
Figure 4.7. CLSM observing anti-miRNA dissociation from micelleplexes. (A) Represented CLSM images. Red: Cy3-anti-miRNA, Green: FITC-micelles, Blue: Nucleus, and the composite of the three pseudocolor images where the Cy3-anti-miRNA concentration was 100 nM in association with micelles at a charge ratio of 30. Scale bar is 20 μm. Top two rows: imaging at 4 hours after delivery; bottom two rows, imaging at 24 hours after delivery, micelles containing medium was replaced with fresh medium at 4 hours to stop further cellular uptake. (B) Quantitative analysis of anti-miRNA dissociation rate. Cy3-anti-miRNA/redox-R_{15} micelleplexes (blue bars) and Cy3-anti-miRNA/nonredox-R_{15} micelleplexes (red bars). Dissociation rate was calculated for 30 individual cells. Data were presented as the mean plus or minus (±) standard error of the mean (S.E.M.). * indicates $p < 0.05$. 157
Figure 4.8. Cytotoxicity of redox and nonredox micelles to U251 cells. Different amount of

micelles were added to U251 cells and cultured in CSF for 4 hours followed by further incubation in full growth medium for 48 hours as in the dual luciferase assay. Data were presented as the mean plus or minus (±) standard error of the mean (S.E.M.). Three independent replicates of each experiment were performed. 159

Figure 4.9. Anti-miR-21/micelleplexes delivery efficiency with dual luciferase assay. The delivery efficiency of redox-R_{15} micelleplexes (blue bars) and nonredox-R_{15} micelleplexes (red bars) were compared by complexing anti-miR-21 and transfecting U251 glioblastoma cells in cerebrospinal fluid. The firefly luciferase level was normalized with renilla luciferase level. Data were presented as the mean plus or minus (±) standard error of the mean (S.E.M.). Three independent replicates of each experiment were performed. *** indicates $p < 0.0001$. 160

Figure A.1. ^{1}H NMR spectrum of mPEG-PLA-PDP. The purified product was dissolved in $CDCl_3$-*d*, which has the four characteristic peaks from the 3-(2-pyridyldithio) proprionyl hydrazide (PDPH), (Red rectangle, aromatic proton, δ 7.52, 1H; 7.91, 1H; 8.02, 1H; 8.68, 1H). 183

Figure B.1. ^{1}H NMR spectrum of mPEG-PLA-AEM. The purified product was dissolved in $CDCl_3$-*d*, which has the characteristic peak from the N-(2 Aminoethyl)maleimide trifluoroacetate (AEM), (a, δ 6.71, 2H). 184

LIST OF TABLES

Table 1.1. General properties of commonly described poly(nucleic acid) therapeutics. .. 5
Table 1.2. Current nonviral gene delivery system for miRNA therapeutics. 19
Table 1.3. Barriers and solutions to miRNA delivery (Adapted from Scholz and Wagner [110]). 21
Table 3.1. Micelle particle size and ζ-potential. 103
Table 3.2. Estimates of the number of oligo-arginine peptides and miRNA associated with micelles. 108
Table 3.3. Thermodynamic parameters for the binding between different micelles and anti-miRNA. 113
Table 3.4. Micelleplexes particle size and ζ-potential. 114

LIST OF ABBREVIATIONS

AMO	Anti-mirna oligonucleotides
APP	Amyloid precursor protein
BBB	Blood-brain barrier
bp	Base pairs
CNS	Central nervous system
CSC	Cancer stem cell
DDAB	Dimethyldioctadecylammonium bromide
DGCR8	Digeorge syndrome critical region gene
DNA	Deoxyribonucleic acid;
DOTMA	1,2-Di-O-octadecenyl-3-trimethylammonium propane
FANA	Fluorine derivatives nucleic acid
GC4	Phage identified internalizing scfvs that target tumor sphere cells
HCV	Hepatitis C virus
iNOP	Nanotransporter interfering nanoparticle-7
IR	Ionizing radiation
LAC	Lung adenocarcinoma
LNA	Locked nucleic acid
LPH	Liposome-hyaluronic acid
2’-Me	2’-methyl

miRNA	MicroRNA
2’-MOE	2’-methoxyethyl
NLE	Neutral lipid emulsion
NSCLC	Non-small cell lung cancer
nt	Nucleotides
ODN	Oligodeoxynucleotides
PEI	Polyethyleneimine
PNA	Peptide nucleic acids
PU	Polyurethane
RNA	Ribonucleic acid
RISC	RNA induced silencing complex
scFv	Single-chain variable fragment
siRNA	Small interfering RNA
TEPA-PCL	Dicetyl phosphate-tetraethylenepentamine-based polycation liposomes
TPGS	D-alpha-tocopheryl polyethylene glycol 1000 succinate
UTR	Untranslated regions
VEGF	Vascular endothelial growth factor
CPPs	Cell penetrating peptides
GBM	Glioblastoma multiforme
MMPs	Matrix metalloproteinases
R_8	Octaarginine

DMEM	Dulbecco's modified Eagle's medium
FBS	Fetal bovine serum
PBS	Phosphate buffered saline
PDCD4	Programmed cell death 4
SERPINB5	Serpin peptidase inhibitor, clade B (ovalbumin), member 5
GAPDH	Glyceraldehyde 3-phosphate dehydrogenase
S.E.M.	Standard error of the mean
Ago2	Argonaute 2
mPEG-PLA	Methoxy-poly(ethylene glycol-b-lactide)
PEG	Poly(ethylene glycol)
EDC	*N*-(3-dimethylaminopropyl)-*N*′-ethylcarbodiimide hydrochloride
NHS	*N*-hydroxysuccinimide
PDPH	3-(2-pyridyldithio) proprionyl hydrazide
CMC	Critical micelle concentration
SD	Standard deviation
ITC	Isothermal titration calorimetry
MD	Molecular dynamics
CNS	Central nervous system
(CSF)	Cerebrospinal fluid
DiI	Dioctadecyl-3,3,3′,3′-tetramethylindocarbocyanine perchlorate
DiO	3,3′-dioctadecyloxacarbocyanine perchlorate

AEM	N-(2-Aminoethyl)maleimide trifluoroacetate salt
TEM	Transmission electron microscopy
FRET	Förster resonance energy transfer

1 Introduction

1.1 Discovery and action of miRNAs

MicroRNAs (miRNAs) are one of a growing number of non-coding RNA molecules that act within a cell [1, 2]. Noncoding RNAs include miRNA, small interfering RNA (siRNA), ribozymes, among others [3]. Both miRNA and siRNA interact with messenger RNA (mRNA), typically marking the mRNA for degradation as will be described in this review. Ribozymes are RNA molecules that bind to mRNA (or other RNAs) and catalyze the degradation of the RNA with no enzyme [4]. Ribozymes are the only RNAs in this class known to act independent of proteins as catalysts to exert their action.

Herein, we focus on microRNAs as a novel class of therapeutic molecules with an emphasis on the methods used for delivery. Discovered little more than a decade ago [5, 6], miRNAs, small (20-24 nt) single stranded endogenous RNAs, are a class of post-transcriptional gene regulators. Since miRNA activity was confirmed in animals [7, 8] and humans [9, 10], miRNAs have attracted significant attention due to their critical regulatory

* Reproduced with permission from: Y Zhang, Z Wang, RA Gemeinhart. J Control Release. 2013 Dec 28;172(3):962-74.

impact on biological functions in development, cell proliferation, differentiation, apoptosis, and metabolism [11-15]. The primary miRNA precursor, pri-miRNA, is first transcribed as capped, polyadenylated RNA strands that form double stranded stem-loop structures (Figure 1.1). These pri-miRNAs are processed in the nucleus by DGCR8 and ribonuclease Drosha into 70 to 100 nt long hairpin structures, called pre-miRNAs. Pre-miRNAs are then exported to the cytoplasm by Exportin-5 and further processed by the RNAse Dicer into approximately 22 nt double-stranded miRNA duplexes [16-18]. The miRNA duplexes enter the miRNA-induced silencing complex (miRISC) and the Argonaute protein in the miRISC unwinds the mature strand from the passenger strand [19]. The mature strand is retained in the miRISC while the passenger strand is released and subsequently degraded.

The majority of miRNA activities [11] are proposed to be through interactions with the miRISC complex (Figure 1.2). Guided by the mature miRNA strand, miRISC binds target mRNAs, and thereby induces translational repression by blocking mRNA translation and degrading the mRNA [20, 21]. This binding is typically to the 3′ untranslated region (UTR) of mRNA; however, 5′-UTR binding and action is also reported [20, 21]. Much like siRNA

and siRISC recognition of mRNA, miRISC recognition of mRNA can be through perfect base pairing of the miRNA with the mRNA strand. But, the binding of miRISC to target mRNAs does not require perfect pairing, which is one factor allowing one miRNA strand to recognize an array of mRNA. Although this promiscuity is thought to be a unique feature of miRNA compared to siRNA (Table 1.1), there is significant overlap in the mechanism of miRISC and siRISC function [22]. There is such overlap that miRNA delivery, particularly when double-stranded approximately 21 nt sequences are delivered, that the terminology si(mi)RNA or simply siRNA is recommended by some [23]. Although the similarity in at least one mechanism of action may be true, we propose the difference between siRNA and miRNA to be the intent to knock down an individual mRNA with siRNA and an array of mRNAs with miRNA. In that, the delivery may converge, but the broad action desired is the primary difference between the two types of small non-coding RNA.

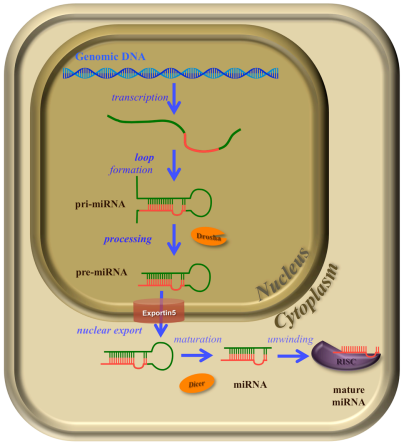

Figure 1.1. Schematic representation of the biogenesis of miRNA. From genomic DNA, RNA is transcribed either as (1) an independent miRNA sequence or (2) an intron that is removed from mRNA. Following loop formation, the pre-miRNA is processed by DROSHA into pre-miRNA. The pre-miRNA is exported from the nucleus by Exportin5 before maturation by Dicer. Upon loading into the RISC complex, the miRNA duplex is unwound and the mature strand (red strand) retained within the miRISC complex. The passenger strand (green strand) is degraded.

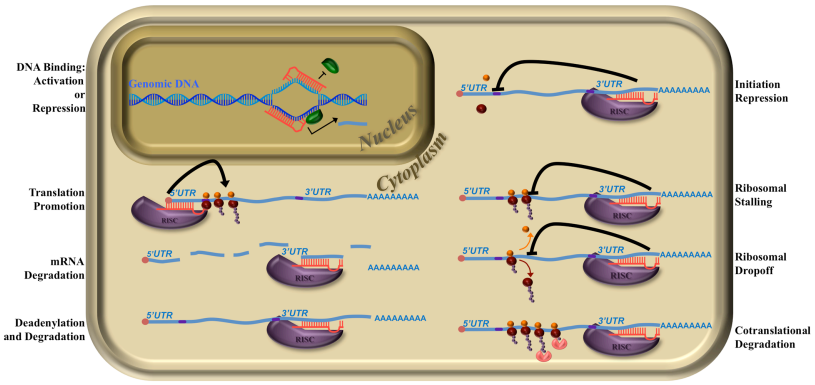

Figure 1.2. Mechanism of natural miRNA-mRNA action. The roles of miRNA in protein production have been proposed to be through many routes. The majority of the actions inhibit protein production, but several modes of promotion of protein production have also been proposed. Binding of miRNA to DNA may promote transcription directly or through the recruitment of other factors. In addition, translation can be promoted by 5'UTR binding. Inhibitory action is likely through a combination of the mechanisms shown which include (1) direct mRNA degradation, (2) deadenylation, (3) initiation repression, (4) ribosomal stalling, (5) ribosomal drop-off, (6) co-translational degradation, and (7) translation repression following DNA binding.

Table 1.1. General properties of commonly described poly(nucleic acid) therapeutics.

Property	miRNA	siRNA	ribozyme	antisense RNA/DNA	gene therapy
Size	~20 bp	~20 bp	≥10 bp	≥20 bp	>1 kbp
DNA or RNA	RNA	RNA	RNA	RNA/DNA	DNA
Structure	Single or double stranded	Double stranded	Single stranded	Single stranded	Double stranded
Proteins directly affected	many	one	one	one	one
Protein production change	downregulated or upregulated	downregulated	downregulated	downregulated	upregulated

The miRISC complex binding to mRNA can either repress or promote translation, although the latter appears to be rare [24]. Degradation of mRNA occurs primarily when prefect base-pairing is present and deadenylation and destabilization of mRNA that is not perfectly base-paired appears to predominate. Even when mRNA is not degraded, initiation may be repressed directly or the mRNA sequestered in regions of the cell (e.g., P-bodies) where low protein production takes place. If initiation takes place, the ribosomes stall during translation and may drop off the mRNA strand resulting in truncation of the protein. Also, proteases are recruited that degrade the protein as translation is underway. Through a combination of these mechanisms, miRNA has significant effect on the proteins produced by cells (Figure 1.2).

Extracellular action is directed through exosome formation [25] and nuclear actions have been proposed [26-34]. The small RNAs have been implicated in direct interactions with DNA, particularly promoter regions, or alterations of the chromatin structure thus altering final mRNA production. Much still remains to be learned about miRNA biosynthesis and actions, but sufficient knowledge has been gained particularly in the expression of miRNAs

in varying tissues and diseases. As we start to understand how altered miRNA expression can be associated with or even cause diseases in humans, including cancer, central nervous system (CNS) disorders, infectious diseases, cardiovascular diseases, metabolic disorders, and autoimmune diseases [35-39], new opportunities for developing novel therapeutics targeting miRNA dysregulation will emerge [36]. To achieve the clinical reality, an understanding of how miRNA therapeutics can act is needed.

1.2 MicroRNA therapeutic approaches

Using high-throughput techniques including miRNA microarrays, unique miRNAs expression profiles are being confirmed to mediate critical pathogenic processes in human disease [37, 40, 41]. These findings are rapidly being translated into recommendations targeting miRNA dysregulation. To translate these discoveries to viable therapies, appropriate, stable molecules must be designed and chemically modified poly(nucleic acids) are typically utilized for miRNA therapy. In addition to stabilization, chemical modifications can also be used to augment the specific binding of miRNA to the miRISC

complex [42, 43]. The current generation of miRNA therapeutics all utilize one or more of the chemical modifications developed over the last 20 years.

1.2.1 Chemical modification to RNA for miRNA therapy

Naked RNA (Figure 1.3) has a very short half-life in blood for several reasons, primarily being degraded by the abundant ribonucleases present in blood stream [44]. Thus, the first generation antisense phosphodiester oligodeoxynucleotides (ODNs), without further chemical modification, were proven to be ineffective in therapeutic applications [45]. The stability of the antisense sequences is augmented using chemically modified oligonucleotides [46]. Chemical modifications (Figure 1.3) include phosphorothioate containing oligonucleotides [47], 2′-O-methyl- (2’-O-Me) or 2′-O-methoxyethyl-oligonucleotides (2′-O-MOE) [48], locked nucleic acid (LNA) oligonucleotides [49], peptide nucleic acids (PNA) [50], fluorine derivatives (FANA and 2′-F) and other chemical modifications [51]. Many of these modifications have evolved previous to the discovery of miRNA first with antisense therapies in the 1980s and 1990s [52] then with siRNA therapies [53-55].

Phosphorothioate ODNs were developed attempting to overcome the stability issue, in which one of the non-bridging oxygen in the phosphate group is replaced by sulfur [56]. This modification dramatically increases nuclease resistance for parenteral administration, eliciting sufficient RNAse H activation for the target RNA cleavage and desired binding to cellular and serum proteins for uptake, absorption and distribution [47, 57-59]. However, limitations include relatively short *in vivo* half-life, low binding affinity to RNA, and nonspecific inhibition of cell growth still hinders the application of phosphorothioate ODNs for therapeutic intervention [58].

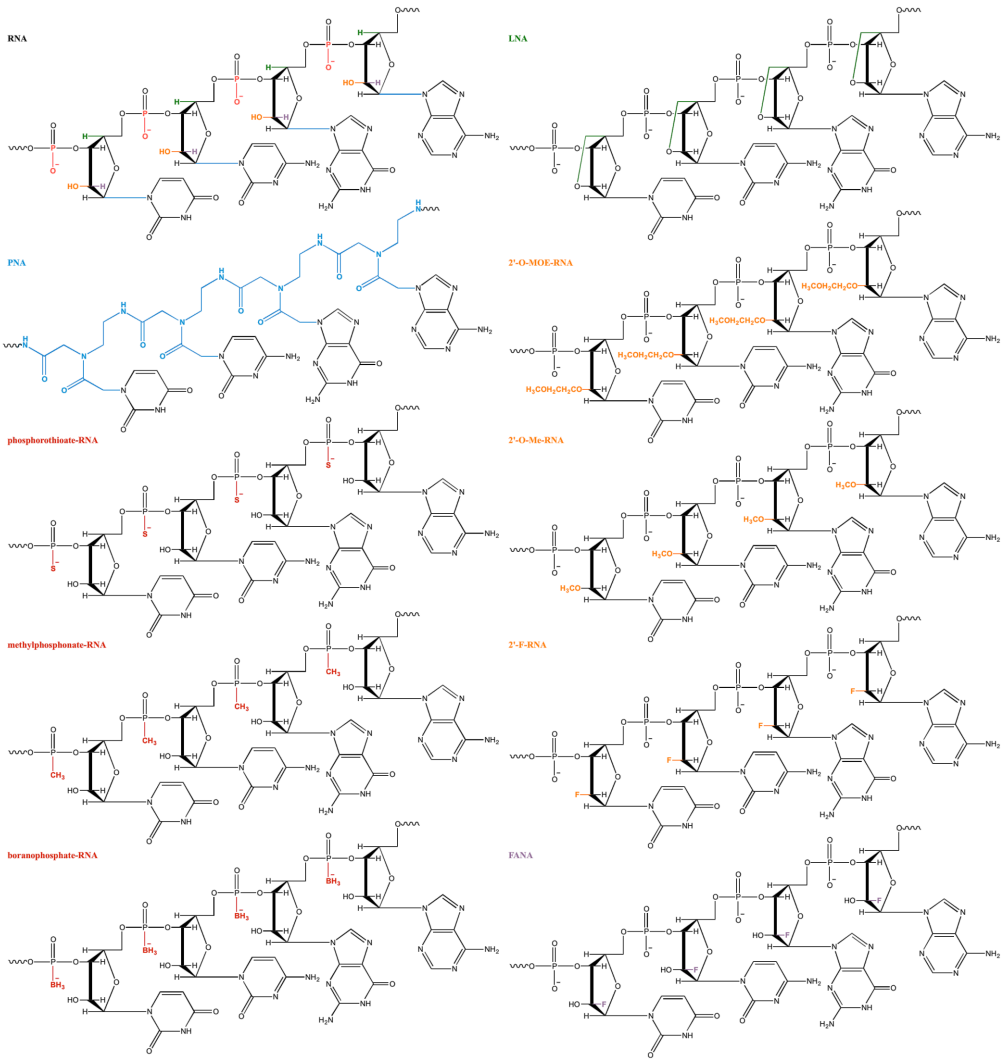

Figure 1.3. Chemistry and structure of miRNA therapeutic molecules. RNA molecules (RNA) has several bonds that have been modified for stability including the alpha oxygen of phosphate (red), 4′ hydrogen (green), 2′ hydroxide (orange), 4′ hydrogen (purple), and the 1′ amide linkage to the base (blue). Peptide nucleic acids (PNAs) substitute a peptide bond at the 1′ amide linkage to the base. Phosphorothioates, methylphosphonates, and boranophosphates substitute a sulfur, methyl, and a borano group, respectively, for the alpha-oxygen of the phosphate. Locked nucleic acids (LNAs) add a secondary linkage between the 4′ carbon and the 2′ hydroxide while 2′-O-(2-methoxyethyl)- (2′-O-MOE), 2'-O-methyl- (2′-O-Me), and 2′-fluoro- (2′-F) RNAs substitutes less reactive groups for the 2′ hydroxyl group.

The introduction of 2′-O-methyl group to the ribose moiety in a phosphorothioate oligoribonucleotides increases binding stability and reduces the non-specific inhibitory effects on cell growth [48]. Similarly, 2′-O-methoxyethyl modification markedly protects phosphorothioate oligoribonucleotides from nuclease degradation and will likely slow down oligoribonucleotides clearance from tissues and cells. The greater stability brought in by 2′-O-methoxyethyl modification and the phosphorothioate backbone should allow for less frequent dosing and may avoid the need for continuous infusions [47].

Further utilizing modifications at the 2'-oxygen, LNAs are RNA analogs with the ribose moiety chemically locked by a bridge connecting the 2'-oxygen and 4'-carbon in a RNA-mimicking N-type (C3′-endo) conformation [60]. Miravirsen or SPC3649 (Santaris Pharma, Horsholm, Denmark), an LNA-based therapeutic used to treat hepatitis C virus (HCV) infection, progressed to Phase II clinical trials in 2010. Miravirsen efficiently suppresses HCV genotype 1a and 1b infections when administered to chimpanzees, with no evidence of apparent viral resistance or side effects [61]. The promising Miravirsen clinical results where a dose-dependent decrease in HCV RNA without evidence of resistance [62]

was observed suggests utilization of the LNA chemistry to develop miRNA therapeutics for the treatment of other diseases.

Peptide nucleic acids (PNA) are uncharged oligonucleotides analogues in which the sugar–phosphodiester backbone of DNA/RNA has been replaced by an achiral structure consisting of N-(2-aminoethyl)-glycine units [63-65]. PNAs exhibit high specificity and stability without generating unwanted toxicity [66]. Most importantly, PNAs frequently do not require assistance of delivery from transfection reagents due to the lack of charge. In addition, cell penetrating peptides can be linked with PNAs to enhance delivery using standard peptide chemistry [42, 67]. Naked PNA-based anti-miR-155 specifically inhibited miR-155 in cultured B cells as well as in mice. However, very high dosage (50 mg PNA/kg/day for 2 days in mice) was required for efficiency and the untargeted mode of delivery poses a challenge for systemic administration [66].

Depending on the expression status of the target miRNA, miRNA therapeutic approaches can be separated into two categories: (1) miRNA inhibition therapy when the miRNA is overexpressed and (2) miRNA replacement therapy when the miRNA is repressed. These

methods can be accomplished with small RNAs directly delivered (Figure 1.4) or by more conventional gene therapy (Table 1.1) approaches where plasmids or virus are delivered to express the therapeutic molecules. The gene therapy approach will not be further discussed as the limits of delivery are equivalent to those of other gene therapy approaches and the activity are similar to the systems described herein.

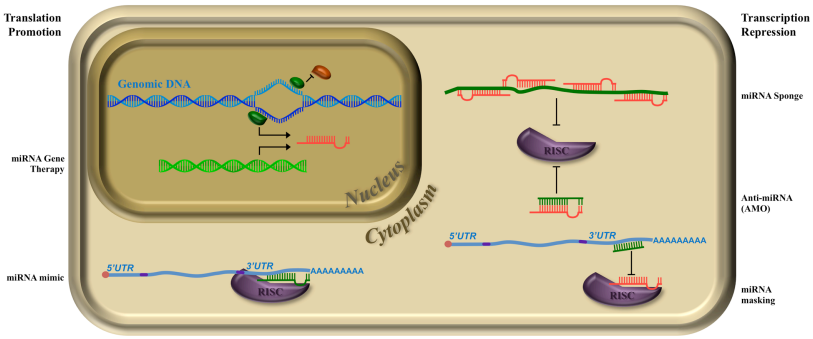

Figure 1.4. Therapeutic Strategies for miRNA activity. Delivered DNA or RNA (green) can act to augment, mimic miRNA activity or prevent activity of miRNA. MicroRNA can be produced by plasmid DNA (gene therapy) that is introduced into the cell, or by introducing agents to increase by translation promoters or cofactors, or delivered directly (in the forms of pri-, pre-, or mature with or without passenger). To prevent the activity of expressed miRNAs, miRNA binding with mRNA may be inhibited by masks of the binding of miRNA with the RISC complex may be inhibited with a sponge or a single binding anti-miRNA. Finally, translation may be directly repressed at the DNA level.

1.2.2 MiRNA inhibition therapy

When an upregulated miRNA contributes to disease pathology, miRNA inhibition therapy can be used to block the miRNAs repression of protein expression (Figure 1.4). Several methods have been used to inhibit miRNA repression of protein expression, but each involves the disruption of the miRISC complex. The most straightforward method utilizes oligonucleotides complementary to the miRNA mature strand, anti-miRNA oligonucleotides (AMOs), to inhibit interactions between miRISC proteins and the miRNA or miRISC and its target mRNAs. This approach mimic the idea of anti-sense DNA and RNA toward the mRNA strand preventing translation of the mRNA [68, 69]; however, the AMO is designed to bind the miRNA (not the mRNA), prevent degradation of the mRNA, and allow the mRNA to be translated. In order to achieve effective inhibition, chemical modifications are often used to enhance selective hybridization with the endogenous miRNAs.

Similar to AMO therapy, miRNA sponges seek to occupy the mature miRNA, but instead of delivering short sequences complementary to the miRNA mature strand, DNA

sequences, typically plasmids, expressing miRNA target mRNA in high copy number are transiently transfected in cells. This approach has recently been reported as similar to natural phenomena occurring in mammalian cells where circular RNA acts as a miRNA sponge inhibiting activity [70]. Those transcripts contain multiple binding sites to the miRNA of interest and saturate the miRISC complex repressing the activity toward natural mRNA [23]. Using this approach, miR-9 sponge, previously identified as having metastasis-promoting function in breast cancer cells, inhibited breast cancer metastasis formation [71]. However, due to limited control and homogeneity of transcripts expression, miRNA sponges could lead to serious unwanted side effect and thus is better suited for studying miRNAs function in cell culture assay *in vitro*.

In contrast to occupying the miRISC complex with decoys, miRNA masks were designed to complement the miRISC binding sites in the 3′ UTR of the target mRNA [72]. In zebrafish, this gene-specific, miRNA-interfering strategy prevented the miR-430 repression of transforming growth factor-β signaling [73]. The most significant advantage of this strategy lies in that signaling pathways regulated by a miRNA can be selectively blocked

by choice of sequence, but this strategy also requires the clear profile of miRNA target genes. Further, the miRNA masks are designed to have specificity for specific mRNA, and thus lose the ability to return protein production for many proteins other than the specific protein that's mRNA is masked.

1.2.3 MicroRNA replacement therapy

MiRNA replacement therapy supplements the lowered level of miRNAs with oligonucleotide mimics containing the same sequence as the mature endogenous miRNA, known as miRNA mimics. In order to achieve the same biological function as the naturally produced miRNA, mimics should possess the ability to enter the RISC complex and affect miRNA target mRNAs. Theoretically speaking, a single strand RNA molecule containing the same sequence, as the mature miRNA would work as a miRNA mimic. However, double stranded miRNA mimics composed of a guide strand and a passenger strand have 100 to 1000 fold higher potency compared with single stranded miRNA mimics [74]. The guide strand contains a sequence identical to the mature miRNA and the passenger strand sequence is complementary to the mature miRNA. For example, intratumoral injection of

cholesterol-conjugated miR-99a mimics significantly inhibited tumor growth in hepatocellular carcinoma-bearing nude mice [75]. In addition to the miRNA mimics having identical sequence as the endogenous mature miRNA, synthetic miRNA precursor mimics with longer sequence ranging from just a few additional nucleotides to full length pri-miRNA have been proposed [76]. Since pri-miRNA is processed in the nucleus, significantly different strategies would be mandated for nuclear targeting of pri-miRNA that would not be necessary for pre-miRNA or mature miRNA. In any case, choosing the appropriate materials to augment the delivery of the miRNA appears to be one of the most important factors influencing the activity of the miRNA.

1.3 Synthetic materials for miRNA and anti-miRNA oligonucleotide delivery

Synthetic materials have demonstrated potential as effective carriers for DNA and siRNA [73, 74]. Under most circumstances, synthetic materials are cationic and condense negatively charged poly(nucleic acid)s through electrostatic interactions. Synthetic delivery systems have considerable advantages over viral-based vector due to the control of their molecular composition, simplified manufacturing, modification and analysis, tolerance for

cargo sizes, and relatively lower immunogenicity [75]. However, synthetic systems have relatively lower efficiency compared to viral vectors. Relative efficiency has been greatly improved by modifying particle size and surface properties to achieve specific biodistribution in vivo. Further, conjugating small molecule ligands to polymeric carrier targeting diseased cell surface specific receptors has been widely used to augment cell uptake in appropriate cells. We have summarized the current synthetic polymer based delivery system for miRNA in Table 1.2.

Table 1.2. Current nonviral gene delivery system for miRNA therapeutics.

Material	Disease model	Targeted miRNA	Therapeutic Approaches	Route	Refs
Lipid-based delivery system: commercially available					
siPORT	Non-small cell lung cancer cells	miR-133b	Replacement	Systemic	[77]
MaxSuppressor	Non-small cell lung cancer	MiR-34a /Let-7	Replacement	Systemic	[78]
LipoTrust	Colorectal tumors	miR-143 /miR-145	Replacement	Intratumoral /systemic	[79]
Lipid-based delivery system: newly explored					
$98N_{12}$-5	Fat and cholesterol metabolism	miR-122	Inhibition	Systemic	[80]
DOTMA:cholesterol: TPGS lipoplexes	Non-small cell lung cancer cells	miR-133b	Replacement	Systemic	[77]
DDAB:cholesterol:TPGS lipoplexes	Head and neck squamous cell carcinoma	miR-107	Replacement	Systemic	[81]
GC4 scFv-targeted LPH nanoparticles	Murine B16F10 melanoma	miR-34a	Replacement	Systemic	[82]
cRGD-targeted LPH nanoparticles	Antiangiogenesis	miR-296	Inhibition	Subcutaneous	[83]
iNOP-7	Fat and cholesterol metabolism	miR-122	Inhibition	Systemic	[84]
Tetraethylenepentamine-based polycation lipoplexes	Colon carcinoma	miR-499	Replacement	Systemic	[85]
Polyethyleneimine (PEI)					
PEI	Colon carcinoma	miR-145/ miR-33a	Replacement	Intratumoral /systemic	[86]
Polyurethane-short branch PEI	Lung adenocarcinoma ; glioblastoma	miR145	Replacement	Systemic; intracranial	[87]
RVG-coupled PEI	Neuron diseases	miR-124a	Replacement	Systemic	[88]
Dendrimers					
Poly(amidoamine)	Glioblastoma	miR-21	Inhibition	Cell culture	[89, 90]
PLA-b-PDMAEMA	Glioma	miR-21	Inhibition	Cell culture	[91]
Poly(lactide-co-glycolide) (PLGA)					
Nonaarginine-modified PLGA nanoparticles	KB cells	miR-155	Replacement	Cell culture	[92]
Penetratin-modified PLGA nanoparticles	Pre-B cell lymphoma	miR-155	Replacement	Systemic	[93]
Micelles					
mPEG-b-PCC-g-GEM-g-DC-g-CAT	Pancreatic cancer	miR-205	Replacement	Systemic	[94]
Natural polymers					
Atelocollagen	Colorectal cancer; Lymphoma; Prostate;	miR-34a; miR-135b; miR-16	Replacement; Inhibition; Replacement	Intratumoral; intratumoral; systemic;	[95-97]

pHLIP peptide	Lymphoma	miR-155	Inhibition	Systemic	[98]
Inorganic materials					
Disialoganglioside-targeting silica nanoparticles	Neuroblastoma	miR-34a	Replacement	Systemic	[99]
RGD modified ultrasmall magnetic nanoparticles	Breast cancer	miR-10b	Inhibition	Systemic	[100]

1.4 Challenges for developing short oligonucleotides delivery system

Over the last several years, miRNA research has made amazingly rapid progress. But despite this, there is a belief that "RNAi is dead" [101] partly due to the departure from or reduction in emphasis on siRNA and miRNA by the pharmaceutical industry [102]. Few siRNA therapeutics and only two candidate miRNAs, SPC3649 (Santaris Pharma, Horsholm, Denmark) [103-108] a miR-122 antisense locked nucleic acid, and MRX34 (Mirna Therapeutics, Inc.) [109] a liposomal miR-34 mimic, have reached clinical trials. There is significant risk for investment by the pharmaceutical companies that is due to the biologically challenging therapeutic molecules, the expense of making and scaling up the therapeutics, and the unproven delivery systems. The field is still in the infancy and will take some time to mature. The costs and challenges will only become more reasonable. Of

all of the scientific (Table 1.3) and commercial challenges, the greatest challenge to translating siRNA and miRNA is delivery [101].

Table 1.3. Barriers and solutions to miRNA delivery (Adapted from Scholz and Wagner [110]).

Barrier/Step to Administration	Solutions
administration	local administration i.v. administration
degradation and elimination	local administration condensation to carrier control of • particle size • particle shape • particle charge • steric stabilization chemical modification
disease accumulation	local administration targeting particle size
cellular entry	targeting ligands non-specific interactions cell penetrating moieties
endosomal/lysosomal	endosomal escape • lytic lipids • fusogenic peptides • fusogenic polymers • osmotic lysis endosomal arrest/lysosomal inhibition MVB targeting
intracellular localization	MVB/P-body targeting for RISC activity

The inherent properties of miRNA are a significant challenge to delivery. Molecular stability before reaching the patient is a concern and this is often ignored. This is coupled with the cost and complexity of the production of the molecules and delivery systems. Once the miRNAs are administered, unprotected miRNAs are rapidly degraded by serum nucleases in bodily fluids. While chemical modifications protect miRNA, these molecules can impair specificity and potentially introducing off-target effects [55, 111]. This is compounded by the clearance of particulate systems even when they adequately protect the miRNA from degradation. When particles reach cells, the miRNA must separate for action to be possible. The limited separation of miRNA from the carrier has forced increased dose of miRNA to be active. Many current systems are focusing on using targeted drug delivery strategies to increase the amount of the drug that reaches the site, but targeting has a limited effect at increasing the total amount of drug that reaches the target organ [112].

The chemical and physical properties are not the only challenges as biologic properties of miRNA present difficulties that must be comprehended to properly deliver the molecules. The property of miRNA being able to regulate a network of genes without perfect pairing

also imposes the challenge of consistency and predictability of miRNA therapeutics. Moreover, the presence of exogenous artificial miRNAs brings the risk of saturation of RNA processing machinery and cause untoward side effect [113, 114]. Most importantly, the expression level and function of miRNAs vary not only between normal and diseased tissues and organs but also between disease stages [115, 116]. For example, a total of 28 epigenetically regulated miRNAs were identified as being associated with poor patient survival when under expressed in neuroblastoma, among which miR-340 induced either differentiation or apoptosis in a cell context dependent manner [117]. This feature is challenging because it requires miRNA therapeutics to achieve both temporal and spatial control over biodistribution *in vivo*.

Even when active, small RNAs can have nonspecific effects that must be examined. Interferon response can occur following activation interferon stimulated genes [118-121]. When this happens, it leads to non-specific inhibition of protein synthesis coupled with non-specific degradation of endogenous mRNA [122]. Therefore, in addition to non-targeting RNA controls, one must rule out the possible interferon response when validating

the small RNA. This can be achieved by determining the expression levels of several key genes involved in the interferon response [123-126]. These responses can be controlled possibly by appropriate delivery and design of the therapeutics.

The efficiency of miRNA-based therapeutic molecules rely largely on the capacity of delivery agent to protect the oligonucleotides against serum degradation, accumulate to the diseased organ or tissue via active targeting, and elicit powerful therapeutic effect without causing unwanted side effects. The delivery of miRNA is limited to parenteral or local injection due to the lack of enteral uptake of RNA although other routes are being examined [127]. Depending upon the disease, the amount of miRNA reaching a target organ (or organs) is limited. The chemical challenges to stabilizing RNAs have been overcome by modification and complexation, but the stability of the RNAs does not improve cellular uptake and escape. The vast majority of delivered RNA never will enter a cell, let alone the target cells. Each of the systems described overcomes some of the numerous challenges, but much improvement is possible.

1.5 Dissertation outline and objectives

The overall objective of this dissertation is to test the hypothesis that systematic study of the assembly and disassembly process of delivery carrier will provide guidance for the development of more efficacious short oligonucleotides delivery technologies. Delivery of miRNAs has substantial therapeutic promise for the treatment of cancer, and we have specifically chosen glioblastoma as a model. Toward this goal, three specific aims are pursued in Chapters 2, 3 and 4.

The majority of gene delivery system uses synthetic polymer with positively charged functional groups for nucleic acid loading and condensation. One possible component of a clinical delivery system is one of several classes of cell penetrating peptides. Cell penetrating peptides are small peptides (6 to 30 amino acid residues) that have membrane translocation activity. They constitute an important category of transfection reagents due to their low toxicity and low immunogenicity [128]. Arginine-rich peptides are one of the most investigated categories of CPPs, and include TAT, protamine and oligoarginine. In particular, the guanidinium groups on arginine are efficient at mediating cellular entry

while maintaining low cytotoxicity [98]. Even though many delivery systems have been developed for double stranded siRNA delivery, it is unclear whether those systems will work seamlessly with single stranded miRNA or anti-miRNA. In Chapter 2, we set out to test the hypothesis that oligoarginine will have different physicochemical interactions with single-stranded anti-miRNA and double-stranded siRNA due to the conformation disparity between single and double-stranded oligonucleotides.

In Chapter 3, to further explore oligoarginine as intracellular anti-miRNAs carrier, we engineered a micelle-based delivery system with methoxy-poly(ethylene glycol-b-lactide-b-arginine) (mPEG-PLA-ss-R_x, x = 8 or 15). Surface properties of the micelles were varied by controlling the oligoarginine block length and conjugation density. We hypothesized that the interaction between charged groups on the micelle surface and miRNA will greatly affect the micelleplexes formation and cellular interaction process.

Micelleplexes formation (complexation) and gene release from the micelleplexes (decomplexation) are major events in polymeric nucleic acid delivery. The unpackaging of nucleic acid from micelleplexes requires thoughtful design considerations because the

release of nucleic acids payloads from carrier in cytoplasm is a necessary step for effective nucleic acids delivery [129]. In Chapter 4, we hypothesized that the polyarginine block will separate from the micelle in the presence of glutathione and the reducing intracellular environment in the cytoplasm and thus facilitate anti-miRNA dissociation from the delivery system.

1.6 References

[1] B. Yan, Z.H. Wang, J.T. Guo, The research strategies for probing the function of long noncoding RNAs, Genomics, 99 (2012) 76-80.

[2] M. Wery, M. Kwapisz, A. Morillon, Noncoding RNAs in gene regulation, Wiley interdisciplinary reviews. Systems biology and medicine, 3 (2011) 728-738.

[3] S. Choudhuri, Small noncoding RNAs: biogenesis, function, and emerging significance in toxicology, Journal of biochemical and molecular toxicology, 24 (2010) 195-216.

[4] R. Robinson, RNAi therapeutics: how likely, how soon?, PLoS biology, 2 (2004) E28.

[5] R.C. Lee, R.L. Feinbaum, V. Ambros, The C. elegans heterochronic gene lin-4 encodes small RNAs with antisense complementarity to lin-14, Cell, 75 (1993) 843-854.

[6] B. Wightman, I. Ha, G. Ruvkun, Posttranscriptional regulation of the heterochronic gene lin-14 by lin-4 mediates temporal pattern formation in C. elegans, Cell, 75 (1993) 855-862.

[7] A.E. Pasquinelli, B.J. Reinhart, F. Slack, M.Q. Martindale, M.I. Kuroda, B. Maller, D.C. Hayward, E.E. Ball, B. Degnan, P. Muller, J. Spring, A. Srinivasan, M. Fishman, J. Finnerty, J. Corbo, M. Levine, P. Leahy, E. Davidson, G. Ruvkun, Conservation of the sequence and temporal expression of let-7 heterochronic regulatory RNA, Nature, 408 (2000) 86-89.

[8] B.J. Reinhart, F.J. Slack, M. Basson, A.E. Pasquinelli, J.C. Bettinger, A.E. Rougvie, H.R. Horvitz, G. Ruvkun, The 21-nucleotide let-7 RNA regulates developmental timing in Caenorhabditis elegans, Nature, 403 (2000) 901-906.

[9] G.A. Calin, C.D. Dumitru, M. Shimizu, R. Bichi, S. Zupo, E. Noch, H. Aldler, S. Rattan, M. Keating, K. Rai, L. Rassenti, T. Kipps, M. Negrini, F. Bullrich, C.M. Croce, Frequent deletions and down-regulation of micro- RNA genes miR15 and miR16 at 13q14 in chronic lymphocytic leukemia, Proc Natl Acad Sci U S A, 99 (2002) 15524-15529.

[10] J. Li, Z. Zhang, miRNA regulatory variation in human evolution, Trends in genetics : TIG, 29 (2013) 116-124.

[11] V. Ambros, The functions of animal microRNAs, Nature, 431 (2004) 350-355.

[12] T. Braun, M. Gautel, Transcriptional mechanisms regulating skeletal muscle differentiation, growth and homeostasis, Nat Rev Mol Cell Biol, 12 (2011) 349-361.

[13] R.T. Lima, S. Busacca, G.M. Almeida, G. Gaudino, D.A. Fennell, M.H. Vasconcelos, MicroRNA regulation of core apoptosis pathways in cancer, Eur J Cancer, 47 (2011) 163-174.

[14] D.P. Bartel, MicroRNAs: genomics, biogenesis, mechanism, and function, Cell, 116 (2004) 281-297.

[15] L. He, G.J. Hannon, MicroRNAs: small RNAs with a big role in gene regulation, Nat Rev Genet, 5 (2004) 522-531.

[16] M.T. Bohnsack, K. Czaplinski, D. Gorlich, Exportin 5 is a RanGTP-dependent dsRNA-binding protein that mediates nuclear export of pre-miRNAs, Rna-a Publication of the Rna Society, 10 (2004) 185-191.

[17] R. Yi, Y. Qin, I.G. Macara, B.R. Cullen, Exportin-5 mediates the nuclear export of pre-microRNAs and short hairpin RNAs, Genes & Development, 17 (2003) 3011-3016.

[18] Y. Lee, C. Ahn, J.J. Han, H. Choi, J. Kim, J. Yim, J. Lee, P. Provost, O. Radmark, S. Kim, V.N. Kim, The nuclear RNase III Drosha initiates microRNA processing, Nature, 425 (2003) 415-419.

[19] A.M. Denli, B.B.J. Tops, R.H.A. Plasterk, R.F. Ketting, G.J. Hannon, Processing of primary microRNAs by the Microprocessor complex, Nature, 432 (2004) 231-235.

[20] L.P. Lim, N.C. Lau, P. Garrett-Engele, A. Grimson, J.M. Schelter, J. Castle, D.P. Bartel, P.S. Linsley, J.M. Johnson, Microarray analysis shows that some microRNAs downregulate large numbers of target mRNAs, Nature, 433 (2005) 769-773.

[21] P.H. Olsen, V. Ambros, The lin-4 regulatory RNA controls developmental timing in Caenorhabditis elegans by blocking LIN-14 protein synthesis after the initiation of translation, Dev Biol, 216 (1999) 671-680.

[22] J.G. Doench, C.P. Petersen, P.A. Sharp, siRNAs can function as miRNAs, Genes Dev, 17 (2003) 438-442.

[23] M.S. Ebert, J.R. Neilson, P.A. Sharp, MicroRNA sponges: competitive inhibitors of small RNAs in mammalian cells, Nat Methods, 4 (2007) 721-726.

[24] S. Vasudevan, Y. Tong, J.A. Steitz, Switching from repression to activation: microRNAs can up-regulate translation, Science, 318 (2007) 1931-1934.

[25] A. Gallo, M. Tandon, I. Alevizos, G.G. Illei, The majority of microRNAs detectable in serum and saliva is concentrated in exosomes, PLoS One, 7 (2012) e30679.

[26] L.C. Li, S.T. Okino, H. Zhao, D. Pookot, R.F. Place, S. Urakami, H. Enokida, R. Dahiya, Small dsRNAs induce transcriptional activation in human cells, Proc Natl Acad Sci U S A, 103 (2006) 17337-17342.

[27] X. Wang, X. Song, C.K. Glass, M.G. Rosenfeld, The long arm of long noncoding RNAs: roles as sensors regulating gene transcriptional programs, Cold Spring Harb Perspect Biol, 3 (2011) a003756.

[28] C. Holz-Schietinger, N.O. Reich, RNA modulation of the human DNA methyltransferase 3A, Nucleic acids research, 40 (2012) 8550-8557.

[29] E. Bernstein, C.D. Allis, RNA meets chromatin, Genes & Development, 19 (2005) 1635-1655.

[30] C.D. Jeffries, H.M. Fried, D.O. Perkins, Nuclear and cytoplasmic localization of neural stem cell microRNAs, RNA, 17 (2011) 675-686.

[31] D.H. Kim, P. Saetrom, O. Snove, Jr., J.J. Rossi, MicroRNA-directed transcriptional gene silencing in mammalian cells, Proc Natl Acad Sci U S A, 105 (2008) 16230-16235.

[32] S.T. Younger, D.R. Corey, Transcriptional gene silencing in mammalian cells by miRNA mimics that target gene promoters, Nucleic acids research, 39 (2011) 5682-5691.

[33] J. Tomikawa, H. Shimokawa, M. Uesaka, N. Yamamoto, Y. Mori, H. Tsukamura, K. Maeda, T. Imamura, Single-stranded noncoding RNAs mediate local epigenetic alterations at gene promoters in rat cell lines, The Journal of biological chemistry, 286 (2011) 34788-34799.

[34] C.L. Jopling, M. Yi, A.M. Lancaster, S.M. Lemon, P. Sarnow, Modulation of hepatitis C virus RNA abundance by a liver-specific MicroRNA, Science, 309 (2005) 1577-1581.

[35] A. Dharap, V.P. Nakka, R. Vemuganti, microRNAs in Ischemic Brain: The Fine-Tuning Specialists and Novel Therapeutic Targets

Translational Stroke Research, in: P.A. Lapchak, J.H. Zhang (Eds.), Springer US, 2012, pp. 335-352.

[36] J. Stanczyk, D.A.L. Pedrioli, F. Brentano, O. Sanchez-Pernaute, C. Kolling, R.E. Gay, M. Detmar, S. Gay, D. Kyburz, Altered expression of microRNA in synovial fibroblasts and synovial tissue in rheumatoid arthritis, Arthritis and Rheumatism, 58 (2008) 1001-1009.

[37] J. Lu, G. Getz, E.A. Miska, E. Alvarez-Saavedra, J. Lamb, D. Peck, A. Sweet-Cordero, B.L. Ebet, R.H. Mak, A.A. Ferrando, J.R. Downing, T. Jacks, H.R. Horvitz, T.R. Golub, MicroRNA expression profiles classify human cancers, Nature, 435 (2005) 834-838.

[38] M. Tatsuguchi, H.Y. Seok, T.E. Callis, J.M. Thomson, J.-F. Chen, M. Newman, M. Rojas, S.M. Hammond, D.-Z. Wang, Expression of microRNAs is dynamically regulated during cardiomyocyte hypertrophy, Journal of Molecular and Cellular Cardiology, 42 (2007) 1137-1141.

[39] K. Jeyaseelan, W.B. Herath, A. Armugam, MicroRNAs as therapeutic targets in human diseases, Expert Opin Ther Targets, 11 (2007) 1119-1129.

[40] Y. Murakami, T. Yasuda, K. Saigo, T. Urashima, H. Toyoda, T. Okanoue, K. Shimotohno, Comprehensive analysis of microRNA expression patterns in hepatocellular carcinoma and non-tumorous tissues, Oncogene, 25 (2006) 2537-2545.

[41] P.T. Nelson, D.A. Baldwin, L.M. Scearce, J.C. Oberholtzer, J.W. Tobias, Z. Mourelatos, Microarray-based, high-throughput gene expression profiling of microRNAs, Nature Methods, 1 (2004) 155-161.

[42] K.A. Lennox, M.A. Behlke, Chemical modification and design of anti-miRNA oligonucleotides, Gene Ther, 18 (2011) 1111-1120.

[43] K.A. Lennox, M.A. Behlke, A direct comparison of anti-microRNA oligonucleotide potency, Pharm Res, 27 (2010) 1788-1799.

[44] F. Czauderna, M. Fechtner, S. Dames, H. Aygun, A. Klippel, G.J. Pronk, K. Giese, J. Kaufmann, Structural variations and stabilising modifications of synthetic siRNAs in mammalian cells, Nucleic acids research, 31 (2003) 2705-2716.

[45] P.D. Cook, Medicinal chemistry of antisense oligonucleotides--future opportunities, Anticancer Drug Des, 6 (1991) 585-607.

[46] J. Krutzfeldt, N. Rajewsky, R. Braich, K.G. Rajeev, T. Tuschl, M. Manoharan, M. Stoffel, Silencing of microRNAs in vivo with antagomirs, Nature, 438 (2005) 685-689.

[47] S.T. Crooke, M.J. Graham, J.E. Zuckerman, D. Brooks, B.S. Conklin, L.L. Cummins, M.J. Greig, C.J. Guinosso, D. Kornbrust, M. Manoharan, H.M. Sasmor, T. Schleich, K.L. Tivel, R.H. Griffey, Pharmacokinetic properties of several novel oligonucleotide analogs in mice, J Pharmacol Exp Ther, 277 (1996) 923-937.

[48] B.H. Yoo, E. Bochkareva, A. Bochkarev, T.C. Mou, D.M. Gray, 2'-O-methyl-modified phosphorothioate antisense oligonucleotides have reduced non-specific effects in vitro, Nucleic acids research, 32 (2004) 2008-2016.

[49] C. Wahlestedt, P. Salmi, L. Good, J. Kela, T. Johnsson, T. Hokfelt, C. Broberger, F. Porreca, J. Lai, K. Ren, M. Ossipov, A. Koshkin, N. Jakobsen, J. Skouv, H. Oerum, M.H. Jacobsen, J. Wengel, Potent and nontoxic antisense oligonucleotides containing locked nucleic acids, Proc Natl Acad Sci U S A, 97 (2000) 5633-5638.

[50] B. Hyrup, P.E. Nielsen, Peptide nucleic acids (PNA): synthesis, properties and potential applications, Bioorg Med Chem, 4 (1996) 5-23.

[51] P.S. Pallan, E.M. Greene, P.A. Jicman, R.K. Pandey, M. Manoharan, E. Rozners, M. Egli, Unexpected origins of the enhanced pairing affinity of 2'-fluoro-modified RNA, Nucleic acids research, 39 (2011) 3482-3495.

[52] S. Akhtar, M.D. Hughes, A. Khan, M. Bibby, M. Hussain, Q. Nawaz, J. Double, P. Sayyed, The delivery of antisense therapeutics, Adv Drug Deliv Rev, 44 (2000) 3-21.

[53] M.A. Behlke, Chemical modification of siRNAs for in vivo use, Oligonucleotides, 18 (2008).

[54] M. Manoharan, RNA interference and chemically modified small interfering RNAs, Curr Opin Chem Biol, 8 (2004) 570-579.

[55] D.R. Corey, Chemical modification: the key to clinical application of RNA interference?, J Clin Invest, 117 (2007) 3615-3622.

[56] J.M. Campbell, T.A. Bacon, E. Wickstrom, Oligodeoxynucleoside phosphorothioate stability in subcellular extracts, culture media, sera and cerebrospinal fluid, J Biochem Biophys Methods, 20 (1990) 259-267.

[57] S.D. Patil, D.G. Rhodes, Influence of divalent cations on the conformation of phosphorothioate oligodeoxynucleotides: a circular dichroism study, Nucleic acids research, 28 (2000) 2439-2445.

[58] T.P. Prakash, A.M. Kawasaki, E.V. Wancewicz, L. Shen, B.P. Monia, B.S. Ross, B. Bhat, M. Manoharan, Comparing in vitro and in vivo activity of 2'-O-[2-(methylamino)-2-oxoethyl]- and 2'-O-methoxyethyl-modified antisense oligonucleotides, J Med Chem, 51 (2008) 2766-2776.

[59] M. Egli, G. Minasov, V. Tereshko, P.S. Pallan, M. Teplova, G.B. Inamati, E.A. Lesnik, S.R. Owens, B.S. Ross, T.P. Prakash, M. Manoharan, Probing the influence of stereoelectronic effects on the biophysical properties of oligonucleotides: comprehensive analysis of the RNA affinity, nuclease resistance, and crystal structure of ten 2'-O-ribonucleic acid modifications, Biochemistry, 44 (2005) 9045-9057.

[60] J. Elmen, M. Lindow, S. Schutz, M. Lawrence, A. Petri, S. Obad, M. Lindholm, M. Hedtjarn, H.F. Hansen, U. Berger, S. Gullans, P. Kearney, P. Sarnow, E.M. Straarup, S. Kauppinen, LNA-mediated microRNA silencing in non-human primates, Nature, 452 (2008) 896-U810.

[61] R.E. Lanford, E.S. Hildebrandt-Eriksen, A. Petri, R. Persson, M. Lindow, M.E. Munk, S. Kauppinen, H. Orum, Therapeutic Silencing of MicroRNA-122 in Primates with Chronic Hepatitis C Virus Infection, Science, 327 (2010) 198-201.

[62] H.L. Janssen, H.W. Reesink, E.J. Lawitz, S. Zeuzem, M. Rodriguez-Torres, K. Patel, A.J. van der Meer, A.K. Patick, A. Chen, Y. Zhou, R. Persson, B.D. King, S. Kauppinen, A.A. Levin, M.R. Hodges, Treatment of HCV Infection by Targeting MicroRNA, The New England journal of medicine, (2013).

[63] E. Vigorito, S. Kohlhaas, D. Lu, R. Leyland, miR-155: an ancient regulator of the immune system, Immunol Rev, 253 (2013) 146-157.

[64] M.M. Fabani, C. Abreu-Goodger, D. Williams, P.A. Lyons, A.G. Torres, K.G. Smith, A.J. Enright, M.J. Gait, E. Vigorito, Efficient inhibition of miR-155 function in vivo by peptide nucleic acids, Nucleic acids research, 38 (2010) 4466-4475.

[65] G. Breipohl, J. Knolle, D. Langner, G. O'Malley, E. Uhlmann, Synthesis of polyamide nucleic acids (PNAs) using a novel Fmoc/Mmt protecting-group combination, Bioorganic & Medicinal Chemistry Letters, 6 (1996) 665-670.

[66] M.M. Fabani, C. Abreu-Goodger, D. Williams, P.A. Lyons, A.G. Torres, K.G.C. Smith, A.J. Enright, M.J. Gait, E. Vigorito, Efficient inhibition of miR-155 function in vivo by peptide nucleic acids, Nucleic acids research, 38 (2010) 4466-4475.

[67] M.M. Fabani, M.J. Gait, miR-122 targeting with LNA/2'-O-methyl oligonucleotide mixmers, peptide nucleic acids (PNA), and PNA, peptide conjugates, RNA, 14 (2008) 336-346.

[68] R. Kole, A.R. Krainer, S. Altman, RNA therapeutics: beyond RNA interference and antisense oligonucleotides, Nat Rev Drug Discov, 11 (2012) 125-140.

[69] R.L. Juliano, X. Ming, O. Nakagawa, Cellular uptake and intracellular trafficking of antisense and siRNA oligonucleotides, Bioconjug Chem, 23 (2012) 147-157.

[70] T.B. Hansen, T.I. Jensen, B.H. Clausen, J.B. Bramsen, B. Finsen, C.K. Damgaard, J. Kjems, Natural RNA circles function as efficient microRNA sponges, Nature, 495 (2013) 384-388.

[71] L. Ma, J. Young, H. Prabhala, E. Pan, P. Mestdagh, D. Muth, J. Teruya-Feldstein, F. Reinhardt, T.T. Onder, S. Valastyan, F. Westermann, F. Speleman, J. Vandesompele, R.A. Weinberg, miR-9, a MYC/MYCN-activated microRNA, regulates E-cadherin and cancer metastasis, Nat Cell Biol, 12 (2010) 247-256.

[72] R. Garzon, G. Marcucci, C.M. Croce, Targeting microRNAs in cancer: rationale, strategies and challenges, Nat Rev Drug Discov, 9 (2010) 775-789.

[73] W.Y. Choi, A.J. Giraldez, A.F. Schier, Target protectors reveal dampening and balancing of Nodal agonist and antagonist by miR-430, Science, 318 (2007) 271-274.

[74] A.G. Bader, D. Brown, J. Stoudemire, P. Lammers, Developing therapeutic microRNAs for cancer, Gene Ther, 18 (2011) 1121-1126.

[75] D. Li, X. Liu, L. Lin, J. Hou, N. Li, C. Wang, P. Wang, Q. Zhang, P. Zhang, W. Zhou, Z. Wang, G. Ding, S.M. Zhuang, L. Zheng, W. Tao, X. Cao, MicroRNA-99a inhibits hepatocellular carcinoma growth and correlates with prognosis of patients with hepatocellular carcinoma, The Journal of biological chemistry, 286 (2011) 36677-36685.

[76] K. Terasawa, K. Shimizu, G. Tsujimoto, Synthetic Pre-miRNA-Based shRNA as Potent RNAi Triggers, J Nucleic Acids, 2011 (2011) 131579.

[77] Y. Wu, M. Crawford, B. Yu, Y. Mao, S.P. Nana-Sinkam, L.J. Lee, MicroRNA Delivery by Cationic Lipoplexes for Lung Cancer Therapy, Molecular Pharmaceutics, 8 (2011) 1381-1389.

[78] P. Trang, J.F. Wiggins, C.L. Daige, C. Cho, M. Omotola, D. Brown, J.B. Weidhaas, A.G. Bader, F.J. Slack, Systemic Delivery of Tumor Suppressor microRNA Mimics Using a Neutral Lipid Emulsion Inhibits Lung Tumors in Mice, Mol Ther, 19 (2011) 1116-1122.

[79] Y. Akao, Y. Nakagawa, I. Hirata, A. Iio, T. Itoh, K. Kojima, R. Nakashima, Y. Kitade, T. Naoe, Role of anti-oncomirs miR-143 and -145 in human colorectal tumors, Cancer Gene Ther, 17 (2010) 398-408.

[80] A. Akinc, A. Zumbuehl, M. Goldberg, E.S. Leshchiner, V. Busini, N. Hossain, S.A. Bacallado, D.N. Nguyen, J. Fuller, R. Alvarez, A. Borodovsky, T. Borland, R. Constien, A. de Fougerolles, J.R. Dorkin, K.N. Jayaprakash, M. Jayaraman, M. John, V. Koteliansky, M. Manoharan, L. Nechev, J. Qin, T. Racie, D. Raitcheva, K.G. Rajeev, D.W.Y. Sah, J. Soutschek, I. Toudjarska, H.-P. Vornlocher, T.S. Zimmermann, R. Langer, D.G. Anderson, A combinatorial library of lipid-like materials for delivery of RNAi therapeutics, Nature Biotechnology, 26 (2008) 561-569.

[81] L. Piao, M. Zhang, J. Datta, X. Xie, T. Su, H. Li, T.N. Teknos, Q. Pan, Lipid-based Nanoparticle Delivery of Pre-miR-107 Inhibits the Tumorigenicity of Head and Neck Squamous Cell Carcinoma, Molecular Therapy, 20 (2012) 1261-1269.

[82] Y. Chen, X. Zhu, X. Zhang, B. Liu, L. Huang, Nanoparticles modified with tumor-targeting scFv deliver siRNA and miRNA for cancer therapy, Mol Ther, 18 (2010) 1650-1656.

[83] X.Q. Liu, W.J. Song, T.M. Sun, P.Z. Zhang, J. Wang, Targeted delivery of antisense inhibitor of miRNA for antiangiogenesis therapy using cRGD-functionalized nanoparticles, Molecular Pharmaceutics, 8 (2011) 250-259.

[84] J. Su, H. Baigude, J. McCarroll, T.M. Rana, Silencing microRNA by interfering nanoparticles in mice, Nucleic acids research, 39 (2011) e38.

[85] H. Ando, T. Asai, H. Koide, A. Okamoto, N. Maeda, K. Tomita, T. Dewa, T. Minamino, N. Oku, Advanced cancer therapy by integrative antitumor actions via systemic administration of miR-499, J Control Release, 181 (2014) 32-39.

[86] A.F. Ibrahim, U. Weirauch, M. Thomas, A. Grunweller, R.K. Hartmann, A. Aigner, MicroRNA Replacement Therapy for miR-145 and miR-33a Is Efficacious in a Model of Colon Carcinoma, Cancer Research, 71 (2011) 5214-5224.

[87] G.Y. Chiou, J.Y. Cherng, H.S. Hsu, M.L. Wang, C.M. Tsai, K.H. Lu, Y. Chien, S.C. Hung, Y.W. Chen, C.I. Wong, L.M. Tseng, P.I. Huang, C.C. Yu, W.H. Hsu, S.H. Chiou, Cationic polyurethanes-short branch PEI-mediated delivery of Mir145 inhibited epithelial-

mesenchymal transdifferentiation and cancer stem-like properties and in lung adenocarcinoma, Journal of Controlled Release, 159 (2012) 240-250.

[88] W. Hwang do, S. Son, J. Jang, H. Youn, S. Lee, D. Lee, Y.S. Lee, J.M. Jeong, W.J. Kim, D.S. Lee, A brain-targeted rabies virus glycoprotein-disulfide linked PEI nanocarrier for delivery of neurogenic microRNA, Biomaterials, 32 (2011) 4968-4975.

[89] Y. Ren, X. Zhou, M. Mei, X.-B. Yuan, MicroRNA-21 inhibitor sensitizes human glioblastoma cells U251 (PTEN-mutant) and LN229 (PTEN-wild type) to taxol, BMC Cancer, 10 (2010) 27.

[90] Y. Ren, C.S. Kang, X.B. Yuan, X. Zhou, P. Xu, L. Han, G.X. Wang, Z. Jia, Y. Zhong, S. Yu, J. Sheng, P.Y. Pu, Co-delivery of as-miR-21 and 5-FU by poly(amidoamine) dendrimer attenuates human glioma cell growth in vitro, J Biomater Sci Polym Ed, 21 (2010) 303-314.

[91] X. Qian, L. Long, Z. Shi, C. Liu, M. Qiu, J. Sheng, P. Pu, X. Yuan, Y. Ren, C. Kang, Star-branched amphiphilic PLA-b-PDMAEMA copolymers for co-delivery of miR-21 inhibitor and doxorubicin to treat glioma, Biomaterials, 35 (2014) 2322-2335.

[92] C.J. Cheng, W.M. Saltzman, Polymer Nanoparticle-Mediated Delivery of MicroRNA Inhibition and Alternative Splicing, Molecular Pharmaceutics, 9 (2012) 1481-1488.

[93] I.A. Babar, C.J. Cheng, C.J. Booth, X. Liang, J.B. Weidhaas, W.M. Saltzman, F.J. Slack, Nanoparticle-based therapy in an in vivo microRNA-155 (miR-155)-dependent mouse model of lymphoma, Proc Natl Acad Sci U S A, (2012).

[94] A. Mittal, D. Chitkara, S.W. Behrman, R.I. Mahato, Efficacy of gemcitabine conjugated and miRNA-205 complexed micelles for treatment of advanced pancreatic cancer, Biomaterials, 35 (2014) 7077-7087.

[95] H. Tazawa, N. Tsuchiya, M. Izumiya, H. Nakagama, Tumor-suppressive miR-34a induces senescence-like growth arrest through modulation of the E2F pathway in human colon cancer cells, Proc Natl Acad Sci U S A, 104 (2007) 15472-15477.

[96] H. Matsuyama, H.I. Suzuki, H. Nishimori, M. Noguchi, T. Yao, N. Komatsu, H. Mano, K. Sugimoto, K. Miyazono, miR-135b mediates NPM-ALK-driven oncogenicity and renders IL-17-producing immunophenotype to anaplastic large cell lymphoma, Blood, 118 (2011) 6881-6892.

[97] F. Takeshita, L. Patrawala, M. Osaki, R.U. Takahashi, Y. Yamamoto, N. Kosaka, M. Kawamata, K. Kelnar, A.G. Bader, D. Brown, T. Ochiya, Systemic delivery of synthetic microRNA-16 inhibits the growth of metastatic prostate tumors via downregulation of multiple cell-cycle genes, Molecular therapy : the journal of the American Society of Gene Therapy, 18 (2010) 181-187.

[98] C.J. Cheng, R. Bahal, I.A. Babar, Z. Pincus, F. Barrera, C. Liu, A. Svoronos, D.T. Braddock, P.M. Glazer, D.M. Engelman, W.M. Saltzman, F.J. Slack, MicroRNA silencing for cancer therapy targeted to the tumour microenvironment, Nature, 518 (2015) 107-110.

[99] A. Tivnan, W.S. Orr, V. Gubala, R. Nooney, D.E. Williams, C. McDonagh, S. Prenter, H. Harvey, R. Domingo-Fernandez, I.M. Bray, O. Piskareva, C.Y. Ng, H.N. Lode, A.M. Davidoff, R.L. Stallings, Inhibition of Neuroblastoma Tumor Growth by Targeted Delivery of MicroRNA-34a Using Anti-Disialoganglioside GD(2) Coated Nanoparticles, PLoS One, 7 (2012) e38129.

[100] M.V. Yigit, S.K. Ghosh, M. Kumar, V. Petkova, A. Kavishwar, A. Moore, Z. Medarova, Context-dependent differences in miR-10b breast oncogenesis can be targeted for the prevention and arrest of lymph node metastasis, Oncogene, (2012).

[101] A.M. Krieg, Is RNAi dead?, Mol Ther, 19 (2011) 1001-1002.

[102] H. Ledford, Drug giants turn their backs on RNA interference, Nature, 468 (2010) 487.

[103] Santaris Pharma A/S, Miravirsen in Combination With Telaprevir and Ribavirin in Null Responder to Pegylated-Interferon Alpha Plus Ribavirin Subjects With Chronic Hepatitis C Virus Infection, in, Bethesda, MD: National Library of Medicine (US), ClinicalTrias.gov, 2013-.

[104] Santaris Pharma A/S, Drug Interaction Study to Assess the Effect of Co-Administered Miravirsen and Telaprevir in Healthy Subjects, in, Bethesda, MD: National Library of Medicine (US), ClinicalTrias.gov, 2012-2012.

[105] Santaris Pharma A/S, Miravirsen Study in Null Responder to Pegylated Interferon Alpha Plus Ribavirin Subjects With Chronic Hepatitis C, in, Bethesda, MD: National Library of Medicine (US), ClinicalTrias.gov, 2012-.

[106] Santaris Pharma A/S, Multiple Ascending Dose Study of Miravirsen in Treatment-Naïve Chronic Hepatitis C Subjects, in, Bethesda, MD: National Library of Medicine (US), ClinicalTrias.gov, 2010-2012.

[107] Santaris Pharma A/S, SPC3649 Multiple Dose Study in Healthy Volunteers, in, Bethesda, MD: National Library of Medicine (US), ClinicalTrias.gov, 2009-2011.

[108] Santaris Pharma A/S, Safety Study of SPC3649 in Healthy Men, in, Bethesda, MD: National Library of Medicine (US), ClinicalTrias.gov, 2008-2009.

[109] Mirna Therapeutics, Inc., A Phase I Study of MRX34 Given Intravenously in Patients With Unresectable Primary Liver Cancer or Metastatic Cancer With Liver Involvement, in, Bethesda, MD: National Library of Medicine (US), ClinicalTrials.gov, 2013-.

[110] C. Scholz, E. Wagner, Therapeutic plasmid DNA versus siRNA delivery: common and different tasks for synthetic carriers, J Control Release, 161 (2012) 554-565.

[111] J.B. Bramsen, M.B. Laursen, A.F. Nielsen, T.B. Hansen, C. Bus, N. Langkjaer, B.R. Babu, T. Hojland, M. Abramov, A. Van Aerschot, D. Odadzic, R. Smicius, J. Haas, C. Andree, J. Barman, M. Wenska, P. Srivastava, C. Zhou, D. Honcharenko, S. Hess, E. Muller, G.V. Bobkov, S.N. Mikhailov, E. Fava, T.F. Meyer, J. Chattopadhyaya, M. Zerial, J.W. Engels, P. Herdewijn, J. Wengel, J. Kjems, A large-scale chemical modification screen identifies design rules to generate siRNAs with high activity, high stability and low toxicity, Nucleic acids research, 37 (2009) 2867-2881.

[112] Y.H. Bae, K. Park, Targeted drug delivery to tumors: myths, reality and possibility, Journal of Controlled Release, 153 (2011) 198-205.

[113] A.A. Khan, D. Betel, M.L. Miller, C. Sander, C.S. Leslie, D.S. Marks, Transfection of small RNAs globally perturbs gene regulation by endogenous microRNAs, Nat Biotech, 27 (2009) 549-555.

[114] D. Grimm, K.L. Streetz, C.L. Jopling, T.A. Storm, K. Pandey, C.R. Davis, P. Marion, F. Salazar, M.A. Kay, Fatality in mice due to oversaturation of cellular microRNA/short hairpin RNA pathways, Nature, 441 (2006) 537-541.

[115] Y. Murakami, H. Toyoda, M. Tanaka, M. Kuroda, Y. Harada, F. Matsuda, A. Tajima, N. Kosaka, T. Ochiya, K. Shimotohno, The progression of liver fibrosis is related with overexpression of the miR-199 and 200 families, PLoS One, 6 (2011) e16081.

[116] E.M. Small, R.J. Frost, E.N. Olson, MicroRNAs add a new dimension to cardiovascular disease, Circulation, 121 (2010) 1022-1032.

[117] S. Das, K. Bryan, P.G. Buckley, O. Piskareva, I.M. Bray, N. Foley, J. Ryan, J. Lynch, L. Creevey, J. Fay, S. Prenter, J. Koster, P. van Sluis, R. Versteeg, A. Eggert, J.H. Schulte, A. Schramm, P. Mestdagh, J. Vandesompele, F. Speleman, R.L. Stallings, Modulation of neuroblastoma disease pathogenesis by an extensive network of epigenetically regulated microRNAs, Oncogene, (2012).

[118] A.J. Bridge, S. Pebernard, A. Ducraux, A.L. Nicoulaz, R. Iggo, Induction of an interferon response by RNAi vectors in mammalian cells, Nat. Genet., 34 (2003) 263-264.

[119] V. Hornung, M. Guenthner-Biller, C. Bourquin, A. Ablasser, M. Schlee, S. Uematsu, A. Noronha, M. Manoharan, S. Akira, A. de Fougerolles, S. Endres, G. Hartmann,

Sequence-specific potent induction of IFN-alpha by short interfering RNA in plasmacytoid dendritic cells through TLR7, Nat. Med., 11 (2005) 263-270.

[120] A.D. Judge, V. Sood, J.R. Shaw, D. Fang, K. McClintock, I. MacLachlan, Sequence-dependent stimulation of the mammalian innate immune response by synthetic siRNA, Nat. Biotechnol., 23 (2005) 457-462.

[121] C.A. Sledz, M. Holko, M.J. de Veer, R.H. Silverman, B.R. Williams, Activation of the interferon system by short-interfering RNAs, Nat. Cell Biol., 5 (2003) 834-839.

[122] J. Lu, Targeted liposomal drug delivery for the treatment of pain and opioid addiction, in, University of Illinois at Chicago, Ann Arbor, 2008, pp. 215.

[123] X. He, M. Pool, K.M. Darcy, S.B. Lim, N. Auersperg, J.S. Coon, W.T. Beck, Knockdown of polypyrimidine tract-binding protein suppresses ovarian tumor cell growth and invasiveness in vitro, Oncogene, 26 (2007) 4961-4968.

[124] S.T. Ong, F. Li, J. Du, Y.W. Tan, S. Wang, Hybrid cytomegalovirus enhancer-h1 promoter-based plasmid and baculovirus vectors mediate effective RNA interference, Hum. Gene Ther., 16 (2005) 1404-1412.

[125] S. Samakoglu, L. Lisowski, T. Budak-Alpdogan, Y. Usachenko, S. Acuto, R. Di Marzo, A. Maggio, P. Zhu, J.F. Tisdale, I. Riviere, M. Sadelain, A genetic strategy to treat sickle cell anemia by coregulating globin transgene expression and RNA interference, Nat. Biotechnol., 24 (2006) 89-94.

[126] S. Xiang, J. Fruehauf, C.J. Li, Short hairpin RNA-expressing bacteria elicit RNA interference in mammals, Nat. Biotechnol., 24 (2006) 697-702.

[127] D.C. Forbes, N.A. Peppas, Oral delivery of small RNA and DNA, J Control Release, 162 (2012) 438-445.

[128] E. Vives, J. Schmidt, A. Pelegrin, Cell-penetrating and cell-targeting peptides in drug delivery, Biochim Biophys Acta, 1786 (2008) 126-138.

[129] C.-K. Chen, Biodegradable Polymeric Materials for Gene and Drug Delivery, in, State University of New York at Buffalo, Ann Arbor, 2013, pp. 249.

2 Arginine-rich, Cell Penetrating Peptide–anti-microRNA Complexes Decrease Glioblastoma Migration Potential

2.1 Abstract

MicroRNAs (miRNAs) are a class of gene regulators originating from non-coding endogenous RNAs. Altered expression, both up- and down-regulation, of miRNAs plays important roles in many human diseases. Correcting miRNA dysregulation by either inhibiting or restoring miRNA function may provide therapeutic benefit. One of the most effective approaches to suppress upregulated miRNAs is single stranded anti-miRNAs. Cell penetrating peptides (CPPs) have been applied for double stranded siRNA delivery. However, to our knowledge, few have examined CPP transfection efficiency with single stranded anti-miRNAs. For the first time, we compare R_8-mediated delivery efficiency of single stranded anti-miRNA and double stranded siRNA. The R_8 peptide condensed both siRNA and anti-miRNA. Greater than 50% of cells had anti-miRNA/R_8 complexes associated and in these cells 68% of anti-miRNA escapes the endosome/lysosome. Single-

* Reproduced with permission from: Y Zhang, M Köllmer, JS Buhrman, MY Tang, RA Gemeinhart. Peptides, 2014, 58:83-90.

stranded antisense miR-21 inhibitor (anti-miR-

21) administered using the R_8 peptide elicited efficient downstream gene upregulation. Glioblastoma cell migration was inhibited by 25% compared to the negative control group. To our knowledge, this is the first demonstration of miRNA modulation with anti-miR-21/R_8 complexes, which has laid the groundwork for further exploring octaarginine as intracellular anti-miRNAs carrier.

2.2 Introduction

Glioblastoma multiforme (GBM) is a fatal brain tumor with an annual incidence of approximately 5 in 100,000 people, equivalent to 17,000 new diagnoses per year [1]. The deadly threat posed by GBM resides in the explosive growth characteristics, extremely invasive behavior, difficulty in treatment due to the blood-brain barrier, and intrinsic resistance to current therapies [2]. The current standard treatment for glioblastoma is surgery and radiotherapy combined with temozolomide. This approach doubles the 2-year survival rate to 27%, but overall prognosis remains poor [1]. New therapies that provide highly specific treatment based on disease pathology characteristics are urgently needed.

One possible new therapeutic option for GBM is microRNA (miRNA) therapy. MiRNAs are short noncoding RNAs that post-transcriptionally regulate gene expression of multiple target genes through seed pairing with 3′ untranslated region (UTR) of mRNA. By binding to the 3′ UTR as part of the miRISC complex, miRNAs block mRNA translation and lead to mRNA degradation [3-5]. MiRNAs play a causative role in the development of cancer [6]. Depending upon the specific miRNA, a gain or a loss of miRNA can occur in the tumor compared to normal tissue [7, 8].

Recently, the delivery of miRNA mimics to supplement lost miRNAs and anti-miRNAs to block elevated miRNAs has attracted enormous attention as new cancer therapies [9-11]. Some view miRNAs as the new "beacon of hope" for cancer patients [1, 12]. A recent analysis on clinical patient samples showed that miR-21 is consistently overexpressed in glioblastoma tumor cells, but not in adjacent normal brain parenchyma, and the miR-21 levels correlated significantly with the grade of glioma [13].

MiR-21 targets key matrix metalloproteinases (MMPs) regulators, promoting glioma invasiveness [14]. MiRNA-21 has also been shown to function as an oncogenic miRNA in glioblastoma through modulating a network of key tumor-suppressive pathways in glioblastoma cells [14-17]. Therefore, a new therapy targeting miR-21 could potentially slow glioma progression and kill the tumor cells. Due to the poor cellular uptake characteristics of polyanionic oligonucleotides, a formulation that can mediate sufficient cellular uptake is needed to achieve efficient miR-21 knockdown. In addition, minimizing toxicity associated with most cationic carriers for gene delivery, such as PEI and dendrimers, is paramount to achieve a clinical delivery system for miRNA [18].

One possible component of a clinical delivery system is one of several classes of cell penetrating peptides. Cell penetrating peptides are small peptides (6 to 30 amino acid residues) that have membrane translocation activity. They constitute an important category of transfection reagent due to their low toxicity and low immunogenicity [19]. Arginine-rich peptides are one of the most investigated categories of CPPs, and include TAT,

protamine and oligoarginine [20]. In particular, the guanidinium groups on arginine are efficient at mediating cellular entry while maintaining low cytotoxicity [21].

Aiming to lower the miR-21 level in glioblastoma, we set out to use octaarginine (R_8) to form complexes with single stranded anti-miR-21. Single stranded anti-miRNAs hybridize with mature miRNAs in the cytoplasm and prevent the miRNAs from recognizing their mRNA targets [22, 23]. Double stranded siRNA has been delivered using TAT and R_9 [24, 25]; however, little is known concerning the differences between double stranded siRNA and single stranded anti-miRNA influence interaction with CPPs. To this end, we sought to investigate the interactions of single stranded anti-miRNA with arginine-rich cell penetrating peptide. Further, we sought to examine anti-miR-21/R_8 complex efficiency of gene silencing and inhibiting glioblastoma cell migration. Given the high fatality rate of glioblastoma multiforme, an anti-miR-21/R_8 formulation with low toxicity could be easily administered by intracranial infusion to brain tumor patients or in the tumor void as a post-operative treatment after resection surgery suggesting that miRNA/R_8 complexes hold potential.

2.3 Materials and Methods

2.3.1 Materials

Acetyl-RRRRRRRR-amide (R_8) was synthesized by UIC research supply center. MirVana™ miRNA-21 inhibitor (sequence:), miRNA inhibitor negative control #1, and Silencer® siRNA negative control #1 were purchased from Ambion (Austin, TX). Cy3-labeled anti-miRNA, Cy3-labeled siRNA and LysoTracker yellow HCK-123 were obtained from Invitrogen. Human glioblastoma U251 cell line was received from Dr. Lena Al-Harthi (Rush University). The cell line was maintained in Dulbecco's modified Eagle's medium (DMEM; Gibco) supplemented with 10% fetal bovine serum (FBS), 1% nonessential amino acids, 1 mM sodium pyruvate, 100 U/mL penicillin, and 100 U/mL streptomycin. Cells were incubated at 37 °C in humidified air and 5% CO_2.

2.3.2 Preparation and characterization of complexes

The anti-miRNA/R_8 or siRNA/R_8 was prepared by combining equal volumes of RNA and peptide in PBS to make complexes at varying positive to negative (+/-) charge ratios, vortexed for 15 sec, and then incubated at room temperature for 20 min before use. The

successful formation of anti-miR-21/R_8 or siRNA/R_8 complexes was confirmed by a gel shift assay. Complexes were prepared by mixing single stranded anti-miRNA or double stranded siRNA (100 pmol) and R_8 at predetermined positive to negative (+/-) charge ratios in RNase free phosphate buffered saline (PBS) and incubated for 20 minutes at 25°C. The resulting solutions were analyzed by electrophoresis using a 20% non-denaturing acrylamide gel for 1 h at 100 V in 1× TBE buffer (89 mM Tris-borate, 2 mM EDTA). Following ethidium bromide (0.5 μg/mL) staining, the gel was visualized using a gel documentation system (GelDoc 2000, Bio-Rad, Hercules, CA). The size distribution and zeta potential of the complexes were measured using a Nicomp 380 Zeta Potential/Particle Sizer in RNAse free water (Particle Sizing Systems, Santa Barbara, CA).

2.3.3 Fluorescence quenching

The fluorescence quenching assay was conducted as previously reported [23]. Briefly, 60 pmol of Cy3-labeled anti-miRNA or Cy3-labeled siRNA was complexed with R_8 at different charge ratios. Cy3-labeled anti-miRNA or Cy3-labeled siRNA without R_8 was used to normalize (100% uncondensed) the loss of fluorescence intensity due to

condensation. Pure R_8 solution of the highest concentration in experimental groups was used as negative control. The samples were incubated for 20 to 30 mins after mixing before being transferred to a Corning black 96 well plate and measured on BioTek Synergy 2 Multi-Mode Microplate Reader (Winooski, VT).

2.3.4 Cell association and uptake

To measure cell association and uptake, 2×10^5 cells were seeded in 12-well plate and incubated overnight. Complexes prepared at different charge ratios with the final anti-miRNA or siRNA concentration maintained constant at 100 nM were added to OPTI MEM medium to make the total media volume 1 mL prior to an addition incubation of 4 hours. Cells were then washed with cold PBS twice followed by trypsinization and centrifugation at 1500 rpm for 5 mins. The pellets were then washed twice with cold PBS and centrifugation before resuspending in 200 μL of 1% formaldehyde and analyzing on MoFlo Legacy cell sorter (Beckman Coulter, Brea, CA) at excitation 543 nm and emission 570 nm.

To further confirm cell internalization, U251 cells were seeded in Lab-Tek^{TM} 8-chambered coverglass (Nunc; Thermo Fisher Scientific, Skokie, IL) at 3×10^4 cells per chamber in 200 μL growth media 24 hours before an experiment. The medium was exchanged with OPTI MEM and complexes were applied to the chamber. Four hours later, cells were rinsed twice with PBS. The nuclei and endosomes were stained with Hoechst 33258 for 5 min and 50 nM LysoTracker yellow for 15 min before CLSM imaging. CLSM images were acquired using a Zeiss LSM 510 META (Carl Zeiss, Germany) with a water immersion 63× objective (C-Apochromat, Carl Zeiss). Excitation wavelengths were 405 nm (Diode 405), 488 nm (argon laser) and 543 nm (HeNe laser) for Hoechst 33258, LysoTracker, and Cy3, respectively. In order to obtain the 3D information of the endosome escape efficiency, 20 slices for 20 cells were obtained with CLSM Z-stack and 20 cells were counted as previously reported [26, 27]. The colocalization ratio between Cy3-labeled anti-miRNA or Cy3-labeled siRNA and endosome was measured with Mender's coefficient, M, using ImageJ, which calculates the percentage of red pixels (Cy3)

colocalizing with green pixels (lysoTracker) with an automatic threshold [28]. The endosome escape efficiency, $\mathcal{E}_{ee}$, was calculated, Equation 1.

$$\mathcal{E}_{ee} = (1 - \mathrm{M}) * 100\% \qquad \text{Equation 1}$$

2.3.5 Transfection

U251 cells were seeded in a 24-well plate at a density of 1.4×10^5 cells/cm^2 and cultivated with 1 mL of DMEM growth medium for 24 h until 60–70% confluent. The cells in each well were replaced with 250 µL OPTI MEM medium containing 27.5 µL of anti-miR-21/R_8 complexes solution (charge ratio = 50/1) with a final anti-miR-21 concentration is 55 nM. Four hours after transfection, media was replaced with fresh DMEM growth media.

2.3.6 Quantitative real-time PCR analysis

Total RNA was extracted using the TRIzol® reagent (Invitrogen) 24-hour post anti-miR-21/R_8 transfection. To maintain a constant RNA purity, PureLink™ RNA Mini Kit (Invitrogen) was used in combination with DNAse (Invitrogen) according to manufacturer's instructions. High Capacity cDNA Reverse Transcription Kit (Applied Biosystems) was used to reverse transcribe the purified RNA to cDNA. The PCR reactions

were performed on an Applied Biosystems StepOnePlus™ PCR machine. The PCR mixture was composed of 5 µL SYBR® Green PCR Master Mix (Applied Biosystems), 2 µL sequence specific primers (0.5 mM, final concentration) and 3 µL cDNA. The conditions for PCR reaction were previously reported [29]. Briefly, 95°C for 10 min followed by 40 cycles of 15 s of denaturation at 95ºC and 60 s of annealing and elongation at 60ºC. Primer sequences used in the PCR were as follows: Programmed cell death 4 (PDCD4) : 5'-CAGTTGGTGGGCCAGTTTATTG-3' (sense), 5'-AGAAGCACGGTAGCCTTATCCA-3' (antisense); Serpin peptidase inhibitor, clade B (ovalbumin), member 5 (SERPINB5) : 5'-ACAGTGGACTAATCCCAGCACCAT-3' (sense), 5'-ATTTGATAGGGCCACTCCCTTGGT-3'(anti-sense); Glyceraldehyde 3-phosphate dehydrogenase (GAPDH): 5'-TTC GAC AGT CAG CCG CAT CTT CTT-3'(sense), 5'-GCC CAA TAC GAC CAA ATC CGT TGA-3'(anti-sense). The relative gene expression level of the gene of interest was determined using delta-delta-Ct method normalized to the endogenous reference gene, GAPDH.

2.3.7 In vitro cell migration assay

The influence of anti-miR-21/R_8 transfection on cell migration potential was measured using a wound healing assay [30]. Cells were seeded and transfected as previously described. Twenty-four hour post transfection, a wounding area was made along the cell monolayer using a 200 µL pipette tip. Cells were carefully washed with pre-warmed PBS without dislodging the cell monolayer followed by further incubation in DMEM growth medium for another 48 hours until images were taken. Cell migration was determined, Equation 2, by the recovery ratio, P, of wound area at 48-hour post scratching, a_{48}, relative to the initial wound area, a_0.

$$P = \frac{(a_0 - a_{48})}{a_0} * 100\% \qquad \text{Equation 2}$$

2.3.8 Statistical analysis

Data were presented as the mean plus or minus (±) standard error of the mean (S.E.M.). Three independent replicates of each experiment were performed. Statistics was determined using Student's t-test or ANOVA using GraphPad Prism v.4.0 (GraphPad Software, San Diego, CA). Post hoc analysis was performed using Turkey's test when *p*-value was less

than 0.05. Statistical significance was expressed as $P<0.05$ (single symbol), $P<0.01$ (double symbol), and $P<0.001$ (triple symbol).

2.4 Results and Discussion

To compare the condensing capacity of R_8 for single stranded anti-miRNA and double stranded siRNA, a gel shift assay was conducted by mixing 100 pmol of anti-miRNA or siRNA with R_8 at different positive to negative charge ratios (+/-). The R_8 peptide successfully formed complexes with both anti-miRNA and siRNA. The mobility of siRNA was retarded at lower charge ratio (Figure 2.1A) suggesting that double stranded siRNA was more readily interacting with the peptide.

To investigate whether there is difference between the binding behavior of double stranded siRNA and that of single stranded anti-miRNA with R_8, we used dye quenching assay. The fluorescence intensity of fluorophore-labeled oligonucleotides is quenched by the close spatial proximity in complexes where many oligonucleotides are compacted. The trend of fluorescence quenching is the same between anti-miRNA/R_8 and siRNA/R_8. However, at higher charge ratios, from 4:1 to 10:1, the extent of fluorescence quenching is

greater with double stranded siRNA than with single stranded anti-miRNA, suggesting there may be tighter binding between siRNA and the R_8 peptide (Figure 2.1B). The particle size of siRNA/R_8 was larger than anti-miRNA/R_8 (Figure 2.1C) at all charge ratios tested, indicating that the structural differences between single stranded anti-miRNA and double stranded siRNA brought differences in complexes physical properties. These differences include the charge density, size, and flexibility of the RNA molecules. The siRNA is present as a double helix with twice the charge in a given area.

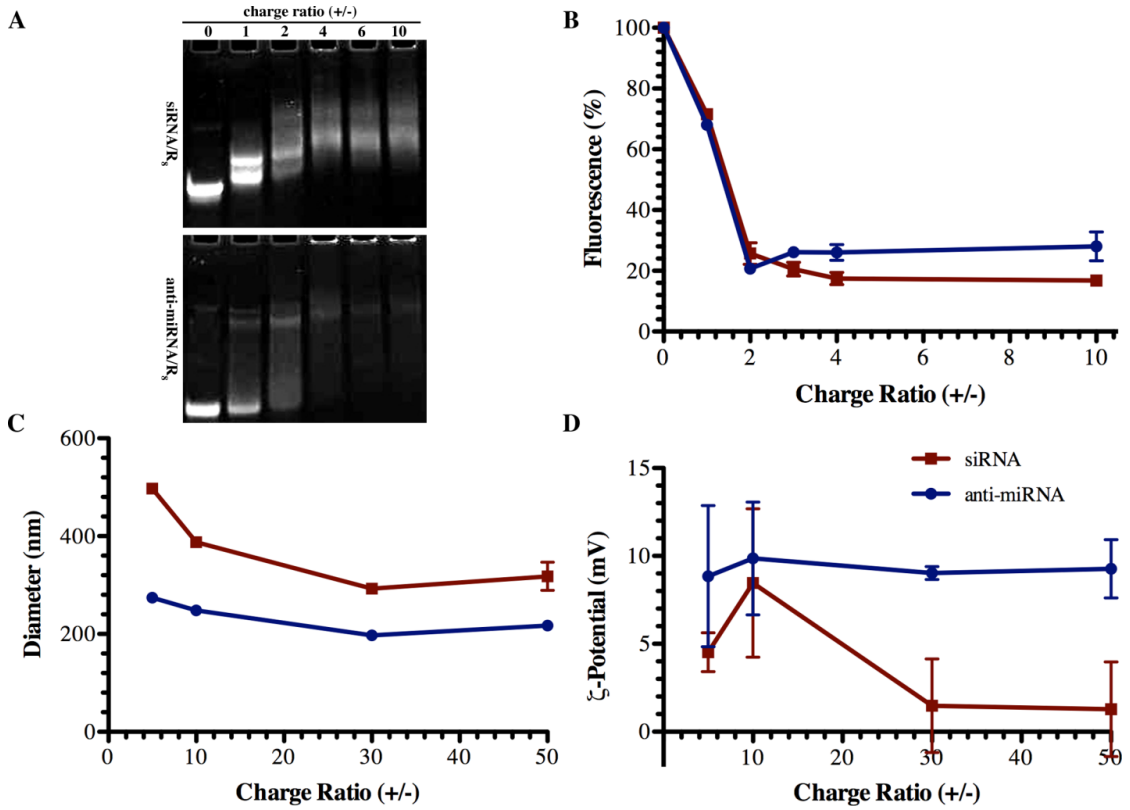

Figure 2.1. Physicochemical characterization of complexes. (A) Mobility of siRNA (upper panel) and anti-miRNA (lower panel) was retarded in the presence of R_8 peptide above a threshold charge (+/-) ratio. (B) Fluorescence was also quenched above a threshold charge (+/-) ratio, indicating double stranded siRNA (■) and single stranded anti-miRNA (◆) were condensed by the R_8 peptide (mean ± S.E.M., n=3). Similarly, R_8 complex (C) diameters and (D) ζ potential were measured by dynamic light scattering (mean ± S.E.M., n=3) for siRNA/R_8 complexes (■) and anti-miRNA/R_8 complexes (◆) further indicating complex formation at the given charge (+/-) ratios (mean ± S.E.M., n=3).

Cell association of siRNA/CPP complexes depends on the complex conformation [24].

MiRNA associated with cells in a dose-dependent manner (Figure 2.2). Given the

differences between the anti-miRNA/R_8 and siRNA/R_8 complexes, we compared the cell association efficiency of the two types of complexes using flow cytometry. SiRNA/R_8 associated with cells to a greater extent than anti-miRNA/R_8 at all of the charge ratios tested (Figure 2.2), confirming our hypothesis that the charge density and flexibility differences between single and double-stranded RNA have an influence on their cell association. It is worth to noting that there is no significant difference between the ζ potential of anti-miRNA/R_8 and siRNA/R_8, which were near neutral (Figure 2.1D).

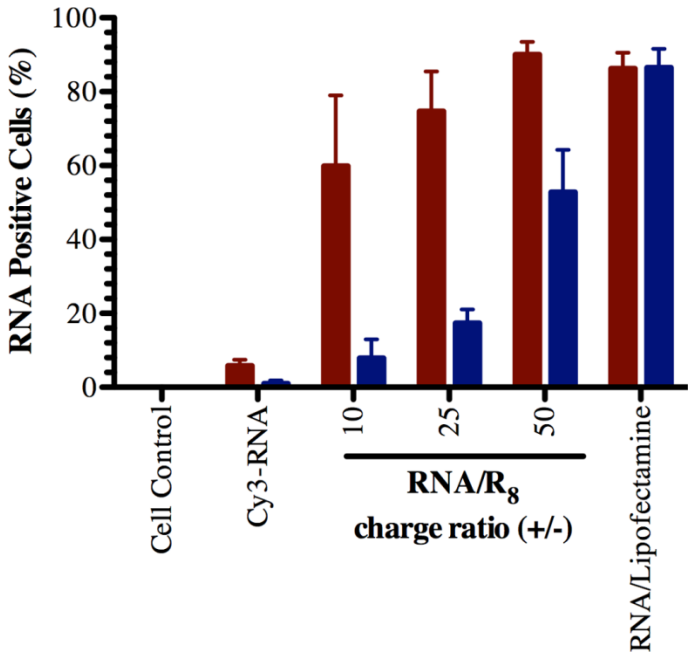

Figure 2.2. Cell association of RNA/R_8 complexes. Relative association of anti-miRNA/R_8 (blue bars) and siRNA/R_8 (red bars) with U251 glioblastoma cells after 4-hour interaction *in vitro* measured by flow cytometry (mean ± S.E.M., n=3).

To illustrate the cellular uptake of the complexes and not just surface association, we observed the presence of Cy3-labeled anti-miRNA/R_8 and Cy3-labeled siRNA/R_8 with confocal microscopy (Figure 2.3). The complexes showed punctate signal in the cytoplasm of the majority of cells. The punctate nature suggested endocytosis-mediated cellular uptake. Endocytosis and macropinocytosis have been reported as the main mechanisms for the cellular uptake of arginine-rich CPPs [31, 32]. Given the difference in cell association between anti-miRNA/R_8 and siRNA/R_8, we speculated that the differences in charge density and flexibility would also contribute to different interactions with the endosome, specifically escape and separation from the peptide.

We compared their endosome escape efficiency by obtaining the colocalization efficiency of Cy3-labeled anti-miRNA or Cy3-labeled siRNA with LysoTracker yellow stained endosomes. By determining the colocalization coefficient in every Z-stack slice, the endosome escape in the cytoplasm measured, while avoiding the bias of utilizing single slice. SiRNA/R_8 more efficiently escaped the endosomes compared to anti-miRNA/R_8, consistent with the cell association. However, we did not control for constant cell entry in

this experiment, *i.e*. the greater separation may be due to the greater amount of siRNA within the endosomes. This should be examined in more detail to better understand the influence of the properties of the complexes and their separation.

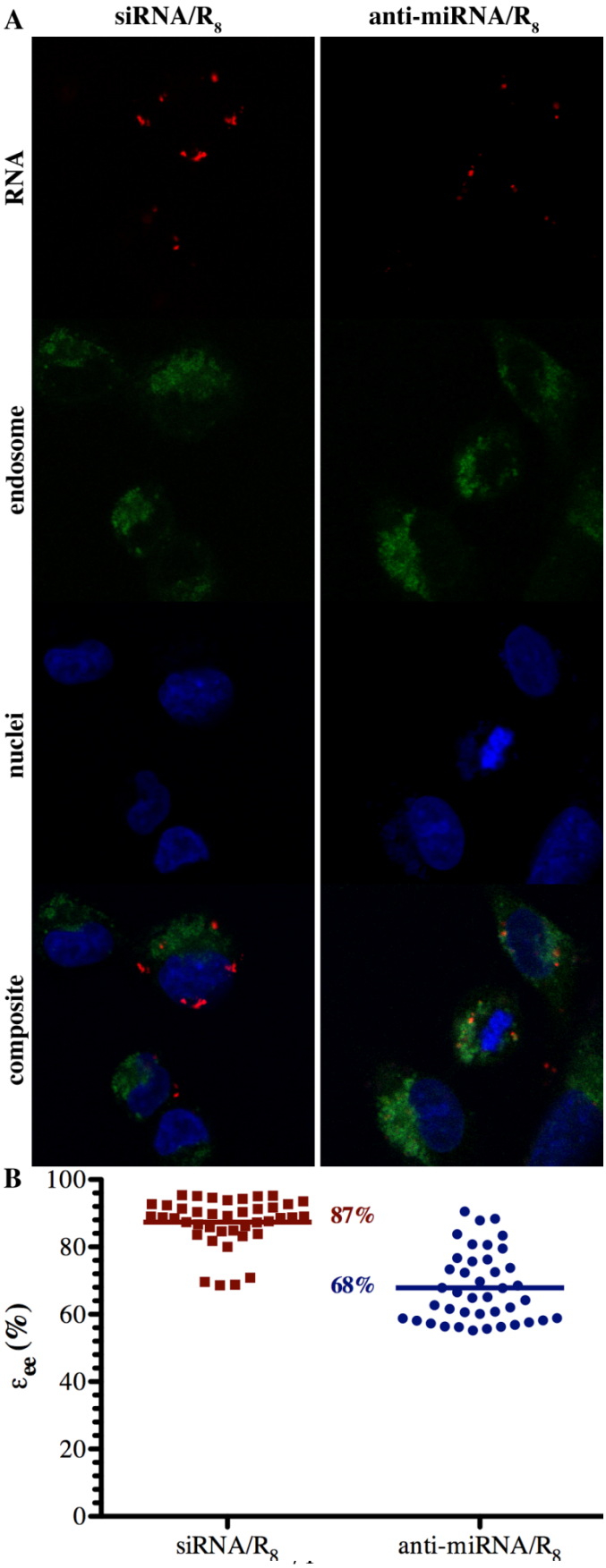
A
siRNA/R8
anti-miRNA/R8
RNA
endosome
nuclei
composite
B
100
80
60
40
20
0
εee (%)
87%
68%
siRNA/R8
anti-miRNA/R8

Figure 2.3. Evaluation of endosomal escape efficiencies of anti-miRNA/R_8 and siRNA/R_8. (A) Representative confocal micrographs of siRNA/R_8 (left) and anti-miRNA/R_8 (right) complex-endosome colocalization showing RNA (red), endosome (green), nuclei (blue), and the composite of the three pseudocolor images where the RNA concentration was 55 nM and mixed with R_8 at a charge ratio of 50. (B) Quantitative comparison of endosome escape efficiency, ε_{ee}, between anti-miRNA/R_8 and siRNA/R_8. Endosome escape efficiency was calculated for 20 random, individual cells ($p < 0.001$).

MiRNA acts as gene regulators by binding to the 3´ untranslated region of targeted mRNA. One miRNA regulates a network of genes because the targeting region is in the untranslated region of the mRNA, is present on many mRNA, and does not require perfect base pairing. Tumor suppressor genes, PDCD4 and SERPINB5, have been reported as being miR-21 suppressed genes [15, 33]. They are transcriptionally regulated by miR-21, specifically, when miR-21 is present, the mRNA of PDCD4 and SERPINB5 degraded. Indirect detection of miRNA activity was chosen due to incomplete miRNA degradation when using anti-miRNAs [11].

Based on our results with cell association and internalization, we observed the best miR-21 knockdown effect when preparing the complexes at charge ratio of 50 to 1 (+/-). As such, formula complexes at this charge ratio were examined. Both PDCD4 and SERPINB5

mRNA levels were significantly increased after anti-miR-21/R_8 transfection comparing with the control groups, indicating successful anti-miR-21 intracellular delivery mediated by R_8 (Figure 2.4).

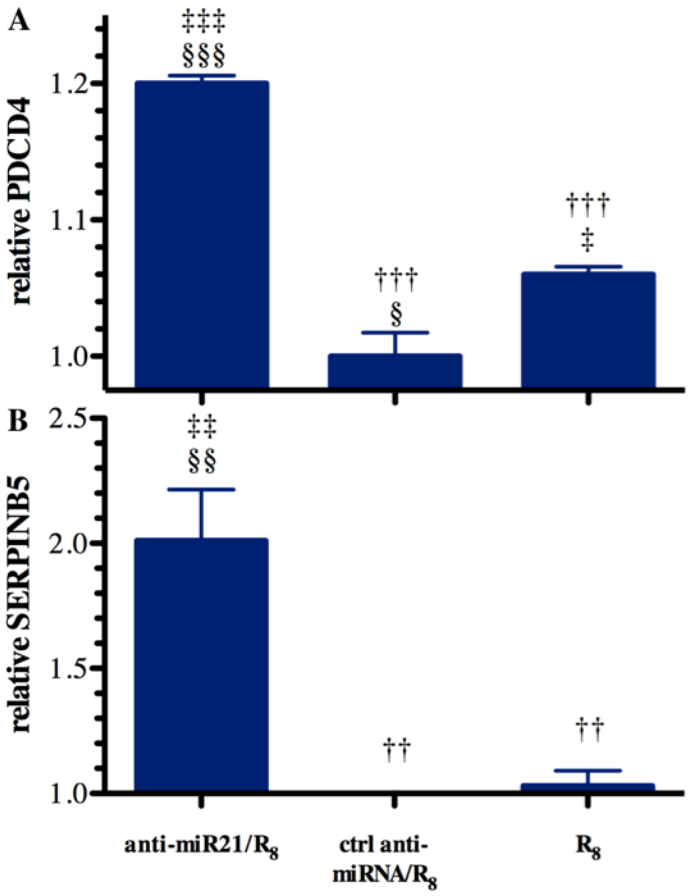

Figure 2.4. Indirect measurement of anti-miRNA activity by detecting the mRNA of downstream miR-21 targets. (A) PDCD4 and (B) SERPINB5 mRNA levels relative to GAPDH mRNA in cells treated with the R_8 peptide, control (ctrl) anti-miRNA/R_8 complexes, and anti-miRNA-21/R_8 complexes where the RNA concentration was 55 nM and mixed with R_8 at a charge ratio of 50 (mean±S.E.M.; n=3). Statistical significance compared to the anti-miRNA/R_8 group (†), ctrl anti-miRNA/R_8 group (‡), and R_8 treatment group (§) is presented as one ($0.01 < p < 0.05$), two ($0.001 < p < 0.01$), or three ($p < 0.001$) symbols.

The delivery of oligonucleotides in many circumstances is associated with cytotoxicity.

None of the complexes showed significant toxicity at the concentrations examined. (Figure

2.5) We, therefore, inferred that the change in mRNA levels were due to the inhibition of miRNA activity and not a result of cell death by some other mechanism. This was further confirmed by the use of the anti-miRNA control, which did not show a change in mRNA level.

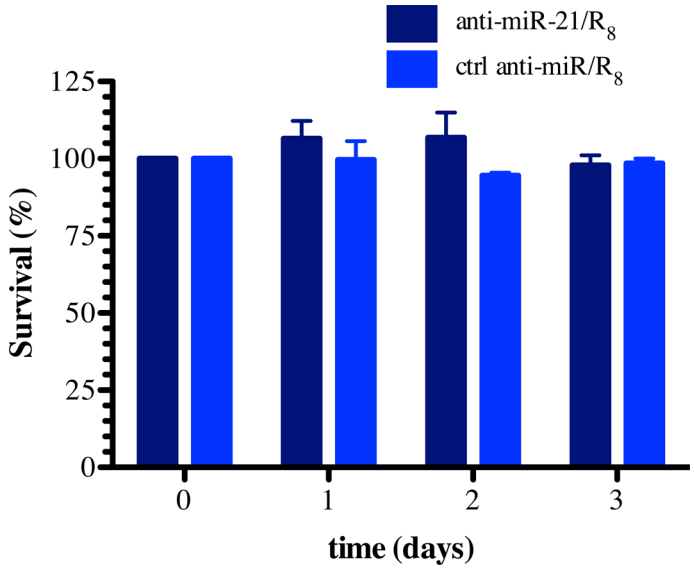

Figure 2.5. Relative U251 survival (mitochondrial activity). After incubation with the anti-miR21/R_8 complex (■) or control (ctrl) anti-miRNA/R_8 complex (■) for varying times (mean±S.E.M.; n=3).

The two selected miRNA-21 targeted genes, PDCD4 and SERPINB5, have also been reported to play inhibitory roles in cancer cell invasion and migration [34-36]. To examine the influence of knockdown of miR-21 by anti-miR-21/R_8 complexes on cell migration, we used a wound-healing assay. In monolayer cell culture, the recovery of wound area was

compared at 72-hour post transfection. The 72-hour time point was chosen based upon preliminary experiments to give sufficient time for anti-miR-21 exert effects on target mRNAs and subsequent proteins expression. Anti-miR-21/R_8 complexes significantly inhibited cell migration by 25% compared with the negative control treated group (Figure 2.6), indicating the amount of anti-miR-21 transfected is biological active.

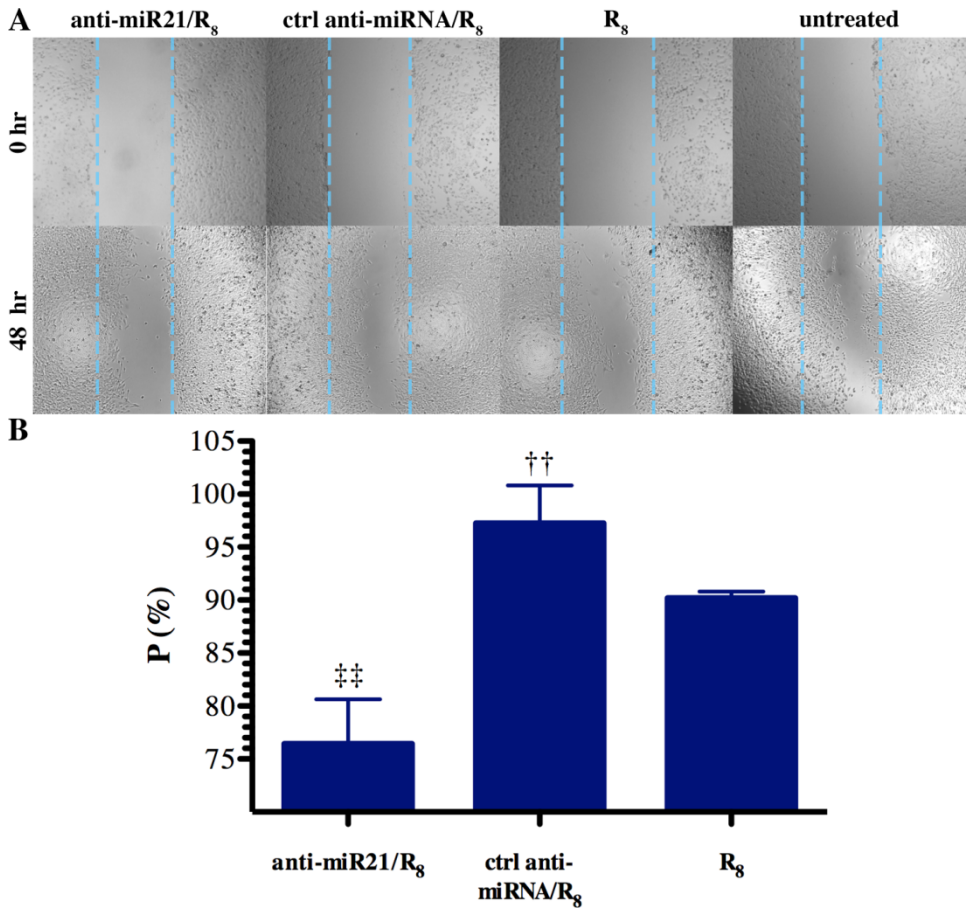

Figure 2.6. Inhibition of U251 cell migration after anti-miR-21/R_8 transfection. (A) Micrographs of U251 cells immediately after (0 hr) and 48 hours after wounding. (B) Wound recovery (P) measured 72 hours post transfection following treatment with R_8 peptide, ctrl anti-miRNA/R_8 complexes, or anti-miRNA-21/R_8 complexes where the RNA concentration was 55 nM and mixed with R_8 at a charge ratio of 50 (mean±S.E.M.; n=3) The wound recovery (P) of the three groups were normalized to the cell control group underwent wounding assay but no treatment. Statistical significance compared to the anti-miRNA/R_8 group (†) and control anti-miRNA/R_8 group (‡) treatment group is presented ($0.001 < p < 0.01$).

Within the last decade, the involvement of miRNA in human cancer oncogenesis and progression has become apparent [37]. Cancer is intimidating because of its

pharmacological complexity and constant development of resistance against therapy. MiRNAs act in accordance with our current understanding of cancer as a "pathway disease" that presumably can only be successfully treated when simultaneously intervening with multiple oncogenic pathways [10].

Even though double stranded siRNA and single stranded anti-miRNA are both seen as RNAi technology, their mechanisms are different. RNAi mediated by double stranded siRNA aims to target one gene at a time by knocking down a specific mRNA. The nascent siRNA associates with Dicer, TRBP, and Argonaute 2 (Ago2) to form the RNA-Induced Silencing Complex (RISC) [38]. Once in RISC, one strand of the siRNA (the passenger strand) is degraded or discarded while the other strand (the guide strand) remains to guide the cleavage of the target mRNA by Ago2, a ribonuclease. Anti-miRNAs sterically block miRNA function by hybridizing and repressing the activity of a mature miRNA whether it exists in single-stranded form, double-stranded form with the natural passenger strand or bound to an Argonaute protein in the miRNA induced silencing complex (miRISC) [22].

Due to this difference in mechanisms and differential effect on a given mRNA, it would be quite difficult and less meaningful to directly compare the gene knockdown efficiency of anti-miRNA/R_8 with siRNA/R_8. Thus, we examined the ability of the peptide to condense anti-miRNA and how the complexes interact with cells, but the knockdown efficiency was not directly compared. Arginine-rich CPPs have been used to deliver double stranded siRNA, but the delivery of single stranded anti-miRNA via arginine-rich CPP in noncovalent manner has never been described to our knowledge. Therefore, our successful delivery of single stranded anti-miRNAs achieving migration repression and gene knockdown is significant and shows therapeutic potential.

Single stranded anti-miRNA is a flexible oligonucleotide that could have many different conformations while double stranded siRNA exists in A-form double helix, the most stable form of RNA secondary structures [39]. Thermodynamically speaking, it will cost more energy to stabilize a system composed of single stranded anti-miRNA than double stranded siRNA. This might explain why R_8 is more efficient at condensing double stranded siRNA than single stranded anti-miRNA in gel shift assay and fluorescence quenching assay. On

the other hand, the rigid structure of double stranded siRNA functions as skeleton and forces R_8 to interact alongside the double helix conformation. Interestingly, this discrepancy leads to different cell association and endosome escape efficiency. It has been reported that the polyplexes formed by circular plasmid DNA/CPPs and siRNA/CPPs differ significantly in terms of physicochemical properties, cellular uptake and endosome escape due to their molecular weight and structure differences [40]. The dramatic difference between anti-miRNA/R_8 and siRNA/R_8 reported here advanced our understanding about the interaction between CPPs and oligonucleotides. Special consideration should be given to the application of single stranded anti-miRNAs transfection with CPPs.

In addition, oligoarginines can be tailored for the establishment of a wide variety of miRNAs therapeutics delivery system since they can be easily encapsulated into or conjugated with other polymeric carrier. Our group has previously reported a matrix metalloproteinases-2 responsive hydrogel drug delivery system aiming for glioblastoma, a great option to combine with the result reported here [41, 42]. Although we have not proceed to in vivo animal experiment yet, Kim et al has shown that HER-2-specific

siRNA/R_{15} complexes resulted in a marked reduction of SKOV-3 xenograft tumor growth in nude mice *in vivo* [43]. Further study is warranted to investigate the miRNA-21 silencing efficiency mediated by anti-miR-21/R_8 complexes *in vivo*.

2.5 Conclusion

For the first time, the difference between single stranded anti-miRNA/R_8 and double stranded siRNA/R_8 was understood by comparing their physicochemical property, cell association and endosome escape efficiency. Single stranded anti-miRNAs pose greater challenge for intracellular delivery via CPPs. In addition, effective *in vitro* miRNA-21 interference was achieved via anti-miR-21/R_8 complexes, resulting in significant inhibition on U251 cell migration, which warrants further exploration of oligoarginine as intracellular anti-miRNA carrier.

2.6 References

[1] A. Omuro, L.M. DeAngelis, Glioblastoma and other malignant gliomas: a clinical review, Jama, 310 (2013) 1842-1850.

[2] H. Zhu, J. Acquaviva, P. Ramachandran, A. Boskovitz, S. Woolfenden, R. Pfannl, R.T. Bronson, J.W. Chen, R. Weissleder, D.E. Housman, A. Charest, Oncogenic EGFR signaling cooperates with loss of tumor suppressor gene functions in gliomagenesis, Proc Natl Acad Sci U S A, 106 (2009) 2712-2716.

[3] D. Baek, J. Villen, C. Shin, F.D. Camargo, S.P. Gygi, D.P. Bartel, The impact of microRNAs on protein output, Nature, 455 (2008) 64-71.

[4] D.P. Bartel, MicroRNAs: genomics, biogenesis, mechanism, and function, Cell, 116 (2004) 281-297.

[5] J.J. Forman, A. Legesse-Miller, H.A. Coller, A search for conserved sequences in coding regions reveals that the let-7 microRNA targets Dicer within its coding sequence, Proc Natl Acad Sci U S A, 105 (2008) 14879-14884.

[6] S. Zadran, F. Remacle, R.D. Levine, miRNA and mRNA cancer signatures determined by analysis of expression levels in large cohorts of patients, Proc Natl Acad Sci U S A, 110 (2013) 19160-19165.

[7] A. Esquela-Kerscher, F.J. Slack, Oncomirs - microRNAs with a role in cancer, Nat Rev Cancer, 6 (2006) 259-269.

[8] G.A. Calin, C.M. Croce, MicroRNA signatures in human cancers, Nat Rev Cancer, 6 (2006) 857-866.

[9] Y. Zhang, Z. Wang, R.A. Gemeinhart, Progress in microRNA delivery, J Control Release, 172 (2013) 962-974.

[10] A.G. Bader, D. Brown, M. Winkler, The promise of microRNA replacement therapy, Cancer Res, 70 (2010) 7027-7030.

[11] J. Stenvang, A. Petri, M. Lindow, S. Obad, S. Kauppinen, Inhibition of microRNA function by antimiR oligonucleotides, Silence, 3 (2012) 1.

[12] A. Bhardwaj, S. Singh, A.P. Singh, MicroRNA-based Cancer Therapeutics: Big Hope from Small RNAs, Mol Cell Pharmacol, 2 (2010) 213-219.

[13] S.K. Hermansen, R.H. Dahlrot, B.S. Nielsen, S. Hansen, B.W. Kristensen, MiR-21 expression in the tumor cell compartment holds unfavorable prognostic value in gliomas, J Neurooncol, 111 (2013) 71-81.

[14] G. Gabriely, T. Wurdinger, S. Kesari, C.C. Esau, J. Burchard, P.S. Linsley, A.M. Krichevsky, MicroRNA 21 promotes glioma invasion by targeting matrix metalloproteinase regulators, Mol Cell Biol, 28 (2008) 5369-5380.

[15] T. Papagiannakopoulos, A. Shapiro, K.S. Kosik, MicroRNA-21 targets a network of key tumor-suppressive pathways in glioblastoma cells, Cancer Res, 68 (2008) 8164-8172.

[16] L.M. Moore, W. Zhang, Targeting miR-21 in glioma: a small RNA with big potential, Expert opinion on therapeutic targets, 14 (2010) 1247-1257.

[17] J.A. Chan, A.M. Krichevsky, K.S. Kosik, MicroRNA-21 is an antiapoptotic factor in human glioblastoma cells, Cancer Res, 65 (2005) 6029-6033.

[18] Y.J. Choi, S.J. Kang, Y.J. Kim, Y.B. Lim, H.W. Chung, Comparative studies on the genotoxicity and cytotoxicity of polymeric gene carriers polyethylenimine (PEI) and polyamidoamine (PAMAM) dendrimer in Jurkat T-cells, Drug and chemical toxicology, 33 (2010) 357-366.

[19] K.M. Wagstaff, D.A. Jans, Protein transduction: cell penetrating peptides and their therapeutic applications, Current medicinal chemistry, 13 (2006) 1371-1387.

[20] E. Vives, P. Brodin, B. Lebleu, A truncated HIV-1 Tat protein basic domain rapidly translocates through the plasma membrane and accumulates in the cell nucleus, J Biol Chem, 272 (1997) 16010-16017.

[21] E.I. Geihe, C.B. Cooley, J.R. Simon, M.K. Kiesewetter, J.A. Edward, R.P. Hickerson, R.L. Kaspar, J.L. Hedrick, R.M. Waymouth, P.A. Wender, Designed guanidinium-rich amphipathic oligocarbonate molecular transporters complex, deliver and release siRNA in cells, Proc Natl Acad Sci U S A, 109 (2012) 13171-13176.

[22] K.A. Lennox, R. Owczarzy, D.M. Thomas, J.A. Walder, M.A. Behlke, Improved Performance of Anti-miRNA Oligonucleotides Using a Novel Non-Nucleotide Modifier, Molecular therapy. Nucleic acids, 2 (2013) e117.

[23] M. Zheng, G.M. Pavan, M. Neeb, A.K. Schaper, A. Danani, G. Klebe, O.M. Merkel, T. Kissel, Targeting the blind spot of polycationic nanocarrier-based siRNA delivery, ACS Nano, 6 (2012) 9447-9454.

[24] A.H. van Asbeck, A. Beyerle, H. McNeill, P.H. Bovee-Geurts, S. Lindberg, W.P. Verdurmen, M. Hallbrink, U. Langel, O. Heidenreich, R. Brock, Molecular parameters of

siRNA--cell penetrating peptide nanocomplexes for efficient cellular delivery, ACS Nano, 7 (2013) 3797-3807.

[25] A. Eguchi, S.F. Dowdy, siRNA delivery using peptide transduction domains, Trends in pharmacological sciences, 30 (2009) 341-345.

[26] A. El-Sayed, I.A. Khalil, K. Kogure, S. Futaki, H. Harashima, Octaarginine- and octalysine-modified nanoparticles have different modes of endosomal escape, The Journal of biological chemistry, 283 (2008) 23450-23461.

[27] H. Akita, R. Ito, I.A. Khalil, S. Futaki, H. Harashima, Quantitative three-dimensional analysis of the intracellular trafficking of plasmid DNA transfected by a nonviral gene delivery system using confocal laser scanning microscopy, Molecular therapy : the journal of the American Society of Gene Therapy, 9 (2004) 443-451.

[28] S. Bolte, F.P. Cordelieres, A guided tour into subcellular colocalization analysis in light microscopy, J Microsc, 224 (2006) 213-232.

[29] M. Kollmer, V. Keskar, T.G. Hauk, J.M. Collins, B. Russell, R.A. Gemeinhart, Stem cell-derived extracellular matrix enables survival and multilineage differentiation within superporous hydrogels, Biomacromolecules, 13 (2012) 963-973.

[30] M.G. Lampugnani, Cell migration into a wounded area in vitro.

[31] I. Nakase, M. Niwa, T. Takeuchi, K. Sonomura, N. Kawabata, Y. Koike, M. Takehashi, S. Tanaka, K. Ueda, J.C. Simpson, A.T. Jones, Y. Sugiura, S. Futaki, Cellular uptake of arginine-rich peptides: roles for macropinocytosis and actin rearrangement, Molecular therapy : the journal of the American Society of Gene Therapy, 10 (2004) 1011-1022.

[32] I. Nakase, T. Takeuchi, G. Tanaka, S. Futaki, Methodological and cellular aspects that govern the internalization mechanisms of arginine-rich cell-penetrating peptides, Adv Drug Deliv Rev, 60 (2008) 598-607.

[33] A.B. Gaur, S.L. Holbeck, N.H. Colburn, M.A. Israel, Downregulation of Pdcd4 by mir-21 facilitates glioblastoma proliferation in vivo, Neuro Oncol, 13 (2011) 580-590.

[34] R.H. Chou, H.C. Wen, W.G. Liang, S.C. Lin, H.W. Yuan, C.W. Wu, W.S. Chang, Suppression of the invasion and migration of cancer cells by SERPINB family genes and their derived peptides, Oncol Rep, 27 (2012) 238-245.

[35] I.A. Asangani, S.A. Rasheed, D.A. Nikolova, J.H. Leupold, N.H. Colburn, S. Post, H. Allgayer, MicroRNA-21 (miR-21) post-transcriptionally downregulates tumor suppressor Pdcd4 and stimulates invasion, intravasation and metastasis in colorectal cancer, Oncogene, 27 (2008) 2128-2136.

[36] H.Y. Shi, L.J. Stafford, Z. Liu, M. Liu, M. Zhang, Maspin controls mammary tumor cell migration through inhibiting Rac1 and Cdc42, but not the RhoA GTPase, Cell Motil Cytoskeleton, 64 (2007) 338-346.

[37] R. Garzon, G. Marcucci, C.M. Croce, Targeting microRNAs in cancer: rationale, strategies and challenges, Nat Rev Drug Discov, 9 (2010) 775-789.

[38] T.P. Chendrimada, R.I. Gregory, E. Kumaraswamy, J. Norman, N. Cooch, K. Nishikura, R. Shiekhattar, TRBP recruits the Dicer complex to Ago2 for microRNA processing and gene silencing, Nature, 436 (2005) 740-744.

[39] I. Tinoco Jr, C. Bustamante, How RNA folds, Journal of Molecular Biology, 293 (1999) 271-281.

[40] C. Scholz, E. Wagner, Therapeutic plasmid DNA versus siRNA delivery: common and different tasks for synthetic carriers, J Control Release, 161 (2012) 554-565.

[41] Y. Zhang, R.A. Gemeinhart, Improving matrix metalloproteinase-2 specific response of a hydrogel system using electrophoresis, Int J Pharm, 429 (2012) 31-37.

[42] J.R. Tauro, B.S. Lee, S.S. Lateef, R.A. Gemeinhart, Matrix metalloprotease selective peptide substrates cleavage within hydrogel matrices for cancer chemotherapy activation, Peptides, 29 (2008) 1965-1973.

[43] S.W. Kim, N.Y. Kim, Y.B. Choi, S.H. Park, J.M. Yang, S. Shin, RNA interference in vitro and in vivo using an arginine peptide/siRNA complex system, Journal of controlled release : official journal of the Controlled Release Society, 143 (2010) 335-343.

3 Charged Group Surface Accessibility Determines Micelleplexes Formation and Cellular Interaction

3.1 Abstract

Micelleplexes are a class of nucleic acid carriers that have gained acceptance due to their size, stability, and ability to synergistically carry small molecules. MicroRNAs (miRNAs) are small non-coding RNA gene regulator that is consists of 19-22 nucleotides. Altered expression of miRNAs plays an important role in many human diseases. Using a model 22-nucleotide miRNA sequence, we investigated the interaction between charged groups on the micelle surface and miRNA. The model micelle system was formed from methoxy-poly(ethylene glycol-b-lactide) (mPEG-PLA) mixed with methoxy-poly(ethylene glycol-b-lactide-b-arginine) (mPEG-PLA-R_x, x = 8 or 15). Surface properties of the micelles were varied by controlling the oligoarginine block length and conjugation density. Micelles were observed to have a core-shell conformation in the aqueous environment where the PLA block constituted the hydrophobic core, mPEG and oligoarginine formed a

* Reproduced with permission from: Y Zhang, Y Liu, S Sen, P Král, RA Gemeinhart. Nanoscale. 2015, 7, 7559-7564.

hydrophilic corona. Significantly different thermodynamic behaviors were observed during the interaction of single stranded miRNA with micelles of different surface properties, and the resulting micelleplexes mediated substantial cellular association. Depending upon the oligoarginine length and density, micelles exhibited miRNA loading capacity directly related to the presentation of charged groups on the surface. The effect of charged group accessibility of cationic micelle on micelleplex properties provides guidance on future miRNA delivery system design.

3.2 Introduction

Over the last decade, miRNA has attracted significant attention due to their critical gene regulatory function in both normal biological process as well as various human diseases [1]. Micelleplexes, complexes formed by binding miRNA to micelles, have been designed for miRNA delivery. To form micelleplexes, miRNA is loaded onto the corona of the pre-formed micelles through multivalent ionic interactions [2-8]. Micelleplexes provide control over particle size through the hydrophobic interactions of the core and hydrophilic stability through the corona. To further develop and optimize micelleplexes for miRNA

delivery, we sought to better understand the physical processes governing the formation, structure, and stability of micelleplexes. While the physical properties of block copolymer micelles have been relatively well studied and understood, much less is known about the processes driving micelleplexes formation and stabilization [9]. For the first time, the effects of charged group surface presentation on miRNA binding are investigated from a thermodynamic standpoint to improve the understanding of the interactions of miRNA with micelles.

Modification of the surface of nanoparticles has significant effect on the stability and biologic interactions of the nanoparticles [10-12]. To promote miRNA-micelle interactions, surface-exposed charged groups have been placed on micelles [2]. Unfortunately, the hydrophilic corona-forming components of micelles also tend to interfere with the binding of miRNA. The hydrophilic corona-forming components, generally poly(ethylene glycol) (PEG), form a 'hydration shell' on nanoparticles excluding the adsorption of proteins resulting in steric stabilization of the micelle [13]. Even with this shell, it is clear that proteins interact with the surface of micelles and other nanoparticles [14-20]. However,

PEG on the surface also impairs cationic polymer interactions with nucleic acids due to decreased positive charge density, hydrogen bonding, and steric hindrance [21, 22]. Moreover, once the micelleplexes arrive at targeted tissue, PEG inhibits interactions between the micelleplexes and cells, reducing cellular uptake of the nanocarrier and resulting in a significant loss of transfection activity [23]. Design criteria that aid in the balance between binding of miRNA and steric stabilization would greatly improve the efficiency of micelleplex design.

3.3 Materials and Methods

3.3.1 Materials

Carboxyl terminal-mPEG2000-PLA3000 was purchased from Advanced Polymer Materials (Montreal, Canada). Ac-CR_8-NH_2 and Ac-CR_{15}-NH_2 peptides were synthesized by VCPBIO (Shenzhen, China). Heparin sulfate, *N*-(3-dimethylaminopropyl)-*N′*-ethylcarbodiimide hydrochloride (EDC) and *N*-hydroxysuccinimide (NHS) were obtained from Sigma Aldrich. 3-(2-pyridyldithio) proprionyl hydrazide (PDPH) crosslinker was obtained from Fisher. Single stranded

anti-miRNA sequence 5'-AUCGAAUAGUCUGACUACAACU-3' was synthesized by Integrated DNA Technologies (IDT) with standard RNA chemistry. Cy-5 labeled single stranded anti-miRNA was from Invitrogen as previously reported [24].

3.3.2 Polymer conjugate synthesis

Carboxyl terminal-mPEG2000-PLA3000, EDC and NHS (100, 40 and 24 mg, respectively) was dissolved in DMSO and stirred for 30 min, after which 14 mg PDPH crosslinker was added, thus modifying mPEG2000-PLA3000 with a pyridyldisulfide functional group at the previous carboxyl termini. Unreacted reagents were removed by dialysis against deionized water for 24 h with a molecular weight cut off of 1000 dialysis membrane. The sample was recovered from the dialysis tube and lyophilized to a white powder. Successful PDPH modification was confirmed with ^{1}H NMR in $CDCl_3$ using a 400 MHz Bruker DPX-400 spectrometer (Bruker BioSpin Corp., Billerica, MA). To couple mPEG-PLA-PDPH with peptide, 40 mg of mPEG-PLA-PDPH and 10 mg CR_{15} or 5.6 mg CR_8 (1:1 molar ratio) was dissolved in argon degased DMSO and reacted for 6 hours in argon environment before purification with a Sep-Pak C_{18} column.

3.3.3 Micelleplex preparation

Micelles were prepared by the film hydration and sonication method as previously reported [25]. Briefly, 10 mg of copolymer was dissolved in 0.5 mL acetonitrile. Solvent was removed by rotovap to form a polymer matrix. RNAse free water (0.5 mL) was added to rehydrate the polymer film followed by sonication for 5 min to form empty micelles. To prepare micelleplexes, micelles were diluted with RNAse free water to the appropriate concentration and added dropwise to RNA solution (10 μM) and incubated for 15 min at room temperature.

3.3.4 Critical micelle concentration

Critical micelle concentration (CMC) was determined by using a pyrene fluorescence probe as previously reported [26]. Briefly, 100 μL of 1.2×10^{-5} M pyrene in acetone was added to a series of amber vials and evaporated in fume hood overnight to form a pyrene film. The final concentration of pyrene upon addition of 2 mL of polymer solution was 6×10^{-7} M. Different copolymer micelle solutions in water (0.1 – 500 mg/L) were added to vials containing pyrene film. The solutions were incubated at room temperature for 24 h on

a shaker before fluorescence measurement. The emission wavelength was set at 390 nm and the excitation spectrum was scanned from 300 nm to 400 nm using a spectrofluorophotometer (RF 1501, Shimadzu, Japan) and the intensity ratio I_{335}/I_{333} against log concentration was plotted. The CMC value was determined from the onset of the change in intensity ratio at high polymer concentrations as previously reported [27].

3.3.5 Particle sizing and ζ-potential

Particle size and ζ-potential were measured in RNAse free water to obtain the parameters before RNA complexation, using a Nicomp 380 Zeta Potential/Particle Sizer (Particle Sizing Systems, Santa Barbara, CA). The data represent the mean plus or minus (±) the standard deviation (SD) from three independent experiments. To mimic a physiologically relevant conditions as previously reported [28]. The particle size and ζ-potential of micelleplexes were measured in 10 mM HEPES buffer (pH 7.4) following RNA complexation. The data represent mean plus or minus (±) the standard deviation (SD) from three independent experiments.

3.3.6 Morphology characterization

The morphology of micelles and micelleplexes were analyzed by transmission electron microscopy (TEM, JEM-1220, JEOL Ltd., Japan). A drop of micelles (1 mg/mL) was placed on a carbon-coated 300 mesh copper grid. The sample was negatively stained with 2% (w/v) uranyl acetate solution, and then dried at room temperature.

3.3.7 Gel shift assay

The successful formation of micelleplexes was confirmed by a gel shift assay. Micelleplexes were prepared as described above at predetermined positive to negative (+/-) charge ratios. The resulting micelleplexes were analyzed by electrophoresis using a 20% non-denaturing polyacrylamide gel for 1 h at 80 V in TBE buffer (89 mM Tris-borate, 2 mM EDTA). Following SYBR gold staining, the gel was visualized using a gel documentation system (GelDoc 2000, Bio-Rad, Hercules, CA).

3.3.8 Heparin competition

With the RNA amount fixed, micelleplexes were prepared as described above at predetermined positive to negative (+/-) charge ratios. To compare the ability of different

micelleplexes in resisting negatively charged macromolecule competition, appropriate amount of heparin solution (2 mg/mL) was added at 4:1 and 8:1 heparin to RNA weight ratios. The RNA was visualized by running the samples in 20% non-denaturing polyacrylamide gel as described in gel shift assay.

3.3.9 Isothermal Titration Calorimetry

Isothermal titration calorimetry (ITC) was carried out on a VP-ITC from Microcal (GE Healthcare Bio-Sciences, Milwaukee, WI, USA) with an active cell volume of 1.4 mL using a stirring rate of 307 rpm [29]. RNAse free water was degassed under vacuum for 10 min and equilibrated to room temperature before use. Measurements were performed at 25℃. The baseline was recorded by titrating an equivalent micelle concentration into water. All experiments were performed by titrating a 3 μL of micelles containing 4.0 mM arginines into the sample cell containing 5 μM anti-miRNA (0.11 mM phosphate). An initial data point from 2 μL first injection was always removed from data analysis to avoid systematic error from syringe filling. The following injections were maintained at 3 μL at intervals of 200 s until the anti-miRNA was saturated with micelles. Injection heat caused

by anti-miRNA binding to micelles during each injection was obtained from the integral of the calorimetric signal after subtraction of the baseline. ITC data were analyzed with Microcal, LLC ITC package for Origin® version 7.0. Each experiment was repeated at least once to ensure reproducibility. The peaks were integrated and corrected with a single-site-binding model. The thermodynamic parameters binding sites, binding constant *K*, enthalpy (ΔH), entropy (ΔS) were reported.

3.3.10 Cellular association

The cellular association was determined as we previously reported [30]. Briefly, 2×10^5 U251 cells were seeded in 12-well plates and incubated overnight. Micelleplexes were prepared at a charge ratio 30:1 with the final anti-miRNA concentration maintained constant at 100 nM. Micelleplexes were added to cells to make the total media volume 1 mL. Following addition of micelleplexes to cells, cells were incubated for an additional 4 h. Cells were then washed with cold PBS twice followed by trypsinization and centrifugation at 1500 rpm for 5 min. The pellets were then washed twice with cold PBS and centrifugation before resuspending in 200 μL of 1% formaldehyde and analyzing on Becton

Dickinson Fortessa flow cytometer (San Jose, CA) at excitation 543 nm and emission 570 nm.

3.3.11 Micelle Modeling

We modeled by atomistic molecular dynamics (MD) simulation of mPEG-PLA-R_8 mixed with mPEG-PLA copolymers in water with different aggregation numbers, N_{agg}, as previously described [26]. Based upon this model, the number of total copolymer monomers to produce a micelle with a size observed by DLS and TEM is between 60 and 100. Using this estimate and the neutral to slightly positive zeta potenital of the micelles, it would be expected that the number of charged phosphate groups would match those of the charged arginine groups, or be slightly below unity. Therefore, the number of oligoarginines and miRNA loading of the micelles was estimated.

3.4 Result and Discussion

Successful polymer conjugation was confirmed by ^{1}H NMR (Figure 3.1) in DMSO-d_6 [8]. The R_x conjugation rate was calculated based on the intensity ratio between the proton peak of the guanidine group (δ 7.43, 4H) and that of the PLA segment (δ 5.19, 1H). The

conjugation rate was controlled by varying functional group molar ratios. For example, a conjugation rate of approximately 28% (relative to total polymer) was achieved when the molar ratio of pyridyldisulfide group to sulfhydryl group in peptide was 1:1, and a 14% conjugation rate was achieved with a molar ratio of 2:1.

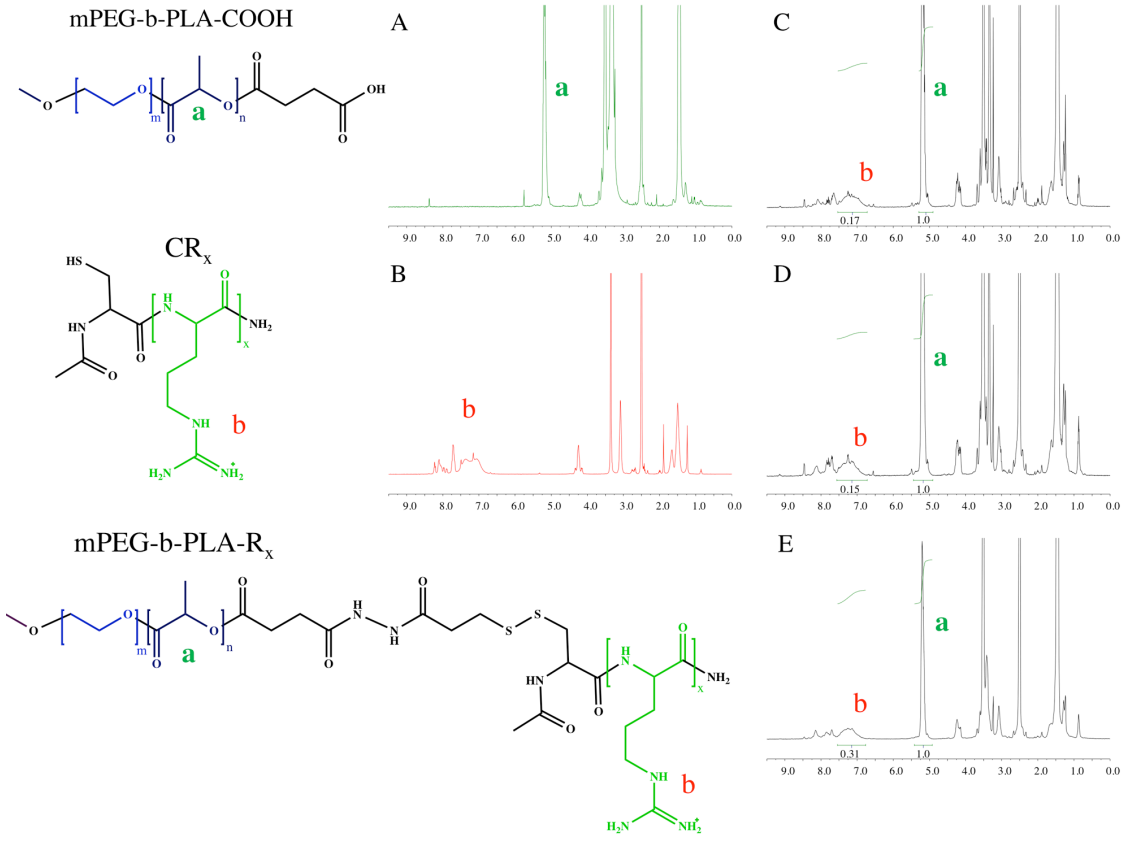

Figure 3.1. ^{1}H NMR spectra of (A) mPEG-PLA-COOH (B) CR_x (C) mPEG-PLA-R_8 (D) mPEG-PLA-R_{15}^{Low} (E) mPEG-PLA-R_{15}^{High}. The purified products have characteristic peaks from both PLA segment (a, δ 5.19, 1H) and guanidine group (b, δ 7.43, 4H) in R_x.

To elucidate the effect of charged group surface presentation of micelles on miRNA loading, stability and cellular uptake, we engineered polymeric micelles that are composed of hydrophilic oligoarginine (R_x, x=8 or 15) conjugated directly to the hydrophobic block of the mPEG-b-PLA block copolymer forming a triblock copolymer, mPEG-PLA-R_x [8] based upon our previous experience with the R_8 oligoarginine [24], the expected extended lengths of the oligoarginine and poly(ethylene glycol), and previously published research [8, 31]. We hypothesized that the mPEG-PLA-R_x micelles would present the oligoarginine block exposed on the surface, dependent upon the length of the oligoarginine block and the poly(ethylene glycol) block. An alternative structure where the oligoarginine block were placed on the poly(ethylene glycol) block, PLA-PEG-R_x, could also be examined and will be in the future to determine if these structures are presented as described for poly(lysine) [32, 33] or oriented toward the interior of the structure [11]. Further, we hypothesized that the surface presentation of the oligoarginine would influence the miRNA-oligoarginine interactions and cellular uptake. In this way, the charged group was accessible for loading after formation, but the presentation at the surface could be controlled unlike systems that

bury the charged groups during the formation of the micelle and limit the loading to the point of formation of the particles [34].

Micelles, mPEG-PLA-R_8, mPEG-PLA-R_{15}^{Low}, and mPEG-PLA-R_{15}^{High}, with arginine block conjugation density (proportion of oligoarginine modified triblock copolymer to total mPEG-PLA polymer) of 27%, 14% and 28% (mol%), respectively, were synthesized by coupling mPEG-PLA with CR_x through disulfide bond exchange reaction. For the purpose of easily distinguishing 14% and 28% R_{15} substituted mPEG-PLA-R_{15} micelles, we denote them as mPEG-PLA-R_{15}^{Low} and mPEG-PLA-R_{15}^{High}, respectively. All of the mPEG-PLA-R_x copolymers have similar critical micelle concentration (CMC) to the mPEG-PLA polymer (Figure 3.2).

Table 3.1. Micelle particle size and ζ-potential.

	Peptide conjugation (mol%)	Micelle size (nm)	Micelle ζ-potential (mV)
mPEG-PLA-R_8	27%	20.13±0.42	30.76±1.16
mPEG-PLA-R_{15}^{Low}	14%	25.00±1.51	19.65±4.7
mPEG-PLA-R_{15}^{High}	28%	20.43±1.50	30.46±1.88

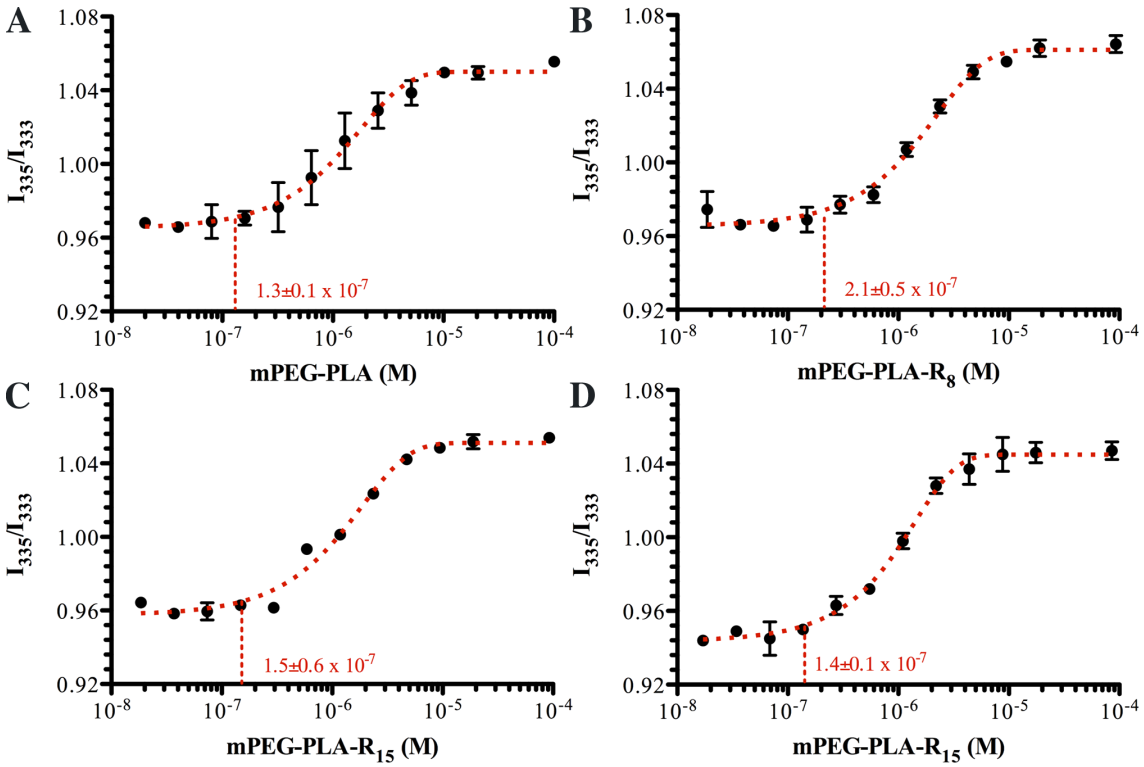

Figure 3.2. mPEG-PLA-R$_x$ copolymers have CMC similar to mPEG-PLA. CMC plots of (A) mPEG-PLA (B) mPEG-PLA-R$_8$ (C) mPEG-PLA-R$_{15}^{Low}$ and (D) mPEG-PLA-R$_{15}^{High}$. Data represent mean ± standard deviation, N=3.

The micelles from each group had similar diameter (Table 3.1**)**. The ζ-potential of mPEG-PLA-R$_8$ micelles (30.76±1.16 nm) was similar to mPEG-PLA-R$_{15}^{High}$ (30.46±1.88 nm), suggesting that only a portion of the oligoarginine contributed directly to the surface charge of the micelles. This was further supported by the ζ-potential of mPEG-PLA-R$_8$ and mPEG-PLA-R$_{15}^{High}$ micelles being higher than mPEG-PLA-R$_{15}^{Low}$ micelles (19.65±4.7

nm). In this way, we produced micelles with similar size, oligoarginine content (mPEG-PLA-R_8 and mPEG-PLA-R_{15}^{Low}) and charge (mPEG-PLA-R_8 and mPEG-PLA-R_{15}^{High}). The morphology of mPEG-PLA-R_8, mPEG-PLA-R_{15}^{Low} and mPEG-PLA-R_{15}^{High} micelles and micelleplexes were observed with transmission electron microscope, all of which demonstrated spherical shape and size similar to DLS measurements (Figure 3.3).

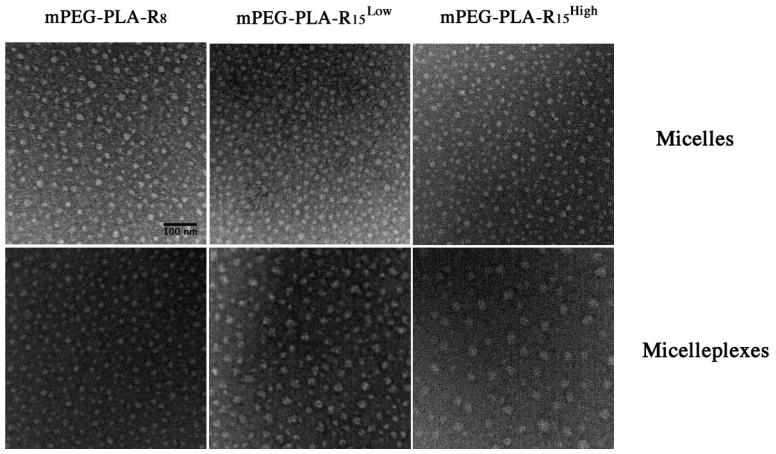

Figure 3.3. TEM images of mPEG-PLA-R_8, mPEG-PLA-R_{15}^{Low} and mPEG-PLA-R_{15}^{High} micelles and micelleplexes (+/- charge ratio 30).

To understand the conformation of the micelles, micelles were prepared in D_2O for solution-phase NMR analysis [35-37]. In this technique, the constituents in the aqueous phase are readily detected but the hydrophobic-phase constituents have repressed signature.

In aqueous solution, the triblock mPEG-b-PLA-R_x polymers formed micelles where the PLA hydrophobic chains collapse, with a disappearance of the PLA proton peaks, to form a hydrophobic core while the PEG chains and the R_x block constitute a hydrophilic corona. While the PLA protons were not detected in D_2O, the terminal methoxyl protons (δ = 3.40, 3H) from mPEG chains (Figure 3.4B), the d methylene protons from arginine side chain (δ = 3.20, 2H) and the a proton (δ = 4.40, 1H, Figure 3.4B) [8] in the peptide backbone of R_x blocks remained detectable in the ^{1}H NMR spectrum. The prominent peaks (δ = 4.7 ppm and δ = 3.7 ppm) correspond to the solvent and methylene proton of poly(ethylene glycol), respectively. Based upon atomistic molecular dynamics simulation (Figure 3.5), the number of total copolymer monomers to produce a micelle with a size observed by DLS and TEM is between 60 and 100 monomers. Using this estimate and the neutral to slightly positive ζ–potenital of the micelles, it would be expected that the number of charged phosphate groups would match those of the charged arginine groups, or be slightly below unity. Therefore, the number of oligoarginines and miRNA loading of the micelles was estimated (Table 3.2). This suggested the presence of oligoarginine block on the micelles surface, *i.e.*

the aqueous phase. Based upon this, each of the micelles presented a portion of the oligoarginine on the surface with access to the aqueous environment.

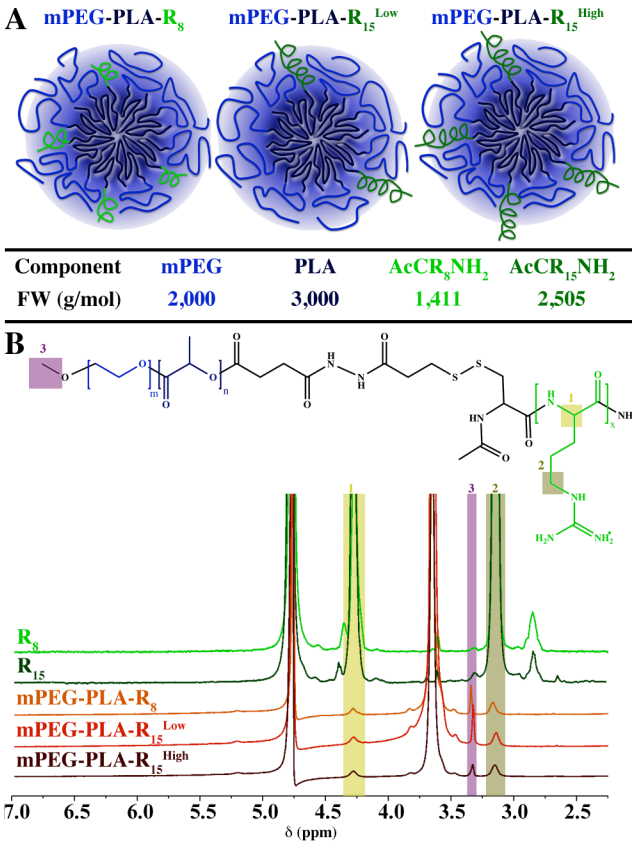

Figure 3.4. Micelles properties and surface oligoarginine presence. (A) Schematic representation of the micelles formed and the relevant molecular weights of the components. (B) ^{1}H NMR analysis of the peptides (CR_8 and CR_{15}) and micelles (mPEG-PLA-R_8, mPEG-PLA-R_{15}^{Low}, and mPEG-PLA-R_{15}^{High}) showing the arginine a proton (1; δ 4.40, 1H), d protons (2; δ 3.20, 2H), or ω-terminal methoxyl protons (arrow; δ 3.40, 3H).

Table 3.2. Estimates of the number of oligo-arginine peptides and miRNA associated with micelles.

N_{agg} (copolymer/micelle)	60		100	
N_Z (oligoargine/micelle or miRNA/micelle)	N_{Rx}	N_{miRNA}	N_{Rx}	N_{miRNA}
mPEG-PLA-R_8	16	6	27	10
mPEG-PLA-R_{15}^{Low}	8	6	14	10
mPEG-PLA-R_{15}^{High}	17	11	28	20

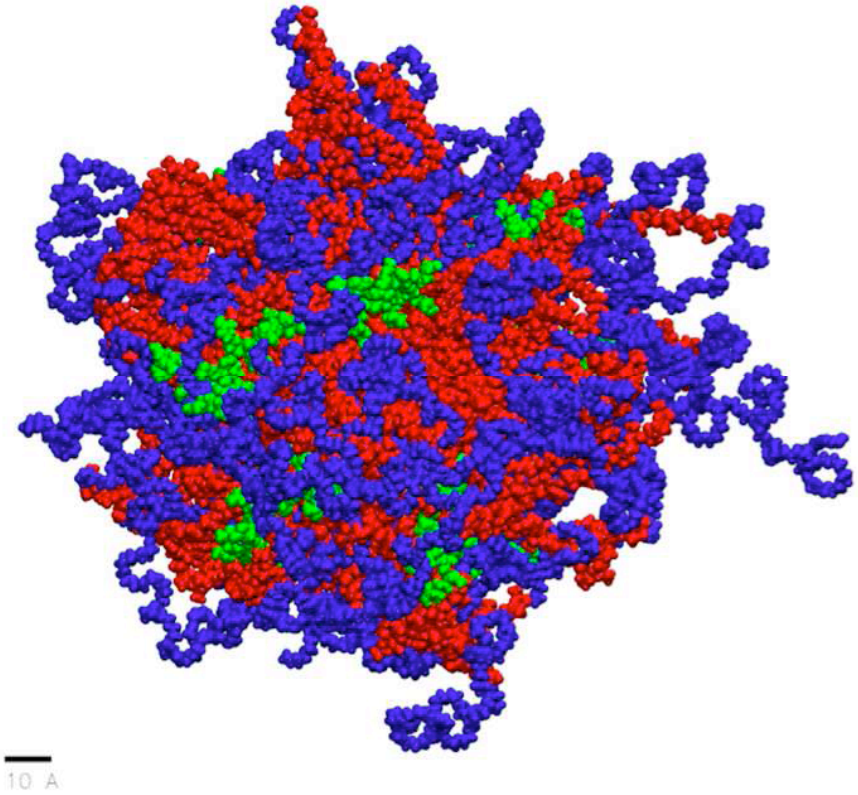

Figure 3.5. Molecular dynamics simulation of mPEG-PLA-R_8 micelle. Each monomer consisted of a methoxy-poly(ethylene-glycol)(mPEG; MW ~ 2,000 g/mol; blue) block coupled to the α-hydroxide of poly(lactide) (PLA; MW ~ 3,000 g/mol; red). As in the experiments, 28% of total monomers were modified with oligoarginine (R_8; green) on the ω-carboxylate of the PLA block. The micelles were prepared with total 60 monomers.

Being present in the aqueous phase, however, does not indicate that the oligoarginine is free to interact with biomolecules in the presence of the PEG corona. To determine the ability of the micelles to interact with miRNA, the gel shift assay was conducted (Figure 3.6A). mPEG-PLA-R_8 micelles were able to fully retard miRNA mobility only at or above

a positive to negative (+/-) charge ratio (arginine to nucleotide) of 30, while mPEG-PLA-R_{15}^{Low} and mPEG-PLA-R_{15}^{High} fully retarded miRNA mobility at a charge ratio of 5. The lower charge ratio needed to fully bind miRNA further suggested that the mPEG-PLA-R_{15} micelles contain arginine that is more accessible to the surface for biomolecular interactions. This is further supported by the fact that mPEG-PLA-R_{15}^{Low} micelles interact with the miRNA as efficiently as the mPEG-PLA-R_{15}^{High} despite the fact that there is approximately half the total arginine present. No significant difference was observed for miRNA interactions with mPEG-PLA-R_{15}^{Low} and mPEG-PLA-R_{15}^{High} at low charge ratios (Figure 3.6B). Based upon the interactions with miRNA, the longer oligoarginine chains are able to more readily interact with biomolecules at the surface of the micelles regardless of overall charge, i.e. zeta potential, of the micelle. This is consistent with observation that PEGylation of cationic polymers generally deteriorates a polymer's ability to interact with DNA and RNA [22].

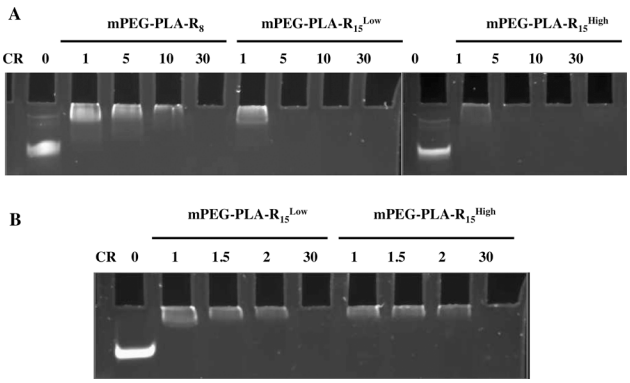

Figure 3.6. MiRNA complexation with micelles occurs at lower charge ratios for longer oligoarginine regardless of oligoarginine density. (A) mPEG-PLA-R_8, mPEG-PLA-R_{15}^{Low}, and mPEG-PLA-R_{15}^{High} complexation with miRNA at +/- charge ratios of 1, 5, 10 and 30 (B) mPEG-PLA-R_{15}^{Low} and mPEG-PLA-R_{15}^{High} complexation with miRNA at +/- charge ratios 1, 1.5, 2 and 30.

To better characterize the interactions and gain information about the events leading to miRNA-micelle interactions, thermodynamic analysis was utilized [29, 38-40]. An initial endothermic peak was observed for mPEG-PLA-R_8, which suggests that a molecular rearrangement took place prior to the ionic interactions between the peptides and the miRNA (Figure 3.7). Unlike mPEG-PLA-R_8, only exothermic processes were observed when miRNA interacts with mPEG-PLA-R_{15}^{Low} or mPEG-PLA-R_{15}^{High}. Only the shorter arginine-containing micelles, mPEG-PLA-R_8, had an unfavorable entropic contribution while all micelles exhibited favorable enthalpy energy (Table 3.3**)**. Water molecules associated with PEG creates a ‘‘hydration shell’’ where the water molecules are oriented in

a structured manner surrounding the micelles [13]. The entropic loss ($-T\Delta S > 0$) during miRNA binding to mPEG-PLA-R_8 process might result from the disturbance of the hydration shell surrounding mPEG-PLA-R_8 in conjunction with unfavorable conformational changes necessary to accommodate the miRNA chain. Because the longer oligoarginine peptides are more accessible, the unfavorable rearrangements and the disruption of the ordered water layer are not necessary to accommodate the miRNA. The interactions of mPEG-PLA-R_{15}^{Low} and mPEG-PLA-R_{15}^{High} with miRNA are very similar to hyperbranched polyethylenimine (PEI) interactions with double strand siRNA [29], suggesting that arginine clusters on the micelle surface could interact with miRNA in similar manner to PEI.

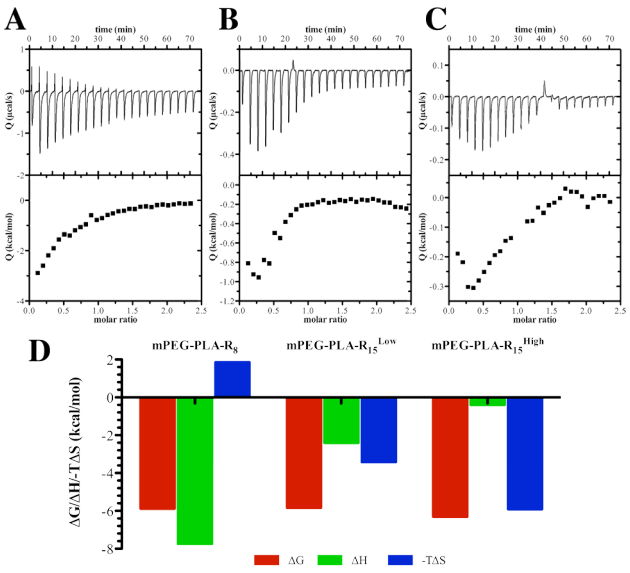

Figure 3.7. Thermodynamic profiles of single stranded miRNA binding to micelles indicate different interactions occur dependent upon oligoarginine length and density. (A) mPEG-PLA-R_8 (B) mPEG-PLA-R_{15}^{Low} (C) mPEG-PLA-R_{15}^{High} (D) Thermodynamic parameters, derived from ITC, of miRNA binding to mPEG-PLA-R_8, mPEG-PLA-R_{15}^{Low}, and mPEG-PLA-R_{15}^{High} micelles.

Table 3.3. Thermodynamic parameters for the binding between different micelles and anti-miRNA.

	N **(sites/arginine)**	***K*** **(x10^3)**	**Δ*H*** **(kcal/mol)**	**Δ*S*** **(cal/mol/deg)**	**Δ*G*** **(kcal/mol)**
mPEG-PLA-R_8	0.32±0.05	21.5±2.82	-7.74±1.48	-6.21	-5.88
mPEG-PLA-R_{15}^{Low}	0.41±0.22	18.8±9.53	-2.41±1.56	11.49	-5.83
mPEG-PLA-R_{15}^{High}	0.73±0.15	42.2±26.2	-0.40±0.11	19.83	-6.31

The entropic energy that was needed to form the complexes was coupled with a lower number of arginines that could interact with the miRNA. The mPEG-PLA-R_8 micelles only

had about 2.6 arginines per peptide available to interact while the mPEG-PLA-R_{15}^{Low} and mPEG-PLA-R_{15}^{High} micelles had 6.2 or 11.0 arginines per peptide available to interact with miRNA, respectively. The differences in available arginines do not mirror the charge on the micelles (Table 3.4), which were all positive, and the density of peptide being the only factor influencing the z-potential. This suggests that the available content of arginine increased on the surface as the amount of peptide in the micelles increased.

Table 3.4. Micelleplexes particle size and ζ-potential.

	Peptide conjugation (mol%)	Micelleplex size (nm)	Micelleplex ζ-potential (mV)
mPEG-PLA-R_8	27%	21.6±1.25	0.93±0.96
mPEG-PLA-R_{15}^{Low}	14%	22.37±4.50	6.01±3.57
mPEG-PLA-R_{15}^{High}	28%	19.9±2.98	4.95±0.43

In addition to the role of the PEG corona shielding the charged groups during complexation, the PEG corona is also thought to influence the stability of the complexes by altering the surface accessibility of charged biomolecules, particularly anionic biomacromolecules that compete with negatively charged nucleic acids on the micelle

surface. In all micelles, the micelleplex ζ-potentials were neutral compared to the original highly positive zeta potential. Using the heparin sulfate competition assay to mimic the natural anionic macromolecules, shorter oligoarginine-containing micelles, mPEG-PLA-R_8, were not able to condense miRNA as tightly as longer oligoarginine containing micelles, mPEG-PLA-R_{15}^{Low} and mPEG-PLA-R_{15}^{High}. mPEG-PLA-R_x micelleplexes migrate in the polyacrylamide gel, but to a lesser extent than miRNA control due to the charge neutralization and the size of the micelleplexes (Figure 3.6). At a charge ratio of 20, heparin did not dissociate miRNA from mPEG-PLA-R_8 micelles at a heparin to miRNA weight ratio of 4:1 (Figure 3.8A), but based upon the diminished dye exclusion the miRNA appears to be less tightly bound to the micelleplex. The association between miRNAs and micelles was similarly loosened in mPEG-PLA-R_{15}^{Low} and mPEG-PLA-R_{15}^{High} micelleplexes in the presence of 8:1 heparin to miRNA. At a charge ratio of 30, heparin was unable to compete with miRNA or loosen the interactions. This suggests that the poorly accessible arginine content in mPEG-PLA-R_8 was less available for interactions, but once the interaction was formed the interaction was stable to heparin competition.

mPEG-PLA-R_{15}^{Low} and mPEG-PLA-R_{15}^{High} have longer peptide sequence and appear to present a greater proportion of miRNAs closer to the surface than in mPEG-PLA-R_8 micelleplexes, and are thus less resistant to heparin competition. At a higher charge ratio of 30 to 1, all micelles were able to maintain the interaction with miRNA (Figure 3.8B**),** suggesting that the interaction was stabilized with further ionic crosslinking. This observation agrees with others who observed that the macromolecules that freely interact with RNA are not necessarily the most stable [41].

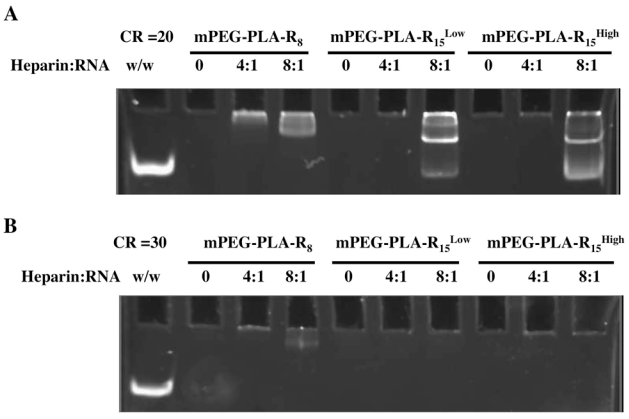

Figure 3.8. Micelleplexes are stable to heparin competition. Micelleplexes were prepared at (A) +/- charge ratio 20 or (B) 30 and incubated with heparin at a heparin to miRNA weight ratio (w/w) of 0:1, 4:1, or 8:1 prior to electrophoresis and staining.

Finally, surface exposed charged groups on the micelles are believed to play key roles in their cellular interactions, with neutral particles (zeta potential -10 to +10 mV) having limited non-specific cellular interactions [11, 42, 43]. mPEG-PLA-R_8 and mPEG-PLA-R_{15}^{High} micelles had higher ζ-potential than mPEG-PLA-R_{15}^{Low}, but the ζ-potential range of all three micelleplexes were generally neutral after miRNA complexation (Table 3.1 & Table 3.4). mPEG-PLA-R_{15}^{Low} and mPEG-PLA-R_{15}^{High} micelleplexes showed significantly more cellular association than mPEG-PLA-R_8 micelleplexes (Figure 3.9). With the similar charge and size, the oligoarginine available on the micelle surface was expected to influence the ability of micelles to associate with or enter cells, but the total arginine and surface charge was not directly related to cellular interaction [24, 44, 45]. Only the available arginine content on the micelle surface correlated with the ability of the micelles to interact with cells. This further supports the idea that the oligoarginine on the mPEG-PLA-R_{15} micelles was more available for interactions.

Despite the fact that mPEG-PLA-R_{15}^{Low} and mPEG-PLA-R_{15}^{High} micelleplexes showed

significantly more cellular association than mPEG-PLA-R_8 micelleplexes in the *in vitro* cellular association testing (Figure 3.9), the tightness, stability and negligible unspecific cellular association of mPEG-PLA-R_8 micelleplexes make it a great candidate for developing targeted nanocarrier *in vivo*. By modifying the PEG terminal with disease or cell type specific targeting moieties (antibodies, ligands and aptamers), targeted PEG-PLA-R_8 micelleplexes could avoid unspecific delivery, mediate active cellular uptake toward diseased cells and effectively release the cargo in the cell. More importantly, such targeted nanocarrier could decrease the dosage of anti-miRNAs needed to achieve effective silencing and minimizing off-target effect.

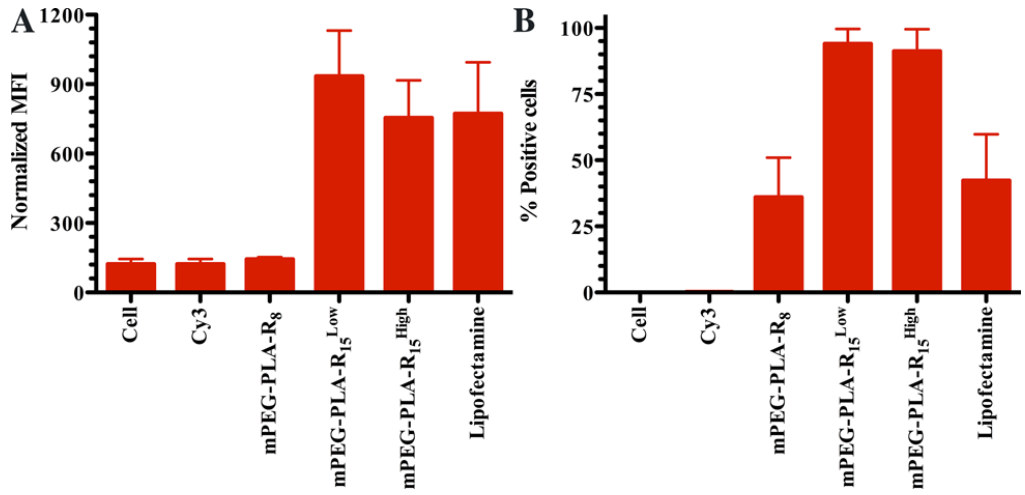

Figure 3.9. Cellular association mediated by different micelleplexes. (A) The mean fluorescence intensity observed on U251 glioma cells following interaction with mPEG-PLA-R_8, mPEG-PLA-R_{15}^{Low}, and mPEG-PLA-R_{15}^{High} micelleplexes or untreated cells or Cy3-labeled miRNA. (B) The relative population (%) of cells associated with the mPEG-PLA-R_8, mPEG-PLA-R_{15}^{Low}, and mPEG-PLA-R_{15}^{High} micelleplexes or untreated cells or Cy3-labeled miRNA. N=3, mean ± standard error of the mean.

The development of nanocarrier often involve a design parameter optimization process, which is to vary the numerical values of different components in order to achieve optimal outcome. Specifically, the final design is determined based on the highest efficacy value at a defined condition without illustrating the mechanism of the balance among different components, which makes those studies hardily instructive to future delivery system development. The investigation of the effect of charged group surface presentation presented here provides a prototype for conducting nanocarrier design optimization with a

mindset targeting both efficacy and mechanistically understanding of nanocarrier engineering.

3.5 Conclusion

In summary, we have presented the synthesis of triblock copolymers that form micelles and expose different amounts of charged groups on their surface. We systematically studied the interactions of the micelles with miRNA and the miRNA-micelle complexes with biologic macromolecules and cells. By precise control of polymer structure, the accessibility of charged groups on micelle surface was used to control the interaction of miRNA with micelles and the eventual interaction with cells. The accessibility of the charged groups has direct impact on miRNA interaction with the micelles, micelleplexes stability and cellular interaction. These results guide the design of materials for RNA/DNA interactions by suggesting that the total charge of the groups used is not the primary factor for determining RNA binding or cellular association. Future work will further elucidate if the shielding of ionic groups can be controlled in alternate architectures. The PEG corona

can shield the ionic groups thus diminishing RNA-micelle binding and minimizing cell binding; however, this PEG corona protects the RNA from competition yielding a more stable micelleplex.

3.6 References

[1] Y. Zhang, Z.J. Wang, R.A. Gemeinhart, Progress in microRNA Delivery, J. Control. Release, 172 (2013) 962-974.

[2] D.J. Gary, H. Lee, R. Sharma, J.S. Lee, Y. Kim, Z.Y. Cui, D. Jia, V.D. Bowman, P.R. Chipman, L. Wan, Y. Zou, G. Mao, K. Park, B.S. Herbert, S.F. Konieczny, Y.Y. Won, Influence of nano-carrier architecture on in vitro siRNA delivery performance and in vivo biodistribution: polyplexes vs micelleplexes, ACS Nano, 5 (2011) 3493-3505.

[3] Y.M. Kim, S.C. Song, Targetable micelleplex hydrogel for long-term, effective, and systemic siRNA delivery, Biomaterials, 35 (2014) 7970-7977.

[4] C.Q. Mao, J.Z. Du, T.M. Sun, Y.D. Yao, P.Z. Zhang, E.W. Song, J. Wang, A biodegradable amphiphilic and cationic triblock copolymer for the delivery of siRNA targeting the acid ceramidase gene for cancer therapy, Biomaterials, 32 (2011) 3124-3133.

[5] R. Sharma, J.S. Lee, R.C. Bettencourt, C. Xiao, S.F. Konieczny, Y.Y. Won, Effects of the incorporation of a hydrophobic middle block into a PEG-polycation diblock copolymer on the physicochemical and cell interaction properties of the polymer-DNA complexes, Biomacromolecules, 9 (2008) 3294-3307.

[6] T.M. Sun, J.Z. Du, Y.D. Yao, C.Q. Mao, S. Dou, S.Y. Huang, P.Z. Zhang, K.W. Leong, E.W. Song, J. Wang, Simultaneous delivery of siRNA and paclitaxel via a "two-in-one" micelleplex promotes synergistic tumor suppression, ACS Nano, 5 (2011) 1483-1494.

[7] H. Yu, Y. Zou, Y. Wang, X. Huang, G. Huang, B.D. Sumer, D.A. Boothman, J. Gao, Overcoming endosomal barrier by amphotericin B-loaded dual pH-responsive PDMA-b-PDPA micelleplexes for siRNA delivery, ACS Nano, 5 (2011) 9246-9255.

[8] Z.X. Zhao, S.Y. Gao, J.C. Wang, C.J. Chen, E.Y. Zhao, W.J. Hou, Q. Feng, L.Y. Gao, X.Y. Liu, L.R. Zhang, Q. Zhang, Self-assembly nanomicelles based on cationic mPEG-PLA-b-Polyarginine(R15) triblock copolymer for siRNA delivery, Biomaterials, 33 (2012) 6793-6807.

[9] D. Schaeffel, A. Kreyes, Y. Zhao, K. Landfester, H.-J.r. Butt, D. Crespy, K. Koynov,

Molecular Exchange Kinetics of Diblock Copolymer Micelles Monitored by Fluorescence Correlation Spectroscopy, ACS Macro Lett, 3 (2014) 428-432.

[10] R.M. Pearson, H.-j. Hsu, J. Bugno, S. Hong, Understanding nano-bio interactions to improve nanocarriers for drug delivery, MRS Bull., 39 (2014) 227-237.

[11] R.M. Pearson, N. Patra, H.J. Hsu, S. Uddin, P. Kral, S. Hong, Positively Charged Dendron Micelles Display Negligible Cellular Interactions, ACS Macro Lett, 2 (2013) 77-81.

[12] L. Vukovic, F.A. Khatib, S.P. Drake, A. Madriaga, K.S. Brandenburg, P. Kral, H. Onyuksel, Structure and dynamics of highly PEG-ylated sterically stabilized micelles in aqueous media, J. Am. Chem. Soc., 133 (2011) 13481-13488.

[13] C. Allen, N. Dos Santos, R. Gallagher, G.N. Chiu, Y. Shu, W.M. Li, S.A. Johnstone, A.S. Janoff, L.D. Mayer, M.S. Webb, M.B. Bally, Controlling the physical behavior and biological performance of liposome formulations through use of surface grafted poly(ethylene glycol), Bioscience reports, 22 (2002) 225-250.

[14] D. Pozzi, V. Colapicchioni, G. Caracciolo, S. Piovesana, A.L. Capriotti, S. Palchetti, S.

De Grossi, A. Riccioli, H. Amenitsch, A. Lagana, Effect of polyethyleneglycol (PEG) chain length on the bio-nano-interactions between PEGylated lipid nanoparticles and biological fluids: from nanostructure to uptake in cancer cells, Nanoscale, 6 (2014) 2782-2792.

[15] E. Casals, T. Pfaller, A. Duschl, G.J. Oostingh, V. Puntes, Time evolution of the nanoparticle protein corona, ACS Nano, 4 (2010) 3623-3632.

[16] T. Cedervall, I. Lynch, S. Lindman, T. Berggard, E. Thulin, H. Nilsson, K.A. Dawson, S. Linse, Understanding the nanoparticle-protein corona using methods to quantify exchange rates and affinities of proteins for nanoparticles, Proc. Natl. Acad. Sci. U. S. A., 104 (2007) 2050-2055.

[17] H.-J. Hsu, S. Sen, R.M. Pearson, S. Uddin, P. Kral, S. Hong, Poly(ethylene glycol) Corona Chain Length Controls End-Group-Dependent Cell Interactions of Dendron Micelles, Macromolecules, 47 (2014) 6911-6918.

[18] M. Lundqvist, J. Stigler, G. Elia, I. Lynch, T. Cedervall, K.A. Dawson, Nanoparticle size and surface properties determine the protein corona with possible implications for biological impacts, Proc Natl Acad Sci U S A, 105 (2008) 14265-14270.

[19] M.P. Monopoli, D. Walczyk, A. Campbell, G. Elia, I. Lynch, F.B. Bombelli, K.A. Dawson, Physical-chemical aspects of protein corona: relevance to in vitro and in vivo biological impacts of nanoparticles, J Am Chem Soc, 133 (2011) 2525-2534.

[20] R.M. Pearson, V.V. Juettner, S. Hong, Biomolecular corona on nanoparticles: a survey of recent literature and its implications in targeted drug delivery, Front. Chem., 2 (2014) Article 108.

[21] C.K. Chen, C.H. Jones, P. Mistriotis, Y. Yu, X. Ma, A. Ravikrishnan, M. Jiang, S.T. Andreadis, B.A. Pfeifer, C. Cheng, Poly(ethylene glycol)-block-cationic polylactide nanocomplexes of differing charge density for gene delivery, Biomaterials, 34 (2013) 9688-9699.

[22] R.E. Fitzsimmons, H. Uludag, Specific effects of PEGylation on gene delivery efficacy of polyethylenimine: interplay between PEG substitution and N/P ratio, Acta Biomater, 8 (2012) 3941-3955.

[23] I. Endo, T. Nagamune, H. Akita, Nano/Micro Biotechnology, Springer, 2010.

[24] Y. Zhang, M. Köllmer, J.S. Buhrman, M.Y. Tang, R.A. Gemeinhart, Arginine-rich,

Cell Penetrating Peptide-anti-microRNA Complexes Decrease Glioblastoma Migration Potential, Peptides, 58 (2014) 83-90.

[25] E. Blanco, E.A. Bey, Y. Dong, B.D. Weinberg, D.M. Sutton, D.A. Boothman, J. Gao, Beta-lapachone-containing PEG-PLA polymer micelles as novel nanotherapeutics against NQO1-overexpressing tumor cells, J. Control. Release, 122 (2007) 365-374.

[26] J.W. Bae, R.M. Pearson, N. Patra, S. Sunoqrot, L. Vukovic, P. Kral, S. Hong, Dendron-mediated self-assembly of highly PEGylated block copolymers: a modular nanocarrier platform, Chem. Commun., 47 (2011) 10302-10304.

[27] J. Aguiar, P. Carpena, J.A. Molina-Bolivar, C. Carnero Ruiz, On the determination of the critical micelle concentration by the pyrene 1:3 ratio method, J Colloid Interf Sci, 258 (2003) 116-122.

[28] D. Gutsch, D. Appelhans, S. Hobel, B. Voit, A. Aigner, Biocompatibility and efficacy of oligomaltose-grafted poly(ethylene imine)s (OM-PEIs) for in vivo gene delivery, Mol Pharm, 10 (2013) 4666-4675.

[29] M. Zheng, G.M. Pavan, M. Neeb, A.K. Schaper, A. Danani, G. Klebe, O.M. Merkel, T.

Kissel, Targeting the blind spot of polycationic nanocarrier-based siRNA delivery, ACS Nano, 6 (2012) 9447-9454.

[30] Y. Zhang, M. Kollmer, J.S. Buhrman, M.Y. Tang, R.A. Gemeinhart, Arginine-rich, cell penetrating peptide-anti-microRNA complexes decrease glioblastoma migration potential, Peptides, 58 (2014) 83-90.

[31] P. Liu, H. Yu, Y. Sun, M. Zhu, Y. Duan, A mPEG-PLGA-b-PLL copolymer carrier for adriamycin and siRNA delivery, Biomaterials, 33 (2012) 4403-4412.

[32] Y. Liu, Z. Chen, C. Liu, D. Yu, Z. Lu, N. Zhang, Gadolinium-loaded polymeric nanoparticles modified with Anti-VEGF as multifunctional MRI contrast agents for the diagnosis of liver cancer, Biomaterials, 32 (2011) 5167-5176.

[33] Y. Liu, C. Liu, M. Li, F. Liu, L. Feng, L. Zhang, N. Zhang, Polymer-polymer conjugation to fabricate multi-block polymer as novel drug carriers: poly(lactic acid)-poly(ethylene glycol)-poly(L-lysine) to enhance paclitaxel target delivery, J Biomed Nanotechnol, 10 (2014) 948-958.

[34] H.X. Wang, X.Z. Yang, C.Y. Sun, C.Q. Mao, Y.H. Zhu, J. Wang, Matrix

metalloproteinase 2-responsive micelle for siRNA delivery, Biomaterials, 35 (2014) 7622-7634.

[35] L. Jongpaiboonkit, Z. Zhou, X. Ni, Y.Z. Wang, J. Li, Self-association and micelle formation of biodegradable poly(ethylene glycol)-poly(L-lactic acid) amphiphilic di-block co-polymers, J. Biomater. Sci. Polym. Ed., 17 (2006) 747-763.

[36] A.S. Darefsky, J.T. King, Jr., R. Dubrow, Adult glioblastoma multiforme survival in the temozolomide era: a population-based analysis of Surveillance, Epidemiology, and End Results registries, Cancer, 118 (2012) 2163-2172.

[37] I.G. Shin, S.Y. Kim, Y.M. Lee, C.S. Cho, Y.K. Sung, Methoxy poly(ethylene glycol)/epsilon-caprolactone amphiphilic block copolymeric micelle containing indomethacin. I. Preparation and characterization, J. Control. Release, 51 (1998) 1-11.

[38] P. Holzerny, B. Ajdini, W. Heusermann, K. Bruno, M. Schuleit, L. Meinel, M. Keller, Biophysical properties of chitosan/siRNA polyplexes: profiling the polymer/siRNA interactions and bioactivity, J. Control. Release, 157 (2012) 297-304.

[39] L. Gu, L.M. Nusblat, N. Tishbi, S.C. Noble, C.M. Pinson, E. Mintzer, C.M. Roth, K.E.

Uhrich, Cationic amphiphilic macromolecule (CAM)-lipid complexes for efficient siRNA gene silencing, J. Control. Release, 184 (2014) 28-35.

[40] L.B. Jensen, G.M. Pavan, M.R. Kasimova, S. Rutherford, A. Danani, H.M. Nielsen, C. Foged, Elucidating the molecular mechanism of PAMAM-siRNA dendriplex self-assembly: effect of dendrimer charge density, Int J Pharm, 416 (2011) 410-418.

[41] S. Mao, M. Neu, O. Germershaus, O. Merkel, J. Sitterberg, U. Bakowsky, T. Kissel, Influence of polyethylene glycol chain length on the physicochemical and biological properties of poly(ethylene imine)-graft-poly(ethylene glycol) block copolymer/SiRNA polyplexes, Bioconjug Chem, 17 (2006) 1209-1218.

[42] C. Fortier, Y. Durocher, G. De Crescenzo, Surface modification of nonviral nanocarriers for enhanced gene delivery, Nanomedicine (Lond), 9 (2014) 135-151.

[43] K. Xiao, Y. Li, J. Luo, J.S. Lee, W. Xiao, A.M. Gonik, R.G. Agarwal, K.S. Lam, The effect of surface charge on in vivo biodistribution of PEG-oligocholic acid based micellar nanoparticles, Biomaterials, 32 (2011) 3435-3446.

[44] X. Xu, Y. Jian, Y. Li, X. Zhang, Z. Tu, Z. Gu, Bio-Inspired Supramolecular Hybrid

Dendrimers Self-Assembled from Low-Generation Peptide Dendrons for Highly Efficient Gene Delivery and Biological Tracking, ACS Nano, 8 (2014) 9255-9264.

[45] Y. Liu, Y.J. Kim, M. Ji, J. Fang, N. Siriwon, L.I. Zhang, P. Wang, Enhancing gene delivery of adeno-associated viruses by cell-permeable peptides, Mol. Ther. Methods Clin. Dev., 1 (2014) 10.1038/mtm.2013.1012.

4 Redox-responsive Anti-miRNAs Delivery System Demonstrates Superior Potential for Releasing MiRNAs

4.1 Abstract

Glioblastoma multiforme (GBM) is a type of central nervous system (CNS) disease that poses great threat to human health. Recently found to play key roles in GBM initiation and progression, microRNA (miRNA) are small gene regulators generated from the DNA nontranscriptional regions. Targeting the misregulated miRNA in the diseased cells might enable the development of novel targeted therapy for GBM. In this chapter, a redox responsive micelle-like nanoparticle delivery system was engineered with methoxy-poly(ethylene glycol-b-lactide-b-arginine) block copolymer (mPEG-PLA-SS-R_{15}). Using confocal laser live cell imaging, the redox responsive feature was found to contribute significantly to oligonucleotides dissociation from the micelleplexes and lead to higher delivery efficiency in dual luciferase assay. More importantly, for the first time, micelleplexes were found to have significantly better stability in cerebrospinal fluid (CSF) than in human plasma, indicating the advantage of applying micelleplexes for CNS disease.

The micelleplexes also demonstrated high delivery efficiency in CSF, suggesting potential performance *in vivo*. The redox responsive delivery system is a promising delivery platform for the treatment of CNS disease with miRNA therapy.

4.2 Introduction

Glioblastoma multiforme (GBM) is a fatal brain tumor with an annual incidence of approximately 5 in 100,000 people, 99% of GBM patients die of the disease with a median survival of 15 months despite aggressive intervention, specifically neurosurgery, radiation and chemotherapy [1]. Unfortunately, over the last two decades, few effective therapeutic advances were reported in the field other than Temozolomide [2]. The intrinsic distinct properties of GBM make new therapy development extremely challenging. The existence of blood-brain barrier limits drug delivery routes. More importantly, instead of metastasizing to other location, GBM resides in non-renewable normal brain tissue and diffusely invade into normal brain parenchyma, limiting treatment options to those that will not cause unacceptable long-term neuro-cognitive dysfunction [3]. Thus, targeted therapy that specifically aims GBM genetic characteristics is one of the most promising directions

for new drug development.

In the last decade, a type of short noncoding RNAs, miRNAs, was discovered to function as gene regulators of multiple target genes through seed pairing with 3' untranslated region (UTR) of mRNA [4]. MiRNAs were found to play critical roles in many steps of the tumorigenic process, including cellular proliferation, invasion, apoptosis, angiogenesis, and stemness of various types of cancer, including GBM [5, 6]. One of the key characteristics of GBM is its cellular heterogeneity, specifically when one specific oncogenic gene is targeted, the tumor cells tend to find alternative compensating pathways [3]. MiRNA can regulate a network of genes through seed pairing. In other words, when a miRNA is artificially modulated, multiple cancer-related signaling pathways could be regulated simultaneously. It is believed that new GBM-targeted therapy could be developed by targeting misregulated miRNAs, especially miR-21 [7-12].

Due to the negatively charged nature and instability of nucleic acids, effective delivery vehicles are needed to achieve cellular uptake and protect nucleic acids against enzymatic degradation *in vivo* [4]. Recently, micelleplexes have attracted significant scientific

attention for nucleic acid delivery, where cationic polymer is attached to hydrophobic polymer block to drive micelles formation in aqueous environment through hydrophobic segment aggregation before loading nucleic acids via electrostatic interactions. In some cases, hydrophilic polymers, such as polyethylene glycol (PEG) blocks, are also included to enhance steric stability of micelleplexes. Thermodynamically speaking, micelleplexes are more stable than polyplexes since hydrophobic and electrostatic interactions are entropically driven processes, which cooperatively contribute to micelleplexes formation and stability [13].

However, micelle-based drug delivery has been plagued by stability issue in systemic administration [14]. Upon injection, charged nanocarriers are confronted with various biological components, mainly blood cells and serum proteins, which causes early release of nucleic acids and system disassembly [15]. Cerebrospinal fluid (CSF) is a clear, colorless body fluid present in the brain and spine [16]. It provides physical support for the brain, and is believed to absorb and carry away toxic metabolic byproducts [17]. The protein concentration in human CSF is 20 mg/dL, much lower than the protein

concentration of 6, 000 mg/dL in human serum [18]. In this study, we hypothesized that micelleplexes have better stability in CSF than human plasma. A micelleplex system was built, which is composed of hydrophilic arginine-rich cell penetrating peptide (R_{15}) conjugated methoxy-poly(ethylene glycol-b-lactide) (mPEG-b-PLA) block copolymer. The miRNAs silencing molecule, anti-miRNAs, were complexed with R_{15} in the hydrophilic corona through electrostatic interactions. The PEG outer layer can ensure steric stability and prevent rapid clearance and PLA is readily biodegradable. (Figure 4.1)

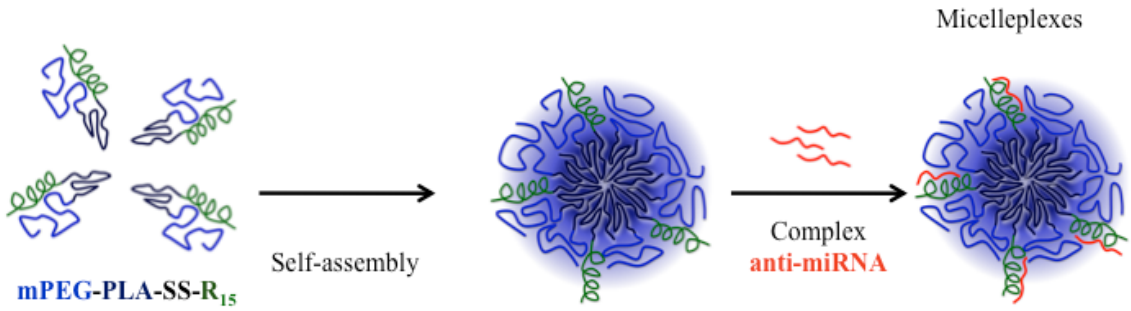

Figure 4.1. Schematic illustration of micelleplexes assembly.

Research has shown that intracellular redox potential is essential for controlling cellular functions by influencing the status of redox-sensitive macromolecules and protect against oxidative stress [19]. Small molecule- and protein-based redox buffer systems, including

GSH/GSSG, cysteine/cystine, and oxidized/reduced thioredoxin, constitute intracellular redox homeostasis [20]. Intracellular glutathione (GSH) concentration (~10 mM) is significantly higher than the level in extracellular environment (<2 μM) [21]. This dramatic difference in redox potential can serve as a trigger for drug delivery. A redox responsive disulfide bond was incorporated between mPEG-b-PLA and R_{15} to enhance anti-miRNAs release by promoting micelle disassembly in GSH rich cytosol. (Figure 4.2)

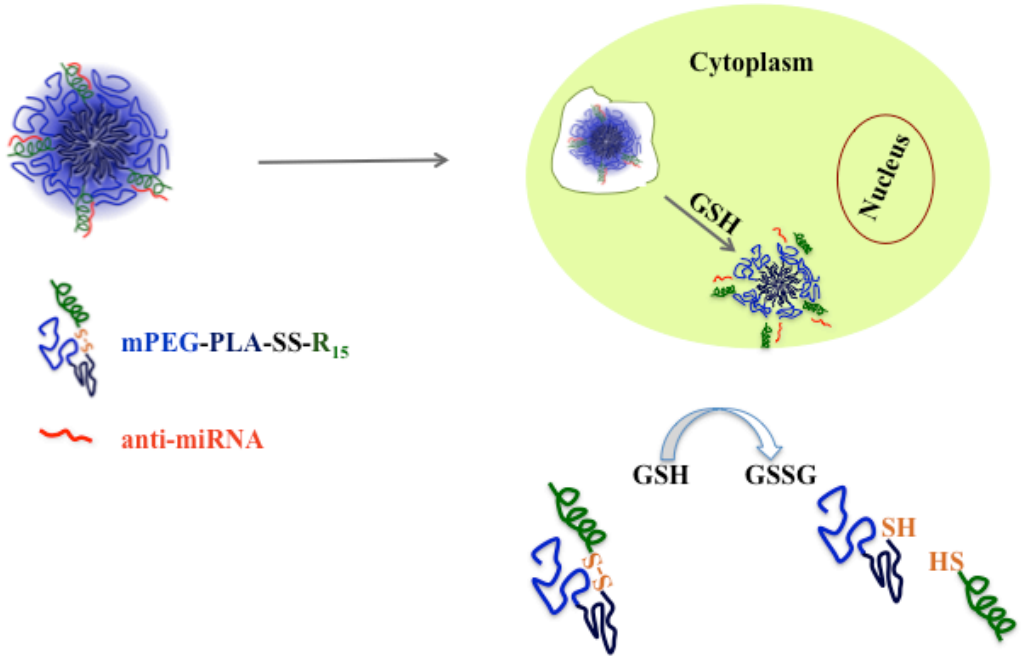

Figure 4.2. Schematic illustration of micelleplexes disassembly in the presence of intracellular reducing environment.

Using GBM as a disease model, we tested the anti-miRNAs delivery efficiency of redox-R_{15} micelleplexes in CSF, where the micelleplexes demonstrated superior stability. Both redox-R_{15} and nonredox-R_{15} micelleplexes successfully delivered anti-miR-21 to glioblastoma cells in CSF, but the redox-R_{15} micelleplexes showed significantly higher delivery efficiency, suggesting the great potential of micelleplexes for treating CNS disease.

4.3 Materials and Methods

4.3.1 Materials

Carboxyl terminal-mPEG2000-PLA3000-COOH was purchased from Advanced Polymer Materials (Montreal, Canada). Ac-CR_{15}-NH_2 and $CR_{15}K(FITC)NH_2$ peptides were synthesized by VCPBIO (Shenzhen, China). *N*-(3-dimethylaminopropyl)-*N*′-ethylcarbodiimide hydrochloride (EDC), *N*-hydroxysuccinimide (NHS), 1,1′-Dioctadecyl-3,3,3′,3′-tetramethylindocarbocyanine perchlorate (DiI), 3,3′-dioctadecyloxacarbocyanine perchlorate (DiO) and N-(2-Aminoethyl)maleimide trifluoroacetate salt (AEM) were purchased from Sigma Aldrich. 3-(2-pyridyldithio) proprionyl hydrazide (PDPH)

crosslinker was obtained from Fisher. Cy-5 labeled single stranded anti-miRNA was from Invitrogen. MirVana^{TM}miRNA-21 inhibitor (miRBase accession# MIMAT0000076, mature miRNA sequence UAGCUUAUCA-GACUGAUGUUGA) and miRNA inhibitor negative control #1 was purchased from Ambion (Austin, TX). Cerebrospinal Fluid (CSF, Cat No# 991-19-S-5 x 1) was obtained [with Institutional Review Board (IRB) Exemption] from Lee Biosolutions, Inc (St. Louis, MO). Anti-coagulated (citrate) human plasma was purchased (with IRB Exemption) from Innovative Research (Novi, MI). The miR-21 Luciferase Reporter Vector was obtained from Signosis, Inc. (Santa Clara, CA) and the renilla control vector was kindly provided by Dr.Yu Hou in University of Illinois Cancer Center.

Human glioblastoma U251 cell line was received from Dr. Lena Al-Harthi (Rush University). The cell line was maintained in Dulbecco's modified Eagle's medium (DMEM; Gibco) supplemented with 10% fetalbovine serum (FBS), 1 mM sodiumpyruvate, 1% nonessential amino acids, 100 U/mL streptomycin , and 100 U/mL penicillin. Cells were incubated in humidified air and 5% CO_2 at 37°C.

4.3.2 Preparation of redox and nonredox polymer conjugates

Redox polymer conjugates were synthesized using disulfide exchange reaction. Methoxy-PEG2000-PLA3000-COOH (mPEG-PLA), EDC and NHS (100, 40 and 24 mg, respectively) was dissolved in DMSO and stirred for 30 min, after which 14 mg PDPH crosslinker was added, thus modifying mPEG2000-PLA3000 with a pyridyldisulfide functional group at the previous carboxyl termini. Unreacted reagents were removed by dialysis against deionized water for 24 h with a molecular weight cut off of 1000 dialysis membrane. The sample was recovered from the dialysis tube and lyophilized to a white powder. Successful PDPH modification was confirmed with ^{1}H NMR (Figure 1, Appendix A) in $CDCl_3$ using a 400 MHz Bruker DPX-400 spectrometer (Bruker BioSpin Corp., Billerica, MA). To couple mPEG-PLA-PDPH with CR_{15}, 40 mg of mPEG-PLA-PDPH and 10 mg CR_{15} were dissolved in argon degased DMSO and reacted for 6 hours in argon environment before purification with a Sep-Pak C_{18} column. Successful conjugation was confirmed by ^{1}H NMR in DMSO-d_6 [22].

Nonredox control polymer conjugates were synthesized using thiol-maleimide coupling.

Carboxyl terminal-mPEG2000-PLA3000-COOH, EDC and NHS (100, 40 and 24 mg, respectively) was dissolved in DMSO and stirred for 30 min, after which 16 mg AEM crosslinker was added, thus modifying mPEG2000-PLA3000 with a maleimide functional group at the previous carboxyl termini. The purification, conjugation and confirmation steps were the same as the redox polymer conjugates. Successful preparation of the mPEG-PLA-AEM and mPEG-PLA-R_{15} polymer conjugates (Figure 1 & 2, Appendix B) was confirmed with ^{1}H NMR spectra.

4.3.3 Micelleplexes preparation

Micelles and micelleplexes were prepared as previously reported by our group [23]. Briefly, 10 mg copolymer was dissolved in 0.5 mL acetonitrile. Solvent was removed by rotovap to form a polymer matrix. RNAse free water (0.5 mL) was added to rehydrate the polymer film followed by sonication for 5 min to form empty micelles. To prepare micelleplexes, micelles were diluted with RNAse free water to appropriate concentration and added dropwise to RNA solution (10 μM) and incubated for 15 min at room temperature.

4.3.4 Gel shift

The successful loading of anti-miRNAs to micelles was confirmed by a gel shift assay [23]. Briefly, micelleplexes were prepared at predetermined positive to negative (+/-) charge ratios and the resulting micelleplexes were analyzed by electrophoresis using a 20% non-denaturing polyacrylamide gel for 1 h at 80 V in TBE buffer (89 mM Tris-borate, 2 mM EDTA). Following SYBR gold staining, the gel was visualized using a gel documentation system (GelDoc 2000, Bio-Rad, Hercules, CA).

4.3.5 Particle sizing and ζ-potential

The particle size and ζ-potential of micelleplexes were measured in 10 mM HEPES buffer (pH 7.4) with a Nicomp 380 Zeta Potential/Particle Sizer (Particle Sizing Systems, Santa Barbara, CA). The data represent the mean plus or minus (±) the standard deviation (SD) from three independent experiments.

4.3.6 Micelle morphology

The morphology of micelles and micelleplexes were characterized by transmission electron microscopy (TEM, JEM-1220, JEOL Ltd., Japan). A drop of micelles (1 mg/mL)

was placed on a carbon-coated 300 mesh copper grid, followed by staining with 2% (w/v) uranyl acetate solution, and then dried at room temperature.

4.3.7 Stability of micelleplexes in cerebrospinal fluid

The stability of micelleplexes was tested with a Förster resonance energy transfer (FRET) based method [24]. The FRET pair, DiO and DiI, were encapsulated in the hydrophobic core of the micelles by dissolving 1% w/w of DiO and DiI in acetonitrile together with polymer conjugates, respectively. Solvent was removed by rotovap to form a polymer matrix, and then deionized water was added to rehydrate the polymer film followed by sonication for 5 min to form FRET micelles. The unencapsulated dye, precipitated as crystals, was removed by filtering the micelle solution with 0.45 μm syringe filter. Based on the balance between cellular association efficiency and vehicle cytotoxicity, micelleplexes were then prepared as described above at +/-charge ratio 30. The FRET micelleplexes (100 μg/mL, final concentration) were incubated with PBS, CSF and human plasma at 37°C for up to 4 hours. The volume ratio between micelleplexes solution and medium is 1:9 and the total volume is 1 mL. Time-resolved spectra were collected on a

spectrofluorophotometer (RF 1501, Shimadzu, Japan) at excitation wavelength of 484 nm and emission wavelength from 480 to 600 nm. To monitor the relative peak shift between I_{499} (the emission of DiO at 499 nm) and I_{561} (the emission of DiI at 561 nm), the FRET ratio, λ, was calculated from the spectra using Equation 1.

$$\lambda = I_{561}/(I_{561} + I_{499}) \qquad \text{Equation 1}$$

Redox-R_{15}/Cy3-anti-miRNA micelleplexes were prepared at +/- charge ratio 30 in RNAse free water. Micelleplexes solution containing 50 pmoles of anti-miRNAs were added to PBS, CSF or human plasma at 37 °C, respectively, in a final total volume of 100 μL. MiRNA or micelles, at the equivanent mass/moles as the micelleplexes, were added to PBS, CSF or human plasma and used as positive and negative control, respectively. The fluorescence recovery of micelleplexes was normalized against fluorescence intensity of Cy3-anti-miRNA in the same medium. The stability of micelleplexes was monitored for 4 hours after adding to PBS, CSF or human plasma and the microplate was sealed and kept in 37 °C incubator between measurement. The experiment was carried out in Corning black

96 well plate and measured on BioTek Synergy2 Multi-Mode Microplate Reader (Winooski, VT) at excitation 543 nm and emission 570 nm.

4.3.8 Anti-miRNA dissociation from micelleplexes with confocal microscopy

To monitor the anti-miRNA dissociation from micelleplexes in cytoplasm, U251 cells were seeded in 4-chamber 35mm glass bottom dish (In Vitro Scientific, Sunnyvale, CA) at 1.5×10^5 cells per chamber in 500 μL growth media 24 hours before an experiment. The medium was exchanged with OPTI MEM and micelleplexes formed from $CR_{15}K(FITC)NH_2$ micelles and Cy3-anti-miRNA were applied to the chamber. Four hours later, cells were rinsed twice with PBS and the medium was replaced with OPTI MEM. Another twenty hours were given to allow anti-miRNAs dissociate from micelleplexes before imaging. The nuclei were stained with Hoechst 33258 for 5 min before CLSM imaging. CLSM images were acquired using a Zeiss LSM 510 META (Carl Zeiss, Germany) with a water immersion 63× objective (C-Apochromat, Carl Zeiss). Excitation wavelengths were 405 nm (Diode 405), 488 nm (argon laser) and 543 nm (HeNe laser) for Hoechst 33258, FITC, and Cy3, respectively. In order to obtain the 3D information of the dissociation efficiency, 20 slices for 30 cells were obtained with CLSM Z-stack and 30

cells were counted as previously reported [25, 26]. The colocalization ratio between Cy3-anti-miRNA and FITC labeled micelles was measured with Mender's coefficient, M, using ImageJ, which calculates the percentage of red pixels (Cy3) colocalizing with green pixels (lysoTracker) with an automatic threshold [27]. The anti-miRNA dissociation efficiency, ε_{ee}, was calculated, Equation 1.

$$\varepsilon_{ee} = (1 - \mathrm{M}) * 100\% \qquad \text{Equation 1}$$

4.3.9 Anti-miR-21/micelleplexes activity

The efficiency of anti-miRNA delivery was tested using a miR-21 luciferase reporter plasmid [28]. A miR-21 complementary sequence was engineered at 3´ untranslated region of luciferase gene. In the presence of miR-21, Firefly luciferase mRNA is rapidly degraded, thereby producing lower levels of Firefly luciferase. Depending on the delivery efficiency of anti-miR-21, Firefly luciferase level will be increased due to miR-21 inhibition. Renilla expression vector is always cotransfected for normalization of well-to-well variation.

U251 cells were seeded in white 96 well plate at 10,000 per well. The cells were cultured

for 24 to 48 hour to achieve at least 80% confluence at the time of transfection. Anti-miR-21/micelleplexes were prepared as described above. The old medium was removed and replaced with CSF containing the micelleplexes. It was shown that culturing U251 cells with CSF up to 4 hours does not affect cell viability. Four hours after the micelleplexes transfection, miR-21 Firefly luciferase vector and Renilla control vector was cotransfected with Dharmacon DharmaFECT™ Duo Transfection Reagents as the company protocol instructed. The Firefly luciferase activity was measured with Dual-Luciferase® Reporter Assay System (Promega) by following the reagent protocol.

4.4 Result and Discussion

To synthesize the mPEG-PLA-SS-R_{15} (Figure 4.3), the carboxyl terminal of mPEG-PLA-COOH was first reacted with the hydrazide group on PDPH crosslinker to bring in the disulfide bond. Successful preparation of redox conjugates were confirmed by ^{1}H NMR after purification with C_{18} column. The guanidine group (-NHCH=NHNH$_2$-, δ 7.43) in CR_{15} and the proton (-CO-CH(CH$_3$)-O-, δ 5.19) in the PLA segment were present in the NMR spectrum of the final product. (Figure 4.4) The R_{15} substitution rate was calculated

based on the intensity ratio between the proton peak of the guanidine group and that of the PLA segment, which is around 30%.

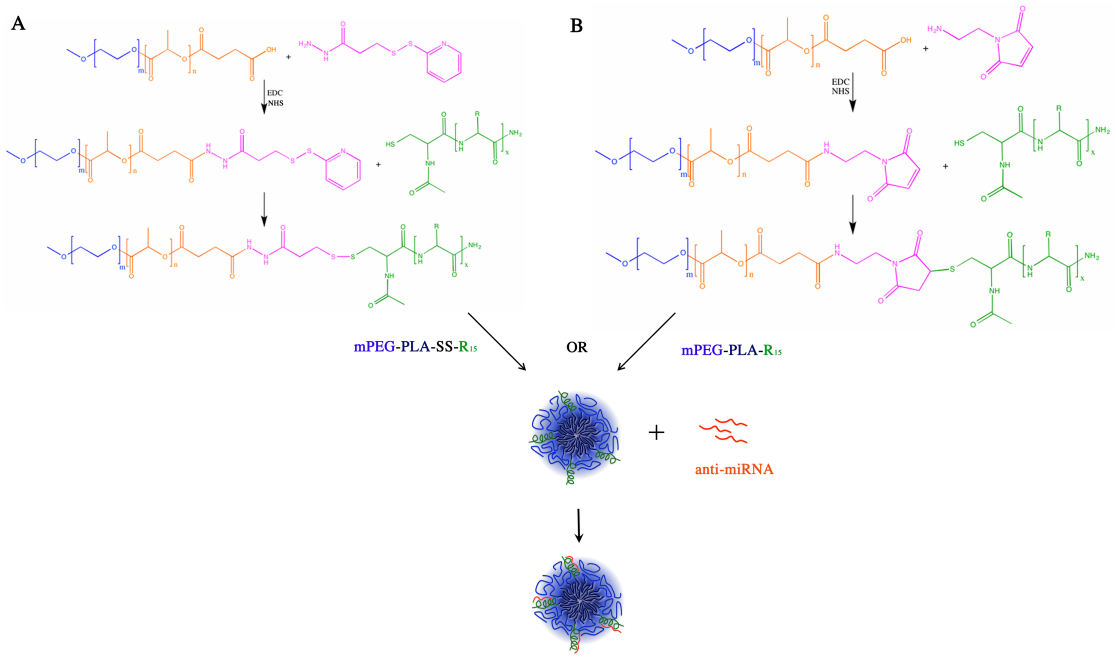

Figure 4.3. Chemical reaction scheme for redox (A) and nonredox (B) polymer conjugates.

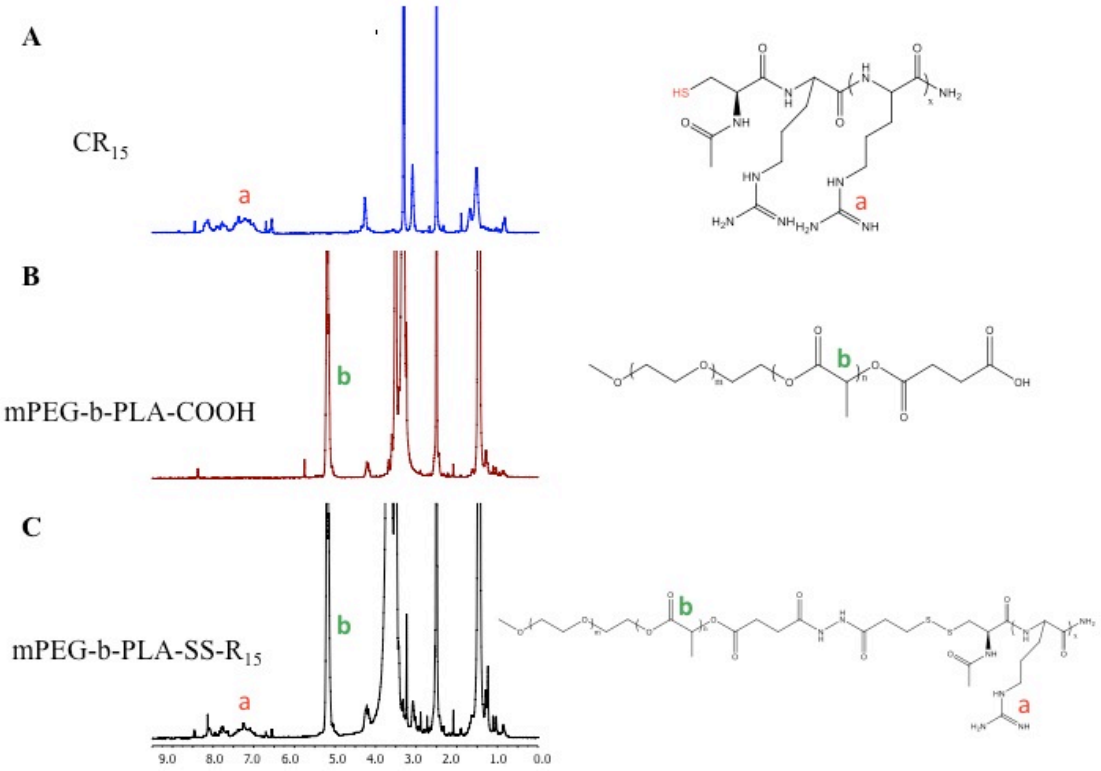

Figure 4.4. ^{1}H NMR spectra of (A) CR_{15} (B) mPEG-PLA-COOH (C) mPEG-PLA-SS-R_{15}. The purified products have characteristic peaks from both guanidine group (a, δ 7.43, 4H) in R_{15} and PLA segment (b, δ 5.19, 1H).

Characterization of micelleplexes

We hypothesized that the triblock copolymer, mPEG-PLA-SS-R_{15} will form micelles with a core-shell conformation in aqueous environment where the hydrophobic block PLA collapse and the mPEG and R_{15} block intertwine to constitute a hydrophilic corona. The oligonucleotides will be loaded onto the micelles through electrostatic interaction with the

oligoarginine block on the surface. We have previously confirmed this conformation with ^{1}H NMR [23]. The antimiRNA condensing ability of micelles were assessed by gel shift assay. As expected, redox-R_{15} and nonredox-R_{15} micelles demonstrated similar anti-miRNA condensing ability due to their very similar oligoarginine conjugation rate, tight micelleplexes were formed at above +/- charge ratio 5. (Figure 4.5A) The particle size and zeta potential of micelles were also tested (Figure 4.5B). The morphology of redox-R_{15} and nonredox-R_{15} micelles before and after loading anti-miRNA was characterized by TEM, all of which demonstrated spherical shape (Figure 4.5C).

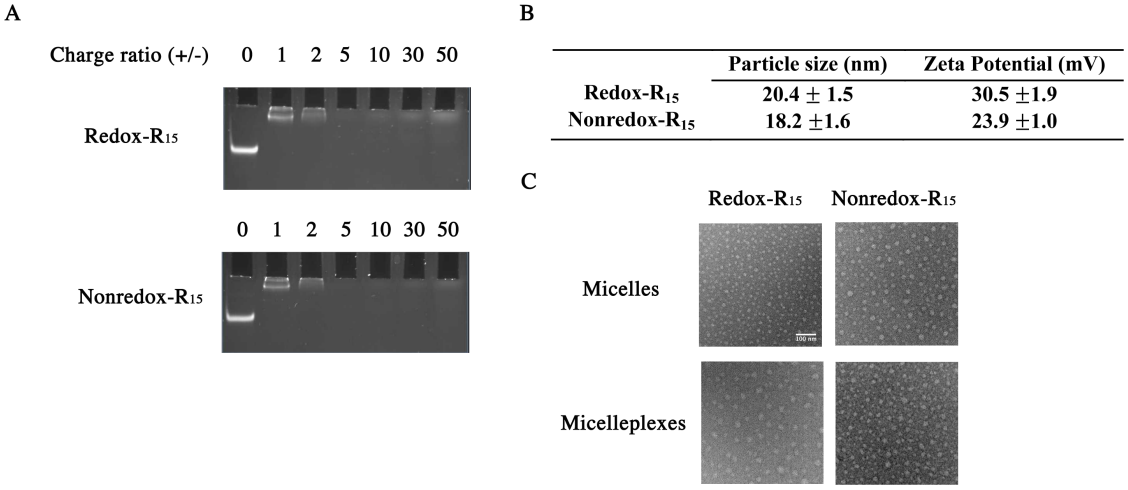

Figure 4.5. Micelleplexes characterization. (A) Redox-R_{15} and Nonredox-R_{15} micelles complexation with anti-miRNA at +/- charge ratios of 1, 2, 5, 10, 30 and 50. (B) Particle size and zeta potential of Redox-R_{15} and Nonredox-R_{15} micelles. (C) TEM characterization of Redox-R_{15} and Nonredox-R_{15} micelles and micelleplexes morphology, the scar bar is 100 nm.

Stability of micelleplexes in Cerebrospinal Fluid

Stability is one of the most critical challenges facing micelles application for drug delivery: small molecule encapsulated micelles tend to fall apart below critical micelle concentration while in micelleplexes the nucleic acid often suffer from early release due to competition from the complex components in the blood serum, mostly blood cells and proteins [13, 14]. Cerebrospinal fluid (CSF) in the brain constitutes a ‘water bath’ within the meninges and acts as a cushion to protect the brain from injury with position or

movement [29]. The CSF contains on average 20 mg/dl protein, significantly lower than the 6, 000 mg/dl protein concentration in plasma [18].

Hence, we hypothesized that micelleplexes will have better stability in human CSF than plasma. A FRET based method was used to test the micelleplexes stability. Two hydrophobic fluorophores, DiO and DiI, were encapsulated in the hydrophobic core of the micelleplexes. The FRET phenomenon will disappear if the DiO and DiI are released due to micelleplexes disassembly. The FRET ratio, λ, was used to monitor the relative peak shift between I_{499} (the emission of DiO at 499 nm) and I_{565} (the emission of DiI at 565 nm) as the stability of micelleplexes changes in the presence of different media [24]. Comparing to micelleplexes in PBS, there was immediate micelleplexes disassembly happening right after the micelleplexes was mixed with CSF and human plasma (Figure 4.6A, t=0 hour). However, micelleplexes demonstrated significantly better stability in CSF than in human plasma, only around 10% lower than in PBS. The stability of redox-R_{15} micelles without anti-miRNA loading was very similar to the redox-R_{15} micelleplexes, suggesting anti-miRNA loading did not affect micelles stability (Figure 4.6B). Due to the fact that the

DiO/DiI pair was loaded in the micelle core, the FRET-based assay can test the stability of micelle polymer assembly but not the electrostatic association between anti-miRNA and micelles. Yet one of the critical challenges facing micelleplexes is the loss of nucleic acids due to competition from complex components in plasma before reaching disease sites.

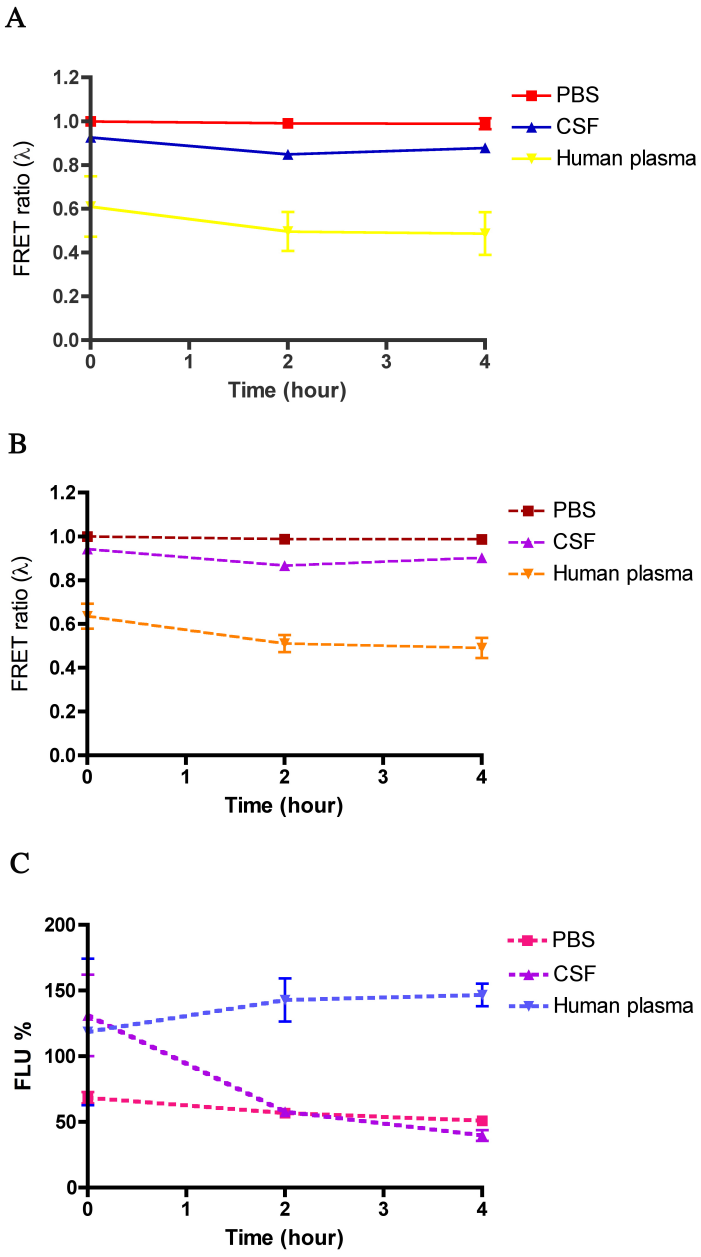

Figure 4.6. Stability of micelleplexes and micelles in different media. (A) Micelleplexes stability in PBS, CSF and human plasma (B) Micelles stability in PBS, CSF and human plasma (C) Stability of the association between Cy3-anti-miRNA and micelles in PBS, CSF and human plasma. Data were presented as the mean plus or minus (±) standard error of the mean (S.E.M.). Three independent replicates of each experiment were performed.

Fluorescence quenching assay is a common method for testing nucleic acids condensation ability of cationic polymer [30, 31]. The fluorescence intensity of fluorophore-labeled nucleic acids is quenched by the close spatial proximity in complexes where many nucleic acids are compacted. On the contrary, the fluorescence intensity of Cy3-anti-miRNA should recover if the nucleic acids are released from the micelleplexes. Figure 4.6C, the fluorescence intensity of Cy3-anti-miRNA/micelleplexes in PBS is around 68.4% that of free Cy3-anti-miRNA in PBS and the fluorescence quenching remain relatively constant in 4 hours, suggesting the anti-miRNAs were tightly condensed by micelleplexes in PBS. The fluorescence intensity of Cy3-anti-miRNA/micelleplexes was recovered immediately after mixing with the human plasma, suggesting Cy3-anti-miRNA release from the micelleplexes due to competition of the complex components in plasma. Surprisingly, the fluorescence intensity of Cy3-anti-miRNA/micelleplexes in CSF dropped to the same level as in PBS at 2 and 4 hours after the initial fluorescence recovery immediately after mixing with CSF. The initial fluorescence recovery could be due to CSF protein competition, which loosened the micelleplexes structure. However, due to the significantly lower protein

concentration in CSF, such competition was not enough to cause anti-miRNA release and/or micelles disassembly. Instead, a protein corona might form on the surface of the micelles, which further condensed the micelleplexes.

Anti-miRNA dissociation from micelleplexes

Micelleplexes formation (complexation) and gene release from the micelleplexes (decomplexation) are major events in polymeric nucleic acid delivery [32]. The unpackaging of nucleic acid from micelleplexes requires thoughtful design considerations because the release of nucleic acids payloads from carrier in cytoplasm is a necessary step for effective nucleic acids delivery [33]. To enhance anti-miRNA release from the micelleplexes after cellular uptake, we included a disulfide bond between the mPEG-PLA block and polyarginine block. We hypothesized that the polyarginine block will leave the micelle in presence of high concentration of glutathione in the cytoplasm and thus facilitate anti-miRNA dissociation from the delivery system. To test the hypothesis, we fluorescently labeled the micelles on the polyarginine block with FITC and prepared micelleplexes with Cy3-labeled anti-miRNA. The dissociation of Cy3-anti-miRNA from the micelleplexes was

monitored with confocal laser living cell microscopy at 4 and 24 hours post delivery. The redox and nonredox micelleplexes had similar RNA dissociation kinetics at 4 hours but redox micelleplexes showed apparently more RNA dissociation at 24 hours. (Figure 4.7A) Using the images obtained from confocal Z-stack mode scanning, RNA dissociation quantification shows that redox responsive micelleplexes had significantly higher dissociation rate than nonredox control group at 24 hours post transfection. (Figure 4.7B) This suggests that redox responsive function contributed to micelleplexes disassembly, which might lead to better anti-miRNA delivery efficiency.

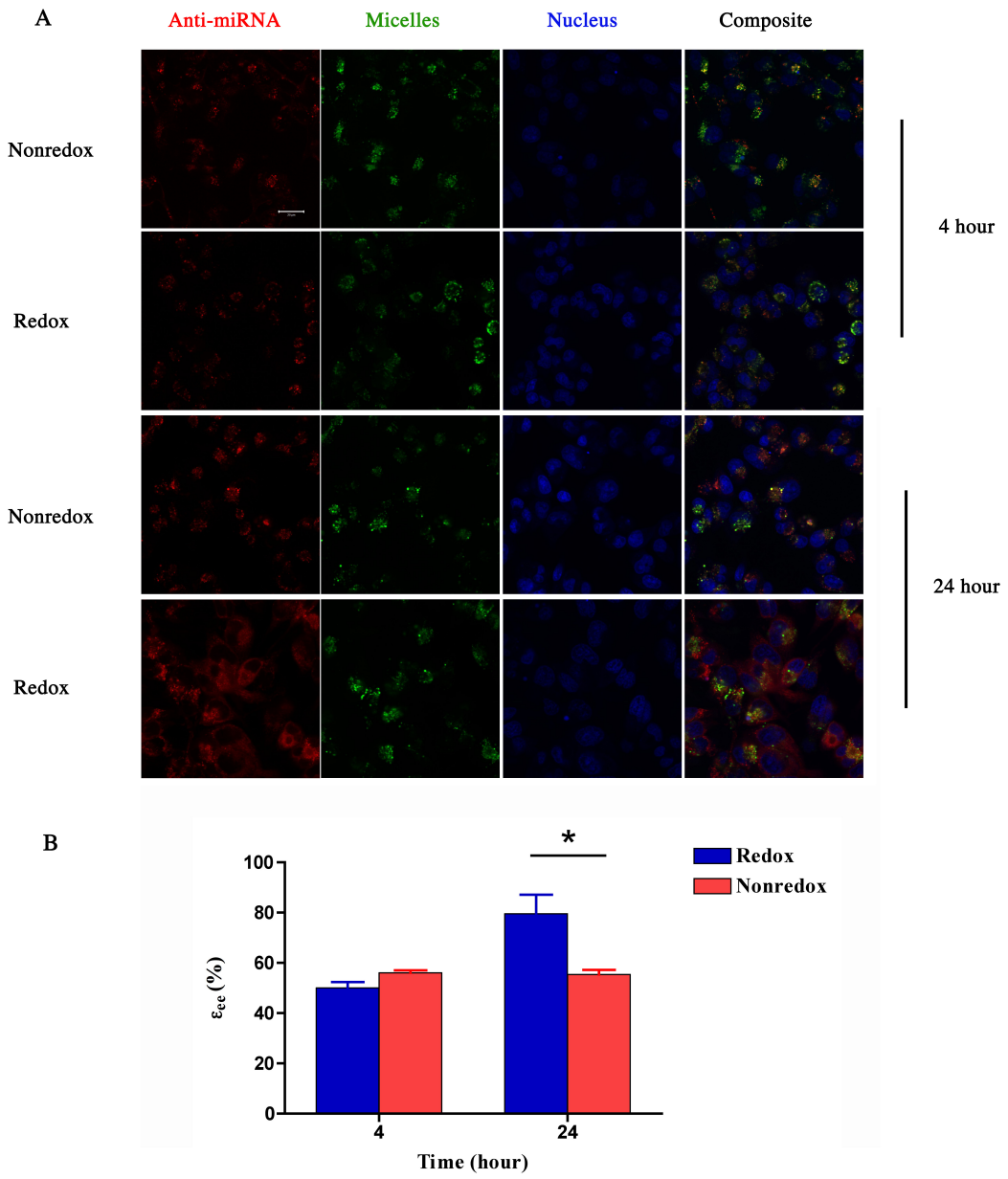

Figure 4.7. CLSM observing anti-miRNA dissociation from micelleplexes. (A) Represented CLSM images. Red: Cy3-anti-miRNA, Green: FITC-micelles, Blue: Nucleus, and the composite of the three pseudocolor images where the Cy3-anti-miRNA concentration was 100 nM in association with micelles at a charge ratio of 30. Scale bar is 20 μm. Top two rows: imaging at 4 hours after delivery; bottom two rows, imaging at 24 hours after delivery, micelles containing medium was replaced with fresh medium at 4 hours to stop further cellular uptake. (B) Quantitative analysis of anti-miRNA dissociation rate. Cy3-anti-miRNA/redox-R_{15} micelleplexes (blue bars) and Cy3-anti-miRNA/nonredox-R_{15} micelleplexes (red bars). Dissociation rate was calculated for 30 individual cells. Data were presented as the mean plus or minus (±) standard error of the mean (S.E.M.). * indicates $p < 0.05$.

Anti-miR-21/micelleplexes delivery efficiency in Cerebrospinal Fluid

To assess the suitability of the micelleplex system for glioblastoma treatment, we tested the anti-miR-21/micelleplexes delivery efficiency with dual luciferase assay in glioblastoma cell line U251. The micelleplexes were incubated with cells in the presence of CSF for 4 hours and then full growth medium containing 2 fold FBS was added to the wells. The amount of redox and nonredox micelles was within the non toxic range of delivery carrier (Figure 4.8). Using CSF as culturing media, redox micelleplexes showed significantly better delivery efficiency than nonredox micelleplexes control, consistent with the anti-miRNA dissociation result (Figure 4.9), which clearly demonstrated the advantage of incorporating the redox responsive feature in anti-miRNA delivery system.

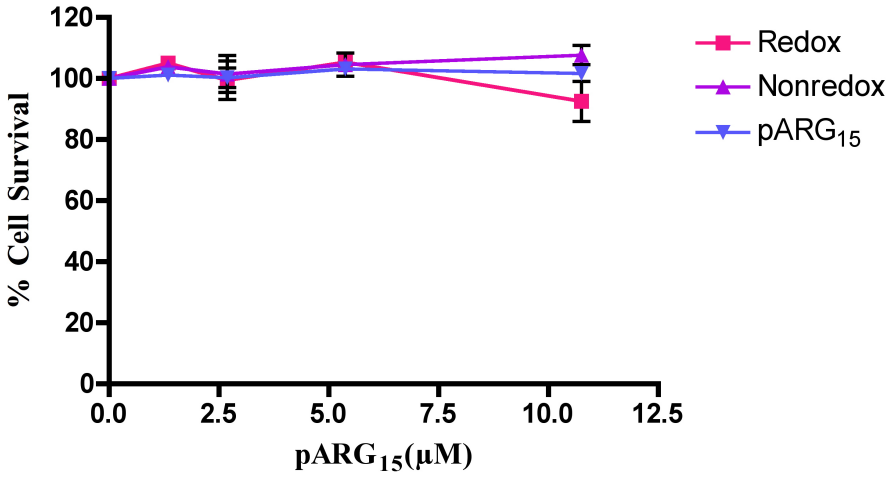

Figure 4.8. Cytotoxicity of redox and nonredox micelles to U251 cells. Different amount of micelles were added to U251 cells and cultured in CSF for 4 hours followed by further incubation in full growth medium for 48 hours as in the dual luciferase assay. Data were presented as the mean plus or minus (±) standard error of the mean (S.E.M.). Three independent replicates of each experiment were performed.

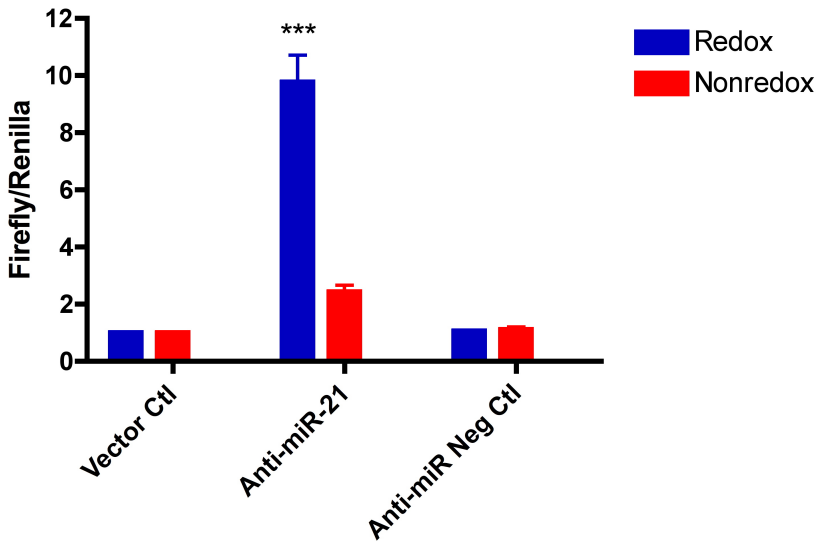

Figure 4.9. Anti-miR-21/micelleplexes delivery efficiency with dual luciferase assay. The delivery efficiency of redox-R_{15} micelleplexes (blue bars) and nonredox-R_{15} micelleplexes (red bars) were compared by complexing anti-miR-21 and transfecting U251 glioblastoma cells in cerebrospinal fluid. The firefly luciferase level was normalized with renilla luciferase level. Data were presented as the mean plus or minus (±) standard error of the mean (S.E.M.). Three independent replicates of each experiment were performed. *** indicates $p < 0.0001$.

Small silencing RNA release from delivery carrier is a rate-limiting step for oligonucleotides delivery and our result shows that redox sensitive disassembly design could lead to more effective delivery. Three-dimension quantification with confocal microscopy supports our hypothesis that redox-responsive feature leads to more anti-miRNAs dissociation from micelleplexes. However, the enhanced anti-miRNAs delivery

efficiency of redox-R_{15} micelleplexes observed in dual luciferase assay may not be exclusively due to increased anti-miRNAs release. When the redox-R_{15} micelleplexes respond to the reducing milieu in cells, it is highly possible that the R_{15} block and anti-miRNAs remain associated after being cleaved from the mPEG-PLA block. Due to the different physicochemical properties of R_{15}/anti-miRNAs polyplexes and nonredox-R_{15} micelleplexes, they could have different intracellular trafficking routes, which are believed to contribute to small silencing RNA delivery efficiency [34]. Thus, it would be beneficial to investigate the effect of incorporating redox responsive feature on micelleplexes intracellular trafficking in future studies.

Most delivery efficiency of nucleic acids carrier was first screened in standard cell culture medium *in vitro*. For the first time, we test the transfection efficiency of micelleplexes in CSF. Upon contacting with biological fluids, nanoparticles are confronted with complex proteins, which form a coating on nanoparticle surface known as the protein corona [35]. It is now believed that "bare" nanoparticle does not exist *in vivo* [36]. Tenzer et al reported that rapid corona formation on silica and polystyrene nanoparticles after mixing with

human plasma affects haemolysis, thrombocyte activation, nanoparticle uptake and endothelial cell death at an early exposure time [37]. However, a lot of studies investigating the effect of nanoparticle design criteria and surface properties were conducted in cell culture medium, which deteriorate the clinical impact of those results. Furthermore, it is of utmost clinical impact to investigate the components of nanoparticle's protein corona after mixing with CSF and the effect of the protein corona in nanoparticle's fate and function inside of the brain.

4.5 Conclusions

A redox responsive micelle delivery system for miRNA therapy was built and the redox responsive feature was found to contribute significantly to delivery efficiency due to enhanced cargo release in the cytoplasm. In addition to the miRNA silencing efficiency, the micelleplexes are nontoxic in the conditions tested and are effective even when administered in CSF, suggesting potential *in vivo* delivery ability. In the recent two decades, a plethora of nonviral synthetic delivery carriers have been developed and

designed for systemic administration. Despite the significant advances in understanding delivery barrier and chemical engineering technology, their critical issue of systemic clearance has not been overcome. For the first time, micelleplexes were demonstrated to have better stability in CSF than in human plasma, suggesting potential advantage of applying such delivery system for brain disease and avoiding the stability challenge that have been plaguing micelle-based drug delivery for systemic administration.

4.6 References

[1] A. Omuro, L.M. DeAngelis, Glioblastoma and other malignant gliomas: a clinical review, Jama, 310 (2013) 1842-1850.

[2] M.M. Mrugala, J. Adair, H.P. Kiem, Temozolomide: Expanding its role in brain cancer, Drugs Today (Barc), 46 (2010) 833-846.

[3] H.A. Fine, New strategies in glioblastoma: exploiting the new biology, Clin Cancer Res, 21 (2015) 1984-1988.

[4] Y. Zhang, Z. Wang, R.A. Gemeinhart, Progress in microRNA delivery, J Control Release, 172 (2013) 962-974.

[5] R. Garzon, G. Marcucci, C.M. Croce, Targeting microRNAs in cancer: rationale, strategies and challenges, Nat Rev Drug Discov, 9 (2010) 775-789.

[6] A.G. Bader, D. Brown, M. Winkler, The promise of microRNA replacement therapy, Cancer Res, 70 (2010) 7027-7030.

[7] J.A. Chan, A.M. Krichevsky, K.S. Kosik, MicroRNA-21 is an antiapoptotic factor in human glioblastoma cells, Cancer Res, 65 (2005) 6029-6033.

[8] G. Gabriely, T. Wurdinger, S. Kesari, C.C. Esau, J. Burchard, P.S. Linsley, A.M. Krichevsky, MicroRNA 21 promotes glioma invasion by targeting matrix metalloproteinase regulators, Mol Cell Biol, 28 (2008) 5369-5380.

[9] A.B. Gaur, S.L. Holbeck, N.H. Colburn, M.A. Israel, Downregulation of Pdcd4 by mir-21 facilitates glioblastoma proliferation in vivo, Neuro Oncol, 13 (2011) 580-590.

[10] S.K. Hermansen, R.H. Dahlrot, B.S. Nielsen, S. Hansen, B.W. Kristensen, MiR-21 expression in the tumor cell compartment holds unfavorable prognostic value in gliomas, J Neurooncol, 111 (2013) 71-81.

[11] L.M. Moore, W. Zhang, Targeting miR-21 in glioma: a small RNA with big potential,

Expert opinion on therapeutic targets, 14 (2010) 1247-1257.

[12] T. Papagiannakopoulos, A. Shapiro, K.S. Kosik, MicroRNA-21 targets a network of key tumor-suppressive pathways in glioblastoma cells, Cancer Res, 68 (2008) 8164-8172.

[13] G. Navarro, J. Pan, V.P. Torchilin, Micelle-like nanoparticles as carriers for DNA and siRNA, Mol Pharm, 12 (2015) 301-313.

[14] S. Kim, Y. Shi, J.Y. Kim, K. Park, J.X. Cheng, Overcoming the barriers in micellar drug delivery: loading efficiency, in vivo stability, and micelle-cell interaction, Expert Opin Drug Deliv, 7 (2010) 49-62.

[15] R.M. Pearson, H.-j. Hsu, J. Bugno, S. Hong, Understanding nano-bio interactions to improve nanocarriers for drug delivery, MRS Bulletin, 39 (2014) 227-237.

[16] N.A. Brunzel, Fundamentals of Urine and Body Fluid Analysis, 3rd ed., Saunders, St. Louis, MI, USA, 2013.

[17] I.R. Manchester, K.S. Andersson, N. Andersson, A.S. Shiriaev, A. Eklund, A nonlinear observer for on-line estimation of the cerebrospinal fluid outflow resistance, Automatica, 44 (2008) 1426-1430.

[18] E.A. Kabat, D.H. Moore, H. Landow, An Electrophoretic Study of the Protein Components in Cerebrospinal Fluid and Their Relationship to the Serum Proteins, J Clin Invest, 21 (1942) 571-577.

[19] R. Banerjee, Redox outside the box: linking extracellular redox remodeling with intracellular redox metabolism, The Journal of biological chemistry, 287 (2012) 4397-4402.

[20] S.E. Moriarty-Craige, D.P. Jones, Extracellular thiols and thiol/disulfide redox in metabolism, Annu Rev Nutr, 24 (2004) 481-509.

[21] R. Cheng, F. Feng, F. Meng, C. Deng, J. Feijen, Z. Zhong, Glutathione-responsive nano-vehicles as a promising platform for targeted intracellular drug and gene delivery, J Control Release, 152 (2011) 2-12.

[22] Z.X. Zhao, S.Y. Gao, J.C. Wang, C.J. Chen, E.Y. Zhao, W.J. Hou, Q. Feng, L.Y. Gao, X.Y. Liu, L.R. Zhang, Q. Zhang, Self-assembly nanomicelles based on cationic mPEG-PLA-b-Polyarginine(R15) triblock copolymer for siRNA delivery, Biomaterials, 33 (2012) 6793-6807.

[23] Y. Zhang, Y. Liu, S. Sen, P. Kral, R.A. Gemeinhart, Charged group surface

accessibility determines micelleplexes formation and cellular interaction, Nanoscale, 7 (2015) 7559-7564.

[24] J. Lu, S.C. Owen, M.S. Shoichet, Stability of Self-Assembled Polymeric Micelles in Serum, Macromolecules, 44 (2011) 6002-6008.

[25] H. Akita, R. Ito, I.A. Khalil, S. Futaki, H. Harashima, Quantitative three-dimensional analysis of the intracellular trafficking of plasmid DNA transfected by a nonviral gene delivery system using confocal laser scanning microscopy, Molecular therapy : the journal of the American Society of Gene Therapy, 9 (2004) 443-451.

[26] A. El-Sayed, I.A. Khalil, K. Kogure, S. Futaki, H. Harashima, Octaarginine- and octalysine-modified nanoparticles have different modes of endosomal escape, The Journal of biological chemistry, 283 (2008) 23450-23461.

[27] S. Bolte, F.P. Cordelieres, A guided tour into subcellular colocalization analysis in light microscopy, J Microsc, 224 (2006) 213-232.

[28] B. Robertson, A.B. Dalby, J. Karpilow, A. Khvorova, D. Leake, A. Vermeulen, Specificity and functionality of microRNA inhibitors, Silence, 1 (2010) 10.

[29] C.D. Aluise, R.A. Sowell, D.A. Butterfield, Peptides and proteins in plasma and cerebrospinal fluid as biomarkers for the prediction, diagnosis, and monitoring of therapeutic efficacy of Alzheimer's disease, Biochim Biophys Acta, 1782 (2008) 549-558.

[30] M. Zheng, G.M. Pavan, M. Neeb, A.K. Schaper, A. Danani, G. Klebe, O.M. Merkel, T. Kissel, Targeting the blind spot of polycationic nanocarrier-based siRNA delivery, ACS Nano, 6 (2012) 9447-9454.

[31] Y. Zhang, M. Kollmer, J.S. Buhrman, M.Y. Tang, R.A. Gemeinhart, Arginine-rich, cell penetrating peptide-anti-microRNA complexes decrease glioblastoma migration potential, Peptides, 58 (2014) 83-90.

[32] H.S. Hwang, H.C. Kang, Y.H. Bae, Bioreducible polymers as a determining factor for polyplex decomplexation rate and transfection, Biomacromolecules, 14 (2013) 548-556.

[33] C.-K. Chen, Biodegradable Polymeric Materials for Gene and Drug Delivery, in, State University of New York at Buffalo, Ann Arbor, 2013, pp. 249.

[34] L. Rajendran, H.J. Knolker, K. Simons, Subcellular targeting strategies for drug design and delivery, Nature reviews. Drug discovery, 9 (2010) 29-42.

[35] D. Docter, D. Westmeier, M. Markiewicz, S. Stolte, S.K. Knauer, R.H. Stauber, The nanoparticle biomolecule corona: lessons learned - challenge accepted?, Chem Soc Rev, 44 (2015) 6094-6121.

[36] M. Masserini, Nanoparticles for brain drug delivery, ISRN Biochem, 2013 (2013) 238428.

[37] S. Tenzer, D. Docter, J. Kuharev, A. Musyanovych, V. Fetz, R. Hecht, F. Schlenk, D. Fischer, K. Kiouptsi, C. Reinhardt, K. Landfester, H. Schild, M. Maskos, S.K. Knauer, R.H. Stauber, Rapid formation of plasma protein corona critically affects nanoparticle pathophysiology, Nat Nanotechnol, 8 (2013) 772-781.

5 Conclusion and Future Work

5.1 MiRNA Delivery Overview

In the recent two decades, nanomedicine has been one of the focuses of drug delivery field, especially when it comes to cancer therapy, due to the unprecedented potential benefits it could bring, such as specificity and high cargo loading [1]. Standing on the advantages of nanoscale delivery vehicle, gene delivery targets the root of a disease instead of the product of the disease pathology, striving to achieve specificity on an even higher hierarchy. The complexity and heterogeneity of signaling pathways involved in cancer, including tumor initiation, progression, metastasis and chemo/radio resistance accounts for the difficulty of developing effective medicine [2]. The discovery of miRNAs might be the critical piece of the cancer research puzzle since one miRNAs can regulate a broad network of genes involved in different signaling pathways.

Many pioneering research groups have dedicated their efforts in developing delivery system for miRNAs [3-5]. However, fundamental understanding of the unique

physicochemical properties of miRNAs and the corresponding requirements these properties impose on delivery system were often neglected. If continued, this trend will inevitably repeats the pattern that many working systems exist but little instructive information could be extracted. In this dissertation, we aim to shed some light to this aspect. Using oligoarginine as a model for cationic polymers, the study has demonstrated the effect of oligonucleotides conformation on delivery system efficiency, and the potential benefit of fundamental understanding of oligonucleotides loading and unpackaging process. Groundwork for study of such kind is established, which is warranted for developing new miRNA delivery system.

5.2 Scientific Contribution of This Study

Significant progress has been made in confirming the ability of different systems to deliver miRNA, but few have made any clinical impact. One of the key reasons lies in that most of the delivery studies focus on developing a "working system", which often undermines fundamental understanding of the effect of the properties of the delivery system on the delivery outcome. In the gene delivery field, it is often found that little instructive

information for developing other systems can be extracted from a successful case while the failed systems were not published.

In Chapter 2, we set out to test the hypothesis that oligoarginine will have different physicochemical interaction with single-stranded anti-miRNA and double-stranded siRNA due to the conformation disparity between single and double-stranded oligonucleotides. It is well known that double-stranded DNA and small double-stranded siRNA have different requirements for delivery vehicle [6]. However, it is not clear whether the single-stranded small oligonucleotides will vary from double-stranded small oligonucleotides. There is no such information available according to a thorough literature search, and yet the information is critical to the development of delivery system. Physicochemical characterization of single-stranded anti-miRNA/R_8 complexes and double-stranded siRNA/R_8 complexes with gel shift assay, fluorescence quenching assay and dynamic light scattering suggests that R_8 have different interaction with single-stranded anti-miRNA in comparison with double-stranded siRNA. Also, siRNA/R_8 associated with cells to a greater extent than anti-miRNA/R_8 at all of the charge ratios tested, confirming our hypothesis that

the charge density and flexibility differences between single and double-stranded RNA have an influence on their cell association [7].

Complexes formation and gene release from the complexes are major events in polymeric nucleic acids delivery. In Chapter 3, we created a micelles-like nanoparticle delivery model with methoxy-poly(ethylene glycol-b-lactide-b-arginine) and investigated the interaction between charged groups on the micelle surface and miRNAs, which greatly affects the micelleplexes formation process. Surface properties of the micelles were varied by controlling the oligoarginine block length and conjugation density. Depending upon the oligoarginine length and density, micelles exhibited miRNA loading capacity directly related to the presentation of charged groups on the surface. The effect of charged group accessibility of cationic micelle on micelleplex properties provides guidance on future miRNA delivery system design [8].

The unpackaging of nucleic acid from micelleplexes requires thoughtful design considerations because the release of nucleic acids payloads from carrier in cytoplasm is a necessary step for effective nucleic acids delivery [9]. To enhance anti-miRNA release

from the micelleplexes after cellular uptake, we included a disulfide bond between the mPEG-PLA block and oligoarginine block. In Chapter 4, we hypothesized that the polyarginine block will leave the micelle in the presence of glutathione and the reduced environment in the cytoplasm and thus facilitate anti-miRNA dissociation from the delivery system. The redox responsive feature was found to contribute significantly to oligonucleotide dissociation from the micelleplex and lead to higher delivery efficiency, indicating the necessity of including self-disassembly function in nucleic acid delivery carrier. Stability issue has been plaguing micelle systematic administration, specifically small molecule drug containing micelles fall apart below critical micelle concentration while micelleplexes prematurely release nucleic acids when facing competition from the complex proteins in human serum. Yet research proposing micelle-based delivery for systematic application keeps being published. For the first time, I found that hydrophobic small molecule containing micelles and micelleplexes have significantly better stability in cerebrospinal fluid (CSF) than in human plasma, indicating the advantage of applying micelleplex for CNS disease.

5.3 Recommended Future Research

Micelleplexes constitutes one of the most ideal delivery vehicles for small oligonucleotides delivery due to their easy assembly, better thermodynamic stability, and small molecule drug codelivery potential [10]. Often used in nucleic acids delivery, cationic polymers facilitate delivery through nonspecific interaction of positively charged functional groups with negatively charged components on cellular membrane such as proteoglycans [11]. PEGylation is introduced to reduce nonspecific interaction but it also greatly diminishes the transfection efficiency [12]. In Chapter 3, we demonstrated that a balance between PEG block and oligoarginine length determines miRNA loading and the resulting micelleplexes' interaction with cellular membrane. Utilizing the acidic condition of tumor microenvironment [13], I envision that including an acidic pH responsive functional group, such as histidine that contains imidazole functional group in the oligoarginine block could allow the R_8 block in mPEG-PLA-R_8 micelleplexes to extend to the surface and mediate efficient cellular interaction after stably circulating to the tumor site under the protection of PEG hydration layer. Additionally, targeted delivery systems could be built on the mPEG-

PLA-oligoarginine micelleplexes prototype by conjugating targeting moieties to the micelles through PEG terminal modification.

In this dissertation, we have discovered that micelleplexes have superior stability in cerebrospinal fluid (CSF) in comparison to human plasma and redox-R_{15} micelleplexes achieved efficient anti-miR-21 delivery in CSF *in vitro*. Further investigation of the stability *in vivo* by tracking micelleplexes in mouse brain model will no doubt lay the groundwork for exploring micelle-like nanoparticle application in brain disease treatment. The brain parenchyma could limit nanoparticle diffusion due to interstitial space limitation and interaction with extracellular components. The pore size of ECS varies based on the models used for the calculation. Most computational models of neurotransmission assume an ECS width of 20 nm, although it is known that varying this parameter can significantly affect results [14].

The "fluid" pore size is especially meaningful since the flow of CSF contributes to the distribution of nanoparticles in the brain. An *in vivo* diffusion analysis predicts a fluid-filled ''pores'' width of 38–64 nm in rat brain [14]. For the first step, the distribution of micelles

in the presence of tissues and CSF could be investigated with similar model by loading quantum dots in the hydrophobic core of micelles as previously described [15]. After revealing the distribution of micelles in living rat brain, the stability of micelles could be monitored by tracking the FRET signal loss *in vivo* using DiO/DiI loaded micelles as in Chapter 4.

Micelle-based delivery vehicles have been administered through intracranial, intranasal and intravenous routes for treating glioblastoma, Parkinson's, and Alzheimer's [16-19]. However, it is not clear how each delivery route will affect the stability and efficacy of micelleplexes, which is a critical question needs to be answered before translating miRNA therapeutics to clinical brain disease treatment. Intranasal delivery provides a noninvasive way to bypass the BBB and avoid toxicity due to systemic administration. Brain system is commonly believed to be lack of immune system, and large macromolecules are removed from the CSF quite slowly, so they distribute throughout the CSF over time [20], which is beneficial to nanoparticles delivered intracranially. When applying nanoparticle intravenously, mechanism of Blood Brain Barrier (BBB) disruption or active targeting

strategy have to always be included in addition to the stability challenge from complex blood components and reticuloendothelial system (RES) clearance.

This dissertation has demonstrated the effect of oligonucleotides conformation on delivery system efficiency, and the potential benefit of fundamental understanding of oligonucleotides loading and unpackaging process. The research methodology and experimental approaches established here could be applied to investigating the effect of different delivery carrier properties on oligonucleotides loading and release process. The research findings provide guidance for developing small oligonucleotides carrier in the future.

5.4 References

[1] E.K. Chow, D. Ho, Cancer nanomedicine: from drug delivery to imaging, Sci Transl Med, 5 (2013) 216rv214.

[2] D.C. Altieri, Survivin, cancer networks and pathway-directed drug discovery, Nature reviews. Cancer, 8 (2008) 61-70.

[3] Y. Zhang, Z. Wang, R.A. Gemeinhart, Progress in microRNA delivery, J Control

Release, 172 (2013) 962-974.

[4] B. Peng, Y. Chen, K.W. Leong, MicroRNA delivery for regenerative medicine, Adv Drug Deliv Rev, 88 (2015) 108-122.

[5] L.H. Nguyen, H.J. Diao, S.Y. Chew, MicroRNAs and their potential therapeutic applications in neural tissue engineering, Adv Drug Deliv Rev, 88 (2015) 53-66.

[6] C. Scholz, E. Wagner, Therapeutic plasmid DNA versus siRNA delivery: common and different tasks for synthetic carriers, J Control Release, 161 (2012) 554-565.

[7] Y. Zhang, M. Kollmer, J.S. Buhrman, M.Y. Tang, R.A. Gemeinhart, Arginine-rich, cell penetrating peptide-anti-microRNA complexes decrease glioblastoma migration potential, Peptides, 58 (2014) 83-90.

[8] Y. Zhang, Y. Liu, S. Sen, P. Kral, R.A. Gemeinhart, Charged group surface accessibility determines micelleplexes formation and cellular interaction, Nanoscale, 7 (2015) 7559-7564.

[9] C.-K. Chen, Biodegradable Polymeric Materials for Gene and Drug Delivery, in, State University of New York at Buffalo, Ann Arbor, 2013, pp. 249.

[10] G. Navarro, J. Pan, V.P. Torchilin, Micelle-like Nanoparticles as Carriers for DNA and siRNA, Mol Pharm, 12 (2015) 301-313.

[11] K.A. Mislick, J.D. Baldeschwieler, Evidence for the role of proteoglycans in cation-mediated gene transfer, Proc Natl Acad Sci U S A, 93 (1996) 12349-12354.

[12] R.E. Fitzsimmons, H. Uludag, Specific effects of PEGylation on gene delivery efficacy of polyethylenimine: interplay between PEG substitution and N/P ratio, Acta Biomater, 8 (2012) 3941-3955.

[13] F. Danhier, O. Feron, V. Preat, To exploit the tumor microenvironment: Passive and active tumor targeting of nanocarriers for anti-cancer drug delivery, J Control Release, 148 (2010) 135-146.

[14] R.G. Thorne, C. Nicholson, In vivo diffusion analysis with quantum dots and dextrans predicts the width of brain extracellular space, Proc Natl Acad Sci U S A, 103 (2006) 5567-5572.

[15] B. Dubertret, P. Skourides, D.J. Norris, V. Noireaux, A.H. Brivanlou, A. Libchaber, In vivo imaging of quantum dots encapsulated in phospholipid micelles, Science, 298 (2002)

1759-1762.

[16] E.J. Chung, Y. Cheng, R. Morshed, K. Nord, Y. Han, M.L. Wegscheid, B. Auffinger, D.A. Wainwright, M.S. Lesniak, M.V. Tirrell, Fibrin-binding, peptide amphiphile micelles for targeting glioblastoma, Biomaterials, 35 (2014) 1249-1256.

[17] T. Kanazawa, K. Morisaki, S. Suzuki, Y. Takashima, Prolongation of life in rats with malignant glioma by intranasal siRNA/drug codelivery to the brain with cell-penetrating peptide-modified micelles, Mol Pharm, 11 (2014) 1471-1478.

[18] Y. Miura, T. Takenaka, K. Toh, S. Wu, H. Nishihara, M.R. Kano, Y. Ino, T. Nomoto, Y. Matsumoto, H. Koyama, H. Cabral, N. Nishiyama, K. Kataoka, Cyclic RGD-linked polymeric micelles for targeted delivery of platinum anticancer drugs to glioblastoma through the blood-brain tumor barrier, ACS Nano, 7 (2013) 8583-8592.

[19] R.A. Morshed, Y. Cheng, B. Auffinger, M.L. Wegscheid, M.S. Lesniak, The potential of polymeric micelles in the context of glioblastoma therapy, Front Pharmacol, 4 (2013) 157.

[20] W.M. Pardridge, Drug delivery to the brain, J Cereb Blood Flow Metab, 17 (1997)

713-731.

APPENDICES

Appendix A

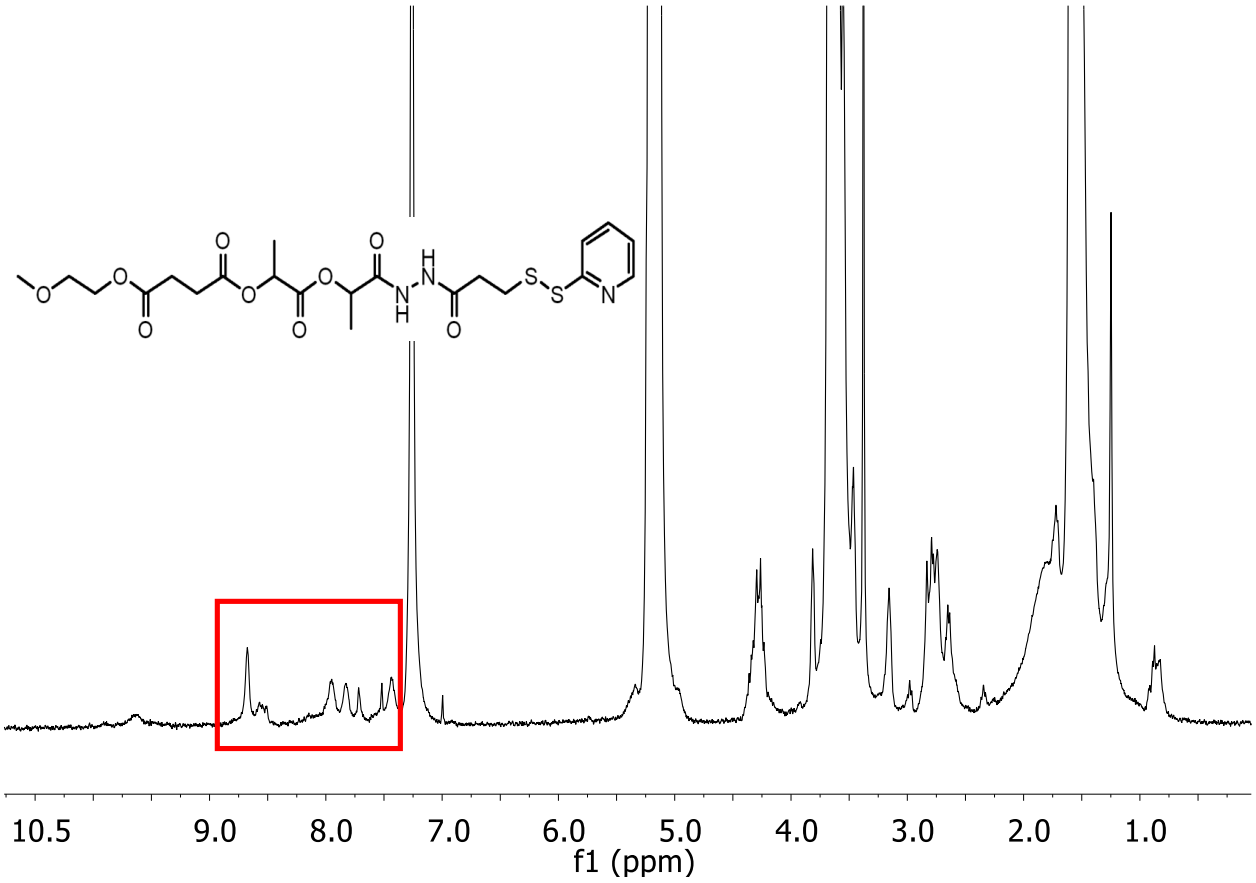

Figure A.1. ^{1}H NMR spectrum of mPEG-PLA-PDP. The purified product was dissolved in $CDCl_3$-*d*, which has the four characteristic peaks from the 3-(2-pyridyldithio) proprionyl hydrazide (PDPH), (Red rectangle, aromatic proton, δ 7.52, 1H; 7.91, 1H; 8.02, 1H; 8.68, 1H).

Appendix B

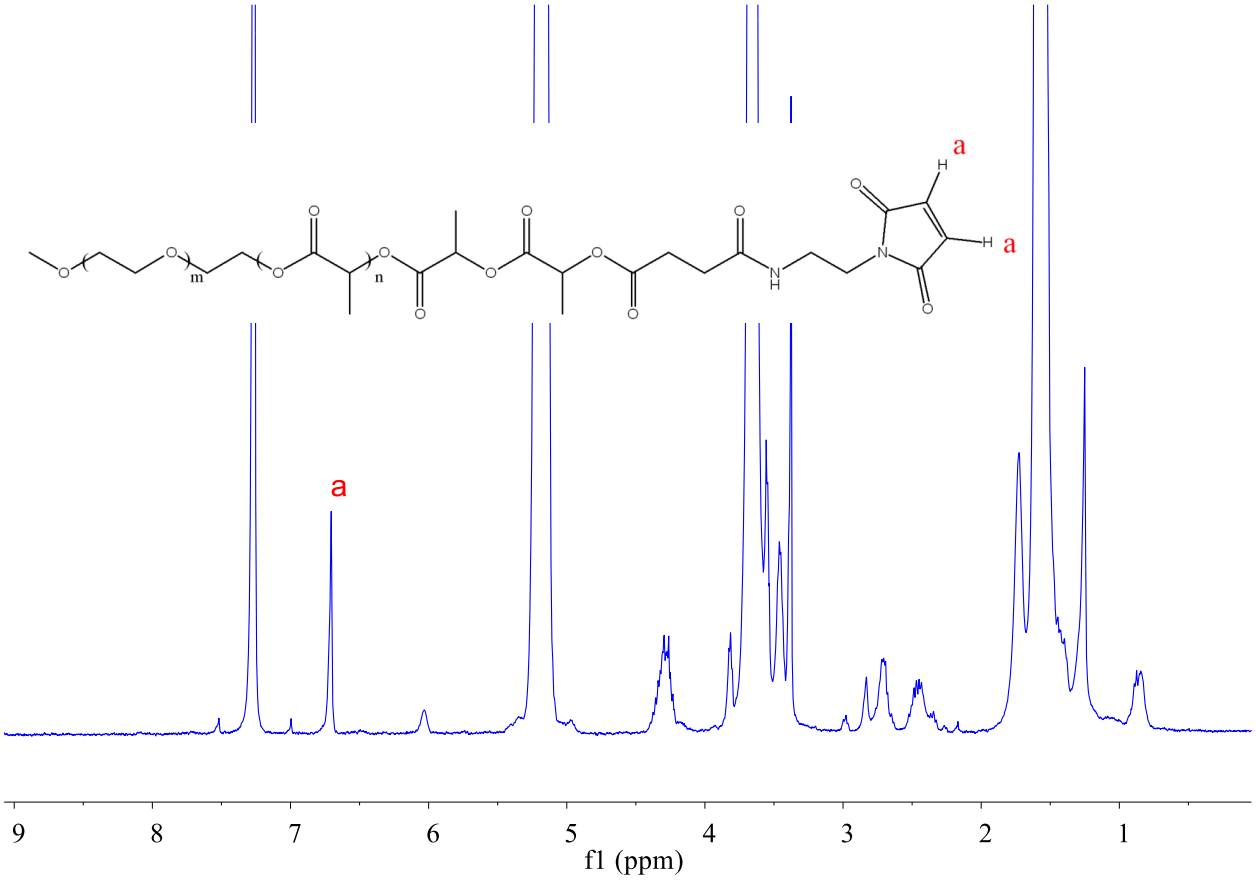

Figure B.1. ^{1}H NMR spectrum of mPEG-PLA-AEM. The purified product was dissolved in $CDCl_3$-*d*, which has the characteristic peak from the N-(2 Aminoethyl)maleimide trifluoroacetate (AEM), (a, δ 6.71, 2H).

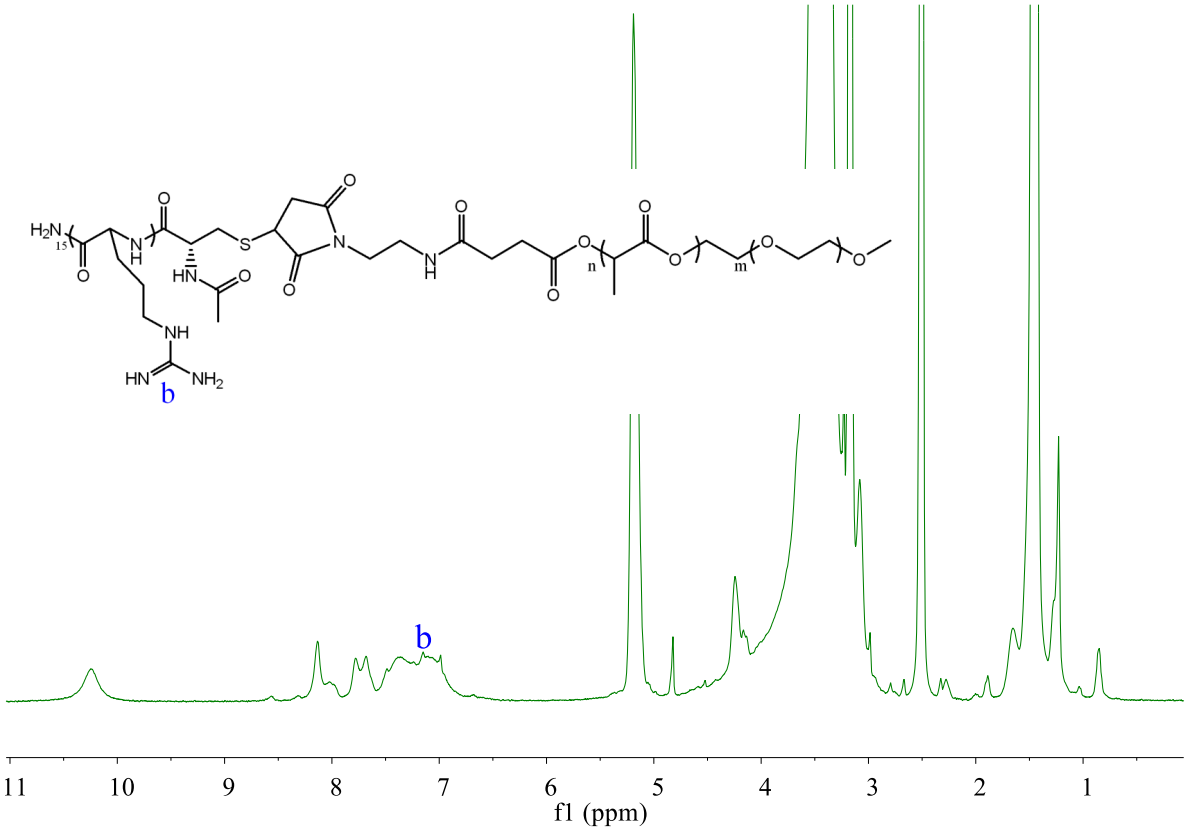

Figure B.2. ^{1}H NMR spectrum of mPEG-PLA-R$_{15}$. The purified product was dissolved in DMSO-d_6, which has the characteristic peaks from the guanidine group in arginine (b, δ 7.20, 4H).

Appendix C

Copyright Clearance Center RightsLink®

Home | Account Info | Help | Live Chat

Title:	Progress in microRNA delivery
Author:	Yu Zhang,Zaijie Wang,Richard A. Gemeinhart
Publication:	Journal of Controlled Release
Publisher:	Elsevier
Date:	28 December 2013

Copyright © 2013 Elsevier B.V. All rights reserved.

Logged in as:
Yu Zhang
University of Illinois
LOGOUT

Quick Price Estimate

I would like to...	reuse in a thesis/dissertation
I would like to use...	full article
My format is...	both print and electronic
I am the author of this Elsevier article...	Yes
I will be translating...	No
My currency is...	USD – $
Quick Price	Click Quick Price

QUICK PRICE CONTINUE

This service provides permission for reuse only. If you do not have a copy of the content, you may be able to purchase a copy using RightsLink as an additional transaction. Simply select 'I would like to..... 'Purchase this content'.

Unclear about who you are?

Exchange rates under license from XE.com.
To request permission for a type of use not listed, please contact Elsevier Global Rights Department.

Are you the author of this Elsevier journal article?

Appendix D

3/3/2015 Rightslink® by Copyright Clearance Center

Copyright Clearance Center RightsLink®

Home | Account Info | Help | Live Chat

Title: Arginine-rich, cell penetrating peptide–anti-microRNA complexes decrease glioblastoma migration potential

Publication: Peptides

Publisher: Elsevier

Date: August 2014

Copyright © 2014 Elsevier Inc. All rights reserved.

Logged in as:
Yu Zhang
University of Illinois

LOGOUT

Quick Price Estimate

I would like to...	reuse in a thesis/dissertation
I would like to use...	full article
My format is...	both print and electronic
I am the author of this Elsevier article...	Yes
I will be translating...	No
My currency is...	USD – $
Quick Price	Click Quick Price

QUICK PRICE CONTINUE

This service provides permission for reuse only. If you do not have a copy of the content, you may be able to purchase a copy using RightsLink as an additional transaction. Simply select 'I would like to..... 'Purchase this content'.

Unclear about who you are?

Exchange rates under license from XE.com.
To request permission for a type of use not listed, please contact Elsevier Global Rights Department.

Are you the author of this Elsevier journal article?

Appendix E

Charged group surface accessibility determines micelleplexes formation and cellular interaction

Y. Zhang, Y. Liu, S. Sen, P. Král and R. A. Gemeinhart, *Nanoscale*, 2015, 7, 7559
DOI: 10.1039/C5NR00095E

Appendix E (continued)

[Original citation] - Reproduced by permission of The Royal Society of Chemistry

If you are the author of this article you still need to obtain permission to reproduce the whole article in a third party publication with the exception of reproduction of the whole article in a thesis or dissertation.

Information about reproducing material from RSC articles with different licences is available on our Permission Requests page.

Appendix F

July 30, 2015

Richard Gemeinhart
Biopharmaceutical Sciences
M/C 865

Dear Dr. Gemeinhart:

The protocol indicated below has been reviewed in accordance with the Institutional Biosafety Committee Policies of the University of Illinois at Chicago and approved on *September 12, 2013* pending the following clarifications. **All clarifications should be in bold, *italic* or highlighted. Please see IBC web site for guidance on editing forms (http://www.research.uic.edu/protocolreview/ibc/forms/editing.shtml).** Only those pages with revisions need to be submitted to the Institutional Biosafety Committee Office, 206 AOB, if revisions result in an exact page-for-page exchange. If an exact page-for-page exchange is not possible, then all pages affected must be resubmitted. Please be sure to address all concerns of the Committee.

Title of Application: Hydrogel Microparticles as Gene Carriers

IBC Number: 13-064

Clarifications:

a. In Form A, item I, remove signature as this assurance and section is N/A to the scope of research proposed.
b. In Form A, item VId, remove check mark from BSL1 and check BSL2 for use of human cells lines.
c. In Biosafety Manual, please address the following:
    i. Item 4.3, please provide specific date of BSC certification.
    ii. Item 4. 3.18, 10% bleach followed by 70 % ethanol needs to be used 70% ethanol is not sufficient for decontamination.
    iii. Item 4.5, contact time must be at least 30 minutes.
    iv. Item 4.7, 10% bleach followed by 70 % ethanol needs to be used 70% ethanol is not sufficient for decontamination.
    i. Item 4.14.4 a and b, please leave this items blank.

Appendix F (continued)

ii. Certification- - All personnel listed in Appendix 1 must read the manual and sign the certification page.

When these clarifications have been made and approved, you will receive a letter of approval. Research may not be initiated under this protocol until that approval is granted.

Thank you for complying with the UIC's Policies and Procedures.

Sincerely,

Randal C. Jaffe, Ph.D.
Chair, Institutional Biosafety Committee

RCJ/mbb
cc: IBC File

Appendix G

UNIVERSITY OF ILLINOIS
AT CHICAGO

Office for the Protection of Research Subjects (OPRS)
Office of the Vice Chancellor for Research (MC 672)
203 Administrative Office Building
1737 West Polk Street
Chicago, Illinois 60612-7227

Notice of Determination of Human Subject Research

October 8, 2014

*20140960
-85327-1*

20140960-85327-1

Richard Gemeinhart, Ph.D.
Biopharmaceutical Sciences
833 S Wood Street, Room 359,
M/C 865
Chicago, IL 60612
Phone: (312) 996-2253 / Fax: (312) 996-2784

RE: **Protocol # 2014-0960**
Protease Activity in Human Plasma

Sponsor: Departmental

Dear Gemeinhart:

☐ The UIC Office for the Protection of Research Subjects received your "Determination of Whether an Activity Represents Human Subjects Research" application, and has determined that this activity **DOES NOT meet the definition of human subject research** as defined by 45 CFR 46.102(f).

You may conduct your activity without further submission to the IRB.

If this activity is used in conjunction with any other research involving human subjects or if it is modified in any way, it must be re-reviewed by OPRS staff.

VITA

Yu Zhang

EDUCATION

2010 –	5th year PhD candidate, Biopharmaceutical Sciences Program, University of Illinois at Chicago
2007 – 2010	Master of Science, Botanical Pharmaceutics, Key Laboratory of Forest Plant Ecology, Ministry of Education, China
2003 – 2007	Bachelor of Science, Life Science, College of Life Sciences, Northeast Forestry University, China

PUBLICATIONS

1. **Zhang Y**, Liu Y, Gemeinhart RA. Charge Group Surface Accessibility Determines Micelleplexes Formation, Stability and Cellular Interaction, Nanoscale. 2015,7, 7559-7564
2. Rayahin JE, Buhrman JS, **Zhang Y**, Gemeinhart RA. High and Low Molecular Weight Hyaluronic Acid Differentially Influence Macrophage Activation, ACS Biomater. Sci. Eng., 2015, 1 (7), pp 481–493
3. **Zhang Y**, Köllmer M, Buhrman JS, Tang MY, Gemeinhart RA. Arginine-rich, Cell Penetrating Peptide-microRNA Inhibitor Complexes Decrease Glioblastoma Migration Potential, Peptides. 2014 Aug;58:83-90.
4. **Zhang Y**, Wang ZJ, Gemeinhart RA. Progress in Nonviral MicroRNA Delivery, J Control Release. 2013 Dec 28;172(3):962-74.
5. Köllmer M, Buhrman JS, **Zhang Y**, Gemeinhart RA. Markers Are Shared Between Adipogenic and Osteogenic Differentiated Mesenchymal Stem Cells. Journal of Developmental Biology and Tissue Engineering. 5(2): 18-25, 2013.
6. **Zhang Y**, Gemeinhart RA. Improving Matrix Metalloproteinase-2 Specific Response of a Hydrogel System Using Electrophoresis. Int J Pharm. 429(1-2): 31-37, 2012.
7. Zu, Y. G., Yuan, S., Zhao, X. H., **Zhang, Y.** & Zhang, X. N. Preparation, activity and

targeting ability evaluation in vitro on folate mediated epigallocatechin-3-gallate albumin nanoparticles. Acta Pharmaceutica Sinica, 2009, 44 (5): 525-531.

8. **Zhang, Y.**, Liu, T. etc. Extracting technique and antioxidant activity of polyphenols from testa of *Quercus Mongolica* Fischer. Bulletin of Botanical Research, 2009, 29 (6): 711-716.
9. Yuangang Zu, **Yu Zhang** etc. Optimization of the preparation process of vinblastine sulfate (VBLS) loaded folate-conjugated bovine serum albumin (BSA) nanoparticles for tumor-targeted drug delivery using response surface methodology (RSM). International Journal of Nanomedicine. 2009:4 321–333.
10. Dongmei Zhao, Xiuhua Zhao, Yuangang Zu, Jialei Li, **Yu Zhang**, Ru Jiang, Zhonghua Zhang. Preparation, characterization, and in vitro targeted delivery of folate-decorated paclitaxel-loaded bovine serum albumin nanoparticles. Int J Nanomedicine. 2010 Sep 20;5:669-77.
11. Liu Yang, Liu Tingting, Yu Xin, **Zhang Yu**, Yang Lei, Zu Yuangang. Optimization for Ultrasound Extraction of Polyphenol from Quercus mongolica Leaves and Its Antioxidant Activity. JOURNAL OF NORTHEAST FORESTRY UNIVERSITY, 2010, 38(1).
12. Qing-yong Li, Liping Yao, Yuan-gang Zu, Hongyan Lv, **Yu Zhang**, Cytotoxicity and Topo I –targeting activity of substituted 10- nitrogenous heterocyclic aromatic group derivatives of SN-38. European Journal of Medicinal Chemistry. 2010, 45(7): 3200-3206.

PATENTS

Gemeinhart RA, **Zhang Y.** Method of Electrophoretic Removal of Unreacted Groups from Materials. Disclosed (DF134; 3/13/2012) and provisional patent application submitted (03/08/2012).

ABSTRACTS AND PROCEEDINGS, PODIA

1. **Yu Zhang**, Jamie E. Rayahin, and Richard A. Gemeinhart. Synthesis of Matrix Metalloproteinase-2 Activable Charged Hydrogel Drug Delivery System. The

Controlled Release Society-Illinois Student Chapter 3rd Annual Symposium. Recent Advances in Nanotechnology for Cancer Therapy. 2011

2. **Yu Zhang (presenting author, 2nd place in poster session)**, Jamie E. Rayahin, and Richard A. Gemeinhart. Use of Pendant Charge with Hydrogels to Modulate Matrix-Mettalloprotease-Stimulated Drug Delivery. Polymers in Medicine and Biology 2011. ACS Division of Polymer Chemistry. Santa Rosa, CA. 2011
3. **Yu Zhang** and Richard A. Gemeinhart. Improving Matrix Metalloproteinase-2 Specific Response of a Hydrogel System Using Electrophoresis. College of Pharmacy Research Day, Chicago, IL. 2012.
4. **Yu Zhang** and Richard A. Gemeinhart. Improving Matrix Metalloproteinase-2 Specific Response of a Hydrogel System Using Electrophoresis. UIC Research Forum, Chicago, IL. 2012.
5. **Yu Zhang**, Melanie Köllmer, Mary Tang, Elizabeth A. Ramirez and Richard A. Gemeinhart. Arginine-rich Cell Penetrating Peptide-microRNA Inhibitor Complexes Decrease Glioblastoma Migration Potential. College of Pharmacy Research Day, Chicago, IL. 2013.
6. Mary Y. Tang, Lillian Nwanah, **Yu Zhang**, and Richard A. Gemeinhart. Multiscale Drug Delivery System: Pluronic F-127 Micelles Encapsulated in PEGDA Hydrogels. College of Pharmacy Research Day, Chicago, IL. 2013.
7. Köllmer M, Buhrman JS, **Zhang Y,** Gemeinhart RA. Markers Are Shared Between Adipogenic and Osteogenic Differentiated Mesenchymal Stem Cells. College of Pharmacy Research Day, Chicago, IL. 2013.
8. **Yu Zhang**, Melanie Köllmer, Mary Tang, and Richard A. Gemeinhart. Arginine-rich Cell Penetrating Peptide-microRNA Inhibitor Complexes Decrease Glioblastoma Migration Potential. The 40th Annual Meeting of the Controlled Release Society, 2013
9. **Yu Zhang,** Yang Liu, Jason Buhrman and Richard A. Gemeinhart. Redox Responsive Polymeric Drug Delivery System for Codelivery of Hydrophobic Drug and Silencing RNAs. College of Pharmacy Research Day, Chicago, IL. 2014.
10. Mary Y. Tang, Lillian Nwanah, **Yu Zhang**, and Richard A. Gemeinhart. Multiscale Drug Delivery System: Pluronic F-127 Micelles Encapsulated in PEGDA Hydrogels.

The 41th, Annual Meeting of the Controlled Release Society, 2014.

11. **Yu Zhang,** Yang Liu, and Richard A. Gemeinhart. Redox Responsive Polymeric Drug Delivery System for Codelivery of Hydrophobic Drug and Silencing RNAs. The 46th Annual Pharmaceutics Graduate Student Research, Chicago, IL. 2014.
12. **Yu Zhang,** Yang Liu, Jason Buhrman and Richard A. Gemeinhart. Redox Responsive Polymeric Drug Delivery System for Codelivery of Hydrophobic Drug and Silencing RNAs. The 41th Annual Meeting of the Controlled Release Society, 2014.
13. Jason Buhrman, Jamie E. Rayahin, **Yu Zhang**, Mary Tang and Richard A. Gemeinhart. Biologically Responsive Recombinant Protein Anchors For Macromolecular Drug Delivery. The 28th Annual Symposium of the Protein Society, San Deigo, CA, 2014. Best Poster Award.
14. Buhrman JS, Rayahin JE, **Zhang Y**, Tang MY, Gemeinhart RA. Biologically responsive recombinant protein anchors for macromolecular drug delivery. Annual Chicago Biomedical Consortium Meeting, Chicago, IL (October 2014).
15. Buhrman JS, Rayahin JE, **Zhang Y**, Tang MY, Gemeinhart RA. Biologically Responsive Recombinant Protein Anchors for Macromolecular Drug Delivery. College of Medicine Research Day, Chicago, IL (November 2014).
16. Rayahin JE, **Zhang Y**, Buhrman JS, Gemeinhart RA. Hyaluronan as a regulator of macrophage function: implications for inflammation and angiogenesis. Annual Meeting of the Society for Glycobiology, Honolulu, HI (November 2014).
17. Buhrman JS, Rayahin JE, **Zhang Y**, Tang MY, Gemeinhart RA. Recombinant protein immobilization and controlled-release mediated by versatile, non-covalent protein anchor. College of Pharmacy Research Day, Chicago, IL (February 2015).
18. Rayahin JE, **Zhang Y**, Buhrman JS, Tang MY, Gemeinhart RA. Hyaluronan as a regulator of macrophage function: implications for inflammation and angiogenesis. College of Pharmacy Research Day, Chicago, IL (February 2015).
19. **Zhang Y**, Liu Y, Buhrman JS, Gemeinhart RA. Controlling miRNA Micelleplex Formation and Disassembly. College of Pharmacy Research Day, Chicago, IL (February 2015).

INDUSTRIAL INTERNSHIP

• Fresenius-Kabi USA, 2013 summer

My project was to investigate the critical factors that contribute to a peptide drug aggregation problem during manufacturing process and validate appropriate detection methods. Supervisor: Dr. Beena Uchil in the Formulation Department.

AWARDS RECEIVED

• Northeast Forestry University First-class Scholarship (2003 – 2007)
• Heilongjiang Provincial Merit Student (2006)
• Northeast Forestry University Outstanding Graduate (2007)
• University of Illinois at Chicago University Fellowship (2010 – 2011)
• Graduate Student Council Travel Award, 2011
• Graduate College Student Presenter Award, 2011.
• Second place in poster session, Polymers in Medicine and Biology 2011, American Chemical Society Polymer Division, CA, USA.
• University of Illinois at Chicago University Fellowship (2013 – 2014)
• Provost's Awards for Graduate Research, 2013
• Graduate Student Council Travel Award, 2013
• Graduate College Student Presenter Award, 2013.
• W.E. Van Doren Scholar, 2013
• University Dean Scholarship 2014
• The 28th Annual Symposium of the Protein Society, San Deigo, CA, 2014, Best Poster Award

LEADERSHIP AND MEMBERSHIP

• President, Controlled Release Society (CRS) - Illinois Student Chapter, 2014 - Current
• Vice president, Controlled Release Society (CRS) - Illinois Student Chapter, May 2012 - 2014
• Phi Kappa Phi Honor Society 2013.03 - current
• Pharmaceutics Graduate Student Research Meeting 2014-UIC Organizing Committee

• Treasurer, Controlled Release Society (CRS) - Illinois Student Chapter, Aug 2010 - April 2012

• Rho Chi Honor Society, 2012.02 - current

• American Association of Pharmaceutical Scientists (AAPS), 2010 - current.

• Controlled Release Society (CRS), 2010 - current.

MENTORING EXPERIENCE

2011-2013 **Elizabeth Ramirez**, undergraduate student, Department of Biology, University of Illinois at Chicago

2015 **Grace Moore**, undergraduate student, Department of Biology, Indiana University